

Bench Scale Apparatus Measurement Uncertainty and Uncertainty Effects on Measurement  
of Fire Characteristics of Material Systems

by

Lei Zhao

A Thesis

Submitted to the Faculty

of the

WORCESTER POLYTECHNIC INSTITUTE

In partial fulfillment of the requirements for the

Degree of Master of Science

In

Fire Protection Engineering

By

---

May 2005

APPROVED:

---

Professor Nicholas A. Dembsey, Major Advisor

---

Dr. John L. de Ris, Co-Advisor  
FM Global Research

---

Dr. Robert Bill, Co-Advisor  
FM Global Research

---

Professor Kathy A. Notarianni, Head of Department

## **ABSTRACT**

Traditional probability and statistics methodologies recommended by ISO and NIST were applied to standardize measurement uncertainty analysis on calorimetry bench scale apparatuses. The analysis was conducted for each component instrument (direct measurement) and each related physics quantity measured indirectly. There were many sources contributing to the ultimate uncertainty, however, initially, we dealt with the intrinsic uncertainty of each measuring instrument and the uncertainty from calibration. All other sources of uncertainty, i.e., drift, data acquisition, data reduction (round off, truncation, and curve smoothing) and personal operation were assumed to be negligible. Results were expressed as an interval having 95% confidence that the “true” value would fall within. A Monte Carlo Simulation technique with sampling size of 10000 was conducted to model the experiments. It showed that at least 95% of the modeled experiment results were inside the estimate interval. The consistency validated our analysis method.

An important characteristic of composite material systems is the ability to “custom design” the system to meet performance criteria such as cost, durability, strength and / or reaction to fire. To determine whether a new system is an improvement over previous ones and can meet required performance criteria, sufficiently accurate and precise instruments are needed to measure the system’s material properties in bench scale testing. Commonly used bench scale apparatuses are the cone calorimeter (Cone) and the FMGR fire propagation apparatus (FPA). For this thesis, thermally “thin” and “thick” specimens of a natural composite, red oak, were tested in the Cone in an air environment and in the FPA in a nitrogen environment. Cone test data of two FRP composite systems from the previous work of Alston are also considered. The material reaction to fire properties were estimated considering both ignition and

pyrolysis measurements made via the Cone and FPA. Investigation of the ultimate uncertainty of these material fire properties based on the intrinsic uncertainty of the component instruments (e.g. load cell) as well as the uncertainty introduced via use of a current ignition and pyrolysis model are considered.

## **ACKNOWLEDGEMENTS**

I am deeply indebted to my advisor Professor Nicholas A. Dembsey for a lot more than his help, encouragement, and advice, and for a lot more than skills and knowledge that I learned from him. His words of wisdom, insight, and philosophy are among the best things that I have learned.

I would also like to thank Dr. John L. de Ris and Dr. Robert Bill for enthusiasm and guidance. Their time and sharing their knowledge and invaluable insight is greatly appreciated.

I am highly appreciative of FM Global Research for providing me continuous and generous financial support. The thesis would not have been possible without the support.

I couldn't have done the thesis without the love and support of my wife and my parents. Especially, my wife has always been there to pick me up during the low points as well as to celebrate the good days. My sanity is indebted to her.

# **TABLE OF CONTENTS**

<b>ABSTRACT</b> .....	<b>i</b>
<b>ACKNOWLEDGEMENTS</b> .....	<b>iii</b>
<b>LIST OF FIGURES</b> .....	<b>vii</b>
<b>LIST OF TABLES</b> .....	<b>x</b>
<b>NOMENCLATURE</b> .....	<b>xi</b>
<b>DOCUMENT ORGANIZATION AND THESIS OVERVIEW</b> .....	<b>1</b>
<b>DOCUMENT ORGANIZATION -- GUIDE TO APPENDICES</b> .....	<b>1</b>
<b>THESIS OVERVIEW</b> .....	<b>5</b>
<b>CONCLUSIONS</b> .....	<b>11</b>
<b>REFERENCES</b> .....	<b>13</b>
<b>APPENDIX A MEASUREMENT UNCERTAINTY ANALYSIS FOR CALORIMETRY APPARATUSES</b> .....	<b>A-1</b>
<b>ABSTRACT</b> .....	<b>A-1</b>
<b>INTRODUCTION</b> .....	<b>A-2</b>
<b>BACKGROUND</b> .....	<b>A-4</b>
<b>UNCERTAINTY ANALYSIS OF COMPONENT INSTRUMENT (DIRECT MEASUREMENT)</b> .....	<b>A-6</b>
<b>1. Load Cell</b> .....	<b>A-6</b>
<b>2. Laser</b> .....	<b>A-15</b>
<b>3. Oxygen Analyzer</b> .....	<b>A-25</b>
<b>4. Pressure Transducer</b> .....	<b>A-30</b>
<b>5. Thermocouple</b> .....	<b>A-31</b>
<b>6. CO/CO<sub>2</sub> Analyzer</b> .....	<b>A-31</b>
<b>UNCERTAINTY ANALYSIS OF INDIRECT MEASUREMENT</b> .....	<b>A-32</b>
<b>1. Heat Release Rate</b> .....	<b>A-34</b>
<b>2. Extinction Coefficient</b> .....	<b>A-49</b>
<b>3. Average Specific Extinction Area</b> .....	<b>A-51</b>
<b>4. Average Heat of Combustion</b> .....	<b>A-54</b>
<b>UNCERTAINTY ANALYSIS METHODS VALIDATION BY MONTE CARLO SIMULATION (MCS)</b> .....	<b>A-56</b>
<b>MANUFACTURER VALUE VS. CURRENT ANALYSIS</b> .....	<b>A-59</b>
<b>CONCLUSIONS</b> .....	<b>A-62</b>
<b>REFERENCES</b> .....	<b>A-64</b>
<b>APPENDIX B UNCERTAINTY EFFECTS ON MEASUREMENT OF FIRE CHARACTERISTICS OF MATERIAL SYSTEMS</b> .....	<b>B-1</b>
<b>ABSTRACT</b> .....	<b>B-1</b>
<b>INTRODUCTION</b> .....	<b>B-1</b>
<b>BACKGROUND</b> .....	<b>B-3</b>
<b>PYROLYSIS MODEL</b> .....	<b>B-3</b>
<b>SPECIMEN PREPARATION</b> .....	<b>B-5</b>
<b>TEST SETUP</b> .....	<b>B-6</b>
<b>PROPERTY ESTIMATION</b> .....	<b>B-7</b>
<b>1. ESTIMATION OF BASELINE PROPERTIES</b> .....	<b>B-8</b>
<b>1.1 Red Oak Tested in Air Environment Using Cone</b> .....	<b>B-8</b>
<b>1.2 Red Oak Tested in Nitrogen Environment Using FPA</b> .....	<b>B-11</b>
<b>1.3 Composites Tested in Air Environment Using Cone</b> .....	<b>B-14</b>
<b>2. PROPERTY ESTIMATION WITH MLR UNCERTAINTY</b> .....	<b>B-16</b>
<b>2.1 MLR and Its Uncertainty Calculation</b> .....	<b>B-17</b>

2.1.1 MLR Calculation .....	B-17
2.1.2 Uncertainty of MLR Calculation .....	B-17
2.2 Property Estimation with One Standard Deviation of MLR.....	B-19
2.2.1 Red Oak Tested in Air Environment Using Cone and in Nitrogen Environment Using FPA .....	B-19
2.2.2 Composites Tested in Air Environment Using Cone.....	B-20
CONCLUSIONS .....	B-21
ACKNOWLEDGEMENTS .....	B-22
REFERENCES.....	B-22
APPENDIX C DERIVATION OF WELCH-SATTERTHWAITE FORMULA <sup>1,2</sup> ....	C-1
1. RELATIONSHIP BETWEEN DISTRIBUTIONS .....	C-1
1-1 Normal and Standard Normal Distribution.....	C-1
1-2 Standard Normal and Chi Squared Distribution.....	C-1
1-3 Summation of Chi Squared Distribution .....	C-2
1-4 Standard Normal, Chi Squared and Student's t Distribution.....	C-2
2. W-S FORMULA DERIVATION .....	C-3
REFERENCES.....	C-5
APPENDIX D C-FACTOR DETERMINATION <sup>1</sup> .....	D-1
REFERENCE.....	D-4
APPENDIX E LASER PHOTODIODES POWER CYCLE INVESTIGATION.....	E-1
APPENDIX F A HYPOTHETICAL CALIBRATION FOR OXYGEN ANALYZER ... .....	F-1
REFERENCES.....	F-4
APPENDIX G STANDARD DEVIATION OF UNIFORM DISTRIBUTION <sup>1</sup> .....	G-1
REFERENCE.....	G-2
APPENDIX H CONE VIs INTRODUCTION .....	H-1
APPENDIX I LOAD CELL SYSTEM AND LASER SYSTEM RESPONSE TIME I-1	
APPENDIX J JUSTIFICATION OF UNCERTAINTY PROPAGATION EQUATION <sup>1</sup> .....	J-1
REFERENCE.....	J-4
Appendix K HRR UNCERTAINTY BASED ON METHANE.....	K-1
REFERENCES.....	K-2
APPENDIX L BACKGROUND OF UNCERTAINTY ANALYSIS RELATED TO RECOMMENDED METHODOLOGIES .....	L-1
REFERENCES.....	L-3
APPENDIX M MEASUREMENT ERROR AND UNCERTAINTY .....	M-1
REFERENCES.....	M-2
APPENDIX N MASS LOSS RATE UNCERTAINTY .....	N-1
REFERENCES.....	N-2
APPENDIX O SENSITIVITY ANALYSIS FOR HRR.....	O-1
REFERENCE.....	O-3
APPENDIX P VOLUME FLOW RATE.....	P-1
REFERENCES.....	P-4
APPENDIX Q SENSITIVITY ANALYSIS FOR EXTINCTION COEFFICIENT... Q-1	
REFERENCE.....	Q-2
APPENDIX R SMOKE PRODUCTION RATE .....	R-1
REFERENCES.....	R-5
APPENDIX S DYNAMIC SPECIFIC EXTINCTION AREA.....	S-1
REFERENCES.....	S-6
APPENDIX T DYNAMIC HEAT OF COMBUSTION .....	T-1

**REFERENCES..... T-3**  
**APPENDIX U CONSTANT MLR GENERATOR FOR FUTURE WORK..... U-1**

## **LIST OF FIGURES**

Figure A-1 Load Cell Residual Dispersion.....	A-9
Figure A-2 Load Cell Measured Values vs. Accepted Values of Reference Materials.....	A-10
Figure A-3 Schematic Diagram of a Control Chart for Load Cell.....	A-14
Figure A-4 Laser Main Photodiode Normalized Residual Dispersion.....	A-18
Figure A-5 Laser Compensation Photodiodes Normalized Residual Dispersion .....	A-19
Figure A-6 Measured Values vs. Accepted Values of Reference Materials for Main Photodiode .....	A-19
Figure A-7 Measured Values vs. Accepted Values of Reference Materials for Compensation Photodiode .....	A-20
Figure A-8 Schematic Diagram of a Control Chart for Laser Main Photodiode.....	A-23
Figure A-9 Schematic Diagram of a Control Chart for Laser Compensation Photodiode .....	A-24
Figure A-10 Manufacturer’s Uncertainty and Current Uncertainty Comparison for Oxygen Analyzer .....	A-30
Figure A-11 Heat Release Rate and Its 95% Confidence Interval for 38mm Red Oak at 40 kW/m <sup>2</sup> External Heat Flux in Cone Test.....	A-36
Figure A-12 Heat Release Rate and Its 95% Confidence Interval of 2mm Red Oak at 40 kW/m <sup>2</sup> External Heat Flux in Cone Test.....	A-37
Figure A-13 Normalized HRR for Ten Days and Its 95% Confidence Uncertainty Band Based on Day-to-Day Variation and 95% Confidence Uncertainty Band based on Calibration for 1 kW Methane Burning Test.....	A-44
Figure A-14 Normalized HRR for Ten Days and Its 95% Confidence Uncertainty Band Based on Day-to-Day Variation and 95% Confidence Uncertainty Band based on Calibration for 3 kW Methane Burning Test.....	A-45
Figure A-15 Normalized HRR for Ten Days and Its 95% Confidence Uncertainty Band Based on Day-to-Day Variation and 95% Confidence Uncertainty Band based on Calibration for 5 kW Methane Burning Test.....	A-45
Figure A-16 HRR Uncertainty and the Normalized HRR Uncertainty (above 100%) of 2mm Red Oak at 70 kW/m <sup>2</sup> External Heat Flux in Cone Test.....	A-46
Figure A-17 HRR Uncertainty and the Normalized HRR Uncertainty (below 100%) of 2mm Red Oak at 70 kW/m <sup>2</sup> External Heat Flux in Cone Test.....	A-47
Figure A-18 R Values of the Component Variables for Heat Release Rate Calculation for 2mm Red Oak at 70 kW/m <sup>2</sup> External Heat Flux in Cone Test .....	A-48
Figure A-19 Extinction Coefficient and Its 95% Confidence Interval of 38mm Red Oak at 40 kW/m <sup>2</sup> External Heat Flux in Cone Test.....	A-50
Figure A-20 R Values of the Component Variables for Extinction Coefficient Calculation for 38mm Red Oak at 40 kW/m <sup>2</sup> External Heat Flux in Cone Test	A-51
Figure A-21 HRR Uncertainty Comparison Between Current Analysis and Manufacturer’s Value for 38mm Red Oak at 40 kW/m <sup>2</sup> External Heat Flux in Cone Test.....	A-60
Figure A-22 HRR Uncertainty Comparison Between Current Analysis and Manufacturer’s Value for 38mm Red Oak at 40 kW/m <sup>2</sup> External Heat Flux in Cone Test.....	A-60
Figure A-23 Normalized HRR Comparison at Different HRR Levels among Current Analysis, Enright et al <sup>12</sup> , Manufacturer Values (of Cone in WPI), and NIST <sup>13</sup> .	A-62
Figure B-1 Measured and Calculated MLR Comparison for Thermally “Thick” Red Oak at 60 kW/m <sup>2</sup> External Heat Flux in Air Using Cone.....	B-9

Figure B-2 Measured and Calculated MLR Comparison for Thermally “Thin” Red Oak at 20 kW/m <sup>2</sup> External Heat Flux in Air Using Cone.....	B-10
Figure B-3 Measured and Calculated MLR Comparison for Thermally “Thick” Red Oak at 50 kW/m <sup>2</sup> External Heat Flux in nitrogen Using FPA.....	B-12
Figure B-4 Measured and Calculated MLR Comparison for Thermally “Thin” Red Oak at 25 kW/m <sup>2</sup> External Heat Flux in nitrogen Using FPA.....	B-13
Figure B-5 Measured and Calculated MLR Comparison for Thermally “Thick” Composite at 50 kW/m <sup>2</sup> External Heat Flux in Air Using Cone. ....	B-15
Figure B-6 Measured and Calculated MLR Comparison for Thermally “Thin” Composite at 50 kW/m <sup>2</sup> External Heat Flux in Air Using Cone. ....	B-15
Figure B-7 MLR and Its Uncertainty Bands for Thermally “Thick” Composite at 50 kW/m <sup>2</sup> External Heat Flux in Air Using Cone Calorimeter.....	B-18
Figure D-1 Illustration of the Vertical Part of the Exhaust Duct of Cone Calorimeter with Orifice Plate and Pressure Ports .....	D-1
Figure E-1 Power Cycle Illustration of Main Photodiode at 16% Reference Obscuration .....	E-2
Figure E-2 Power Cycle Illustration of Compensation Photodiode at 16% Reference Obscuration.....	E-2
Figure E-3 Power Cycle Illustration of Main Photodiode at 100% Reference Obscuration.....	E-3
Figure E-4 Power Cycle Illustration of Compensation Photodiode at 100% Reference Obscuration.....	E-3
Figure E-5 Output Voltage Standard Deviation of Main Photodiode at Different Reference Obscuration Level.....	E-6
Figure E-6 Output Voltage Standard Deviation of Compensation Photodiode at Different Reference Obscuration Level.....	E-6
Figure I-1 Main and Compensation Photodiodes Response Time shown by Changing from 100% Obscuration to 0% Obscuration .....	I-1
Figure I-2 Main and Compensation Photodiodes Response Time shown by Changing from 0% Obscuration to 100% Obscuration.....	I-2
Figure I-3 Load Cell System Response Time by Weight dropped on the Load Cell .....	I-3
Figure I-4 Load Cell System Response Time by Weight Taken Away from the Load Cell .....	I-3
Figure M-1 Illustration of Systematic Error, Random Error and Total Measurement Error (The Figure is Modified from Figure 4.1 of Test Uncertainty <sup>2</sup> ) .....	M-1
Figure N-1 MLR and Its 95% Confidence Interval of 2mm Red Oak at 70 kW/m <sup>2</sup> External Heat Flux in Cone Test .....	N-2
Figure P-1 Five-point Average of Volume Flow Rate and Its 95% Confidence of Interval for 38mm Red Oak at 40 kW/m <sup>2</sup> External Heat Flux in Cone Test.....	P-2
Figure P-2 R Values of the Component Variables of Volume Flow Rate Calculation for 38mm Red Oak at 40 kW/m <sup>2</sup> External Heat Flux in Cone Test.....	P-3
Figure R-1 Smoke Production Rate and Its 95% Confidence Interval for 38mm Red Oak at 40 kW/m <sup>2</sup> External Heat Flux in Cone Test.....	R-3
Figure R-2 R Values of the Component Variables of Smoke Production Rate Calculation for 38mm Red Oak at 40 kW/m <sup>2</sup> External Heat Flux in Cone Test..	R-5
Figure S-1 Five-Point Average of Dynamic Specific Extinction Area and Its 95% Confidence Interval of 38mm Red Oak at 40 kW/m <sup>2</sup> External Heat Flux in Cone Test .....	S-2

**Figure S-2 R Values of C Factor, Pressure, and Temperature for Dynamic Specific Extinction Area Calculation for 38mm Red Oak at 40 kW/m<sup>2</sup> External Heat Flux in Cone Test.....S-4**

**Figure S-3 R Value of Mass Loss Rate for Dynamic Specific Extinction Area Calculation of 38mm Red Oak at 40 kW/m<sup>2</sup> External Heat Flux in Cone Test.....S-5**

**Figure S-4 R Values of Main and Compensation Photodiodes for Dynamic Specific Extinction Area Calculation of 38mm Red Oak at 40 kW/m<sup>2</sup> External Heat Flux in Cone Test.....S-5**

**Figure T-1 Five-Point Average of R Values of Component Variables for Dynamic HOC Calculation for 38mm Red Oak at 40 kW/m<sup>2</sup> External Heat Flux in Cone Test.. T-2**

**Figure T-2 R Values of Component Variables for Dynamic HOC Calculation for 38mm Red Oak at 40 kW/m<sup>2</sup> External Heat Flux in Cone Test ..... T-3**

**Figure U-1 Constant Mass Loss Rate Generator for MLR Uncertainty Estimate..... U-1**

## **LIST OF TABLES**

Table A-1 HRR Uncertainty Estimation Comparison.....	A-38
Table A-2 Average HRR and the Standard Deviation of HRR at Steady State Burning Duration of Thick PMMA .....	A-38
Table A-3 HRR Uncertainty Based on Day-to-Day Variation and HRR Uncertainty Based on Component Instrument Calibration.....	A-40
Table A-4 Normalized HRR Uncertainty based on Day-to-Day Variation and Normalized HRR Uncertainty Based on Component Instrument Calibration...	A-43
Table A-5 R Values of C Factor, Pressure, Temperature, Main Photodiode, compensation Photodiode, and Mass for Average SEA Calculation.....	A-54
Table A-6 Hypothetical True Values for HRR Variables.....	A-57
Table A-7 Monte Carlo Simulation Results .....	A-58
Table A-8 HRR Uncertainty and Its Normalized Uncertainty Comparison among Current Analysis, Enright et al <sup>12</sup> , Manufacturer Value, and NIST <sup>13</sup> .....	A-61
Table B-1 Comparison of Estimated Properties (Using Cone Data in Air without Uncertainties) and Literature <sup>13, 14, 15, 0</sup> Values of Red Oak. ....	B-11
Table B-2 Comparison of Estimated Properties (Using FPA Data in nitrogen without Uncertainties) and Literature Values of Red Oak. ....	B-14
Table B-3 Comparison of Estimated Properties of Thin and Thick Composites .....	B-16
Table B-4 Comparisons Between the “Worst” Estimations and the Baseline Values for Red Oak. ....	B-20
Table B-5 Comparisons Between the “Worst” Estimations and the Baseline Values for FRP Composite.....	B-21
Table E-1 Average and Standard Deviation of Output Voltage of Main Photodiode..	E-4
Table E-2 Average and Standard Deviation of Output Voltage of Compensation Photodiode .....	E-5
Table O-1 SC of Each variable Being Used to Calculate HRR .....	O-2
Table P-1 SC of Each Variable Being Used to Calculate VFR.....	P-3
Table Q-1 SC of Each variable Being Used to Calculate Extinction Coefficient.....	Q-1
Table R-1 SC of Each variable Being Used to Calculate SPR.....	R-4
Table S-1 SC of Each variable Being Used to Calculate Dynamic SEA.....	S-3

## NOMENCLATURE

$A_1$  : inside diameter of the duct (m);  
 $A_2$  : orifice diameter (m);  
b: intercept of an instrument linear function;  
C: orifice constant (C factor);  
 $C_d$  : discharge coefficient;  
 $c_i$  : control value of main or compensation photodiode;  
 $c_{ij}$  : control value of main or compensation photodiode at obscuration of 100%;  
 $c_{ij}$  : control value of main or compensation photodiode at obscuration of 16%;  
 $d_i$  : control value of load cell;  
 $d_{ij}$  : control value at 230g (g);  
 $d_{ij}$  : control value 0g (g);  
 $e_{nk}$  : residual;  
F ratio: the ratio of  $\hat{\delta}_1^2$  and  $\hat{\delta}_p^2$ ;  
F(): F distribution;  
 $f'$  : degrees of freedom;  
 $H$  : relative humidity in percent;  
 $\Delta h_c / r_0$  : net heat of combustion consuming 1kg oxygen (kJ/kg);  
I: actual beam intensity (%);  
 $I_0$ : beam intensity without smoke (%);  
J: times at which the measurements were made;  
K: number of measurements;  
k: extinction coefficient (1/m);  
 $k_p$  : uncertainty coverage factor;  
L: extinction beam path length (m);  
 $L_c$  : lower control limit for main or compensation photodiode;  
 $L_d$  : lower control limit for load cell;  
m: 1) slope of an instrument linear function; 2) number of RMs selected for control method;  
 $m_1$ : initial mass (g);  
 $m_2$ : final mass (g);  
N: number of reference material  
 $NK = N \times K$   
N(): normal distribution;  
n: number of measurements;  
 $O_{2span}$  % : oxygen analyzer span gas concentration (%);  
 $O_{2zero}$  % : oxygen analyzer zero gas concentration (%);  
 $P_1$  : pressure of upstream fluid in duct (Pa);  
 $P_2$  : pressure of downstream fluid in duct (Pa);  
 $P_{H_2O}$  : vapor pressure of water in mm Hg at the ambient temperature;  
 $\Delta P$  : pressure differential across the orifice reported by pressure transducer (Pa);

$Q$ : volumetric flow rate in the duct ( $\text{m}^3/\text{s}$ );  
 $\dot{Q}(t)$ : heat release rate;  
 $\dot{q}_i(t)$ : heat released (kW);  
 $R$  value: the ratio of  $UN_i$  and  $UN_t$  (%);  
 $SC$ : sensitivity coefficient;  
 $SSE$ : the sum of the squared residuals;  
 $SSP$ : the sum of the squared deviations between  $y_{nk}$  and  $y_n$ ;  
 $T_0$ : ambient temperature (K);  
 $T_e$ : fluid temperature in duct (K);  
 $T$ : stack temperature (K);  
 $\Delta t$ : time interval for data collecting, one second;  
 $U$ : uncertainty used to express a quantity;  
 $U_c$ : upper control limit for main or compensation photodiode;  
 $u_c(x_i)$ : standard uncertainty of a direct measured quantity;  
 $u(V)$ : standard uncertainty of voltage output;  
 $u_c(y)$ : standard uncertainty of an indirect measured quantity;  
 $U_d$ : upper control limit for load cell;  
 $UN_i$ : variance of indirect measured quantity calculated from only one of the component variables;  
 $UN_t$ : total variance of indirect measured quantity calculated from all of the component variables;  
 $V$ : voltage output (volt);  
 $V_1$ : velocity of upstream fluid in duct (m/s);  
 $V_2$ : velocity of downstream fluid in duct (m/s);  
 $V_{span}$ : span gas voltage output (volt);  
 $V_{zero}$ : zero gas voltage output (volt);  
 $\nu_{eff}$ : degrees of freedom of indirect measured quantity;  
 $\nu_i$ : degrees of freedom of direct measured quantity;  
 $\dot{V}$ : Volume flow rate in duct ( $\text{m}^3/\text{s}$ );  
 $w_n$ : reciprocal of  $n^{\text{th}}$  RM;  
 $\bar{w}$ : average of  $w_n$ ;  
 $WSSE$ : sum of squared normalized residual at  $n^{\text{th}}$  RM;  
 $WSSP$ : sum of squared deviations between  $z_{nk}$  and  $z_n$ ;  
 $x$ : 1) direct measured quantity; 2) random variable;  
 $X_{H_2O}^0$ : volume fraction of water vapor in ambient;  
 $X_{O_2}$ : mole fraction of oxygen reported by oxygen analyzer (%);  
 $X_{O_2}^0$ : mole fraction of oxygen in the incoming air (%);  
 $x_n$ : the accepted value of the  $n^{\text{th}}$  RM ( $n=1, \dots, N$ );  
 $x^*$ : transformed value;  
 $\bar{x}$  is the average of the accepted value of the reference material;  
 $y$ : 1) indirect measured quantity; 2) random variable;

$y_n$  is the average of the measured values of an accepted value of reference material ( $y_{nk}$ );

$y_0$ : measured value;

$y_{nk}$ : the  $k^{\text{th}}$  measurement of the  $n^{\text{th}}$  RM ( $k=1, \dots, K$ );

$\bar{y}$  is the average of  $y_n$ ;

$\hat{y}_n$  is the fitted value of an accepted value of a reference material;

$z_n$ : average of normalized measured value at  $n^{\text{th}}$  RM;

$z_{nk}$ : normalized measured value at  $n^{\text{th}}$  RM;

$\bar{z}$ : average of  $z_n$ ;

### **Greek Symbols**

$\alpha$ : significance level;

$\beta_0 + \beta_1 x_n$ : represents the expected value of the measurements of the  $n^{\text{th}}$  RM for instrument under the assumption of constant residual standard deviation;  $\beta_0$  is the intercept and  $\beta_1$  is the slope;

$\hat{\beta}_0$  is an estimate of  $\beta_0$ , for a “perfect” instrument  $\hat{\beta}_0$  should be zero;

$\hat{\beta}_1$  is an estimate of  $\beta_1$ , for a “perfect” instrument  $\hat{\beta}_1$  should be one;

$\delta$ : 1) standard uncertainty of weight (g); 2) standard deviation;

$\hat{\delta}$ : standard deviation of residual;

$\hat{\delta}_1^2$ : mean square of the deviation of SSE and SSP;

$\delta b$ : intercept uncertainty with 95% confidence;

$\hat{\delta}_{cal}$ : standard uncertainty of load cell;

$\delta m$ : slope uncertainty with 95% confidence;

$\hat{\delta}_p^2$ : mean square of SSP;

$\epsilon_{nk}$ : the deviation between  $y_{nk}$  and the expected value of the measurement of the  $n^{\text{th}}$  RM for instrument under the assumption of constant residual standard deviation;

$\gamma_0 + \gamma_1 x_n$ : represents the expected value of the measurement of the  $n^{\text{th}}$  RM for instrument under the assumption of proportional residual standard deviation,  $\gamma_0$  is intercept, and  $\gamma_1$  is slope.

$\eta_{nk}$ : deviation between  $y_{nk}$  and the expected measurement of the  $n^{\text{th}}$  RM,  $y_{nk}$  is determined based on measured voltage and calibration factor;

$\rho$ : fluid density ( $\text{kg/m}^3$ );

$\rho_0$ : air density at temperature  $T_0$ ;

$\rho_e$ : 1) fluid density in duct ( $\text{kg/m}^3$ ); 2) air density at temperature  $T_e$ ;

$\tau$ : standard uncertainty coefficient of obscuration;

$\hat{\tau}^2$ : mean square of WSSE.

$\hat{\tau}_1^2$ : mean square of the deviation of WSSE and WSSP;

$\hat{\tau}_{cal}$ : standard uncertainty of main or compensation photodiode;

$\hat{\tau}_p^2$ : mean square of the WSSP;

$\mu$ : expected value;

$\xi$ : significance level associated with each individual RM and with the limits  $U_d$  and  $L_d$  such that the overall significance of  $\alpha$  is obtained for all the m RMs simultaneously;  
 $\hat{\cdot}$ : an estimate of a true value;  
 $[\cdot]$ : mean of random variable;

### **Superscripts**

$\overset{0}{\cdot}$ : ambient;  
 $\overset{*}{\cdot}$ : transformed value;  
 $\overset{\cdot}{\cdot}$ : moment of a random variable;  
 $\bar{\cdot}$ : average;

### **Subscripts**

c: combined;  
eff: effective;  
h: high;  
l: low;  
p: confidence level

### **Abbreviations**

ANOVA: analysis of variance;  
ASTM: American Society for Testing and Materials;  
BIPM: International Bureau of Weights and Measures;  
CIPM: International Committee for Weights and Measures;  
CLT: Central Limit Theorem;  
FDM: finite difference method;  
FPA: fire propagation apparatus;  
FRP: fiber reinforced plastic;  
HOC: heat of combustion (kJ/g);  
HRR: heat release rate (kW/m<sup>2</sup>);  
[HRR]: averaged HRR;  
[NorHRR]: averaged normalized HRR;  
IEC: International Electrotechnical Committee;  
OIML: International Organization of Legal Metrology;  
ISO: International organization for Standardization;  
MCS: Monte Carlo simulation;  
MLR: mass loss rate (kg/sm<sup>2</sup>);  
NIST: National Institute of Standards and Technology;  
PMMA: polymethylmethacrylate;  
RM: reference material;  
SC: sensitivity coefficient  
SEA: specific extinction area (m<sup>2</sup>/kg);  
SPR: smoke production rate (m<sup>2</sup>/s);  
SD: standard deviation;  
VFR: volume flow rate (m<sup>3</sup>/s);

# **DOCUMENT ORGANIZATION AND THESIS OVERVIEW**

## **DOCUMENT ORGANIZATION -- GUIDE TO APPENDICES**

The text of this document is divided into two parts. The first part briefly describes the contents of the appendices. The second part is an overview of the work performed and conclusions drawn. Appendix A is intended to serve as a draft of a peer-reviewed paper. Appendix B was a conference paper published in Fire and Materials 2005. Appendices C through U give additional information relevant to this MS thesis that was not included in Appendices A and B.

### **Appendix A Measurement Uncertainty Analysis for Calorimetry Bench Scale**

#### **Apparatuses**

The measurement uncertainty analysis was conducted for each component instrument (direct measurement) and each related physics quantity measured indirectly. The component instruments are: oxygen analyzer, CO/CO<sub>2</sub> analyzer, load cell, laser photodiodes, pressure transducer, and thermocouples. Indirectly measured physics quantities are: heat release rate, volume flow rate, extinction coefficient, smoke production rate, specific extinction area, and heat of combustion, etc. According to ISO<sup>1,2</sup> and NIST<sup>3</sup>, results were expressed as an interval having 95% confidence that the “true” value would be within.

### **Appendix B Uncertainty Effects on Measurement of Fire Characteristics of Material Systems**

The effects of measurement uncertainty on estimation of material properties were analyzed by using a finite difference pyrolysis model. A natural composite system—red oak and two systems of FRP composite were tested by using calorimetry bench scale apparatuses, and the properties of red oak and the FRP composite were estimated. The properties were: Density of

virgin and char, thermal conductivity of virgin and char, specific heat of virgin and char, pyrolysis temperature, pre-exponential coefficient, vaporization heat, and surface emmissivity, etc.

### **Appendix C Derivation of Welch-Satterthwaite Formula**

Shows the derivation of the Welch-Satterthwaite formula.

### **Appendix D C-Factor Determination**

Introduced the fluid dynamic method to determine the C factor of the orifice plate in the exhaust duct of cone calorimeter.

### **Appendix E Laser Photodiodes Power Cycle Investigation**

It was found that the voltage output at a specific reference obscuration has a “sine” wave pattern. This is why the estimated uncertainties of laser related quantities are “large”.

### **Appendix F A Hypothetical Calibration for Oxygen Analyzer**

A hypothetical calibration for oxygen analyzer is conducted at 15% and 25% oxygen. The uncertainty of oxygen analyzer is estimated by using assumed voltage output standard deviation and the uncertainty of bottled oxygen.

### **Appendix G Standard Deviation of Uniform Distribution**

Shows the derivation of the standard deviation of uniform distribution.

### **Appendix H Cone VIs Introduction**

This Appendix will serve as a guide for the user to use the Cone VIs step by step.

## **Appendix I Load Cell System and Laser System Response Time**

Response time for load cell system is tested by weight drop test. Response time for laser system is tested by changing the obscuration of 0% and 100%.

## **Appendix J Justification of Uncertainty Propagation Equation**

Shows the derivation of the uncertainty propagation equation.

## **Appendix K HRR Uncertainty Based on Methane**

HRR uncertainty is estimated based on methane mass flow rate and methane heat of combustion

## **Appendix L Background of Uncertainty Analysis Related to Recommended Methodologies**

In this appendix, the history of ISO and NIST Guide was introduced. Central Limit Theorem and Monte Carlo Simulation technique were also briefly described.

## **Appendix M Measurement Error and Uncertainty**

The relationship and different between measurement error and uncertainty was introduced.

## **Appendix N Mass Loss Rate Uncertainty**

Mass loss rate was determined experimentally and statistically.

## **Appendix O Sensitivity Analysis for HRR**

It was evaluated that to which component parameter the HRR is sensitive. The component parameters are C factor, Heat of combustion per mass of oxygen, temperature, pressure, and oxygen concentration.

#### **Appendix P Volume Flow Rate**

In this Appendix, volume flow rate uncertainty was estimated as well as sensitivity analysis.

#### **Appendix Q Sensitivity Analysis for Extinction Coefficient**

It was evaluated that to which component parameter the extinction coefficient is sensitive. The component parameters are the obscuration measured by main and compensation diodes.

#### **Appendix R Smoke Production Rate**

In this Appendix, smoke production rate uncertainty was estimated as well as sensitivity analysis.

#### **Appendix S Dynamic Specific Extinction Area**

In this Appendix, dynamic extinction area uncertainty was estimated as well as sensitivity analysis.

#### **Appendix T Dynamic Heat of Combustion**

In this Appendix, dynamic heat of combustion uncertainty was estimated as well as sensitivity analysis.

#### **Appendix U Constant MLR Generator for Future Work**

In this Appendix, an initial idea for designing a constant mass loss rate generator is introduced.

## **THESIS OVERVIEW**

This thesis is intended to be accessible to anyone who has interest in uncertainty analysis on calorimetry bench scale test apparatuses, such as cone calorimeter and FPA (Fire Propagation Apparatus), etc. It demonstrates how to estimate uncertainties of direct measured quantities, such as oxygen concentration, smoke obscuration, etc, for component instruments of calorimetry bench scale apparatus, and how those uncertainties propagate to indirect measured quantities such as, HRR, extinction coefficient, etc. It also shows the measurement uncertainty effects on the material property estimate for a natural composite system—red oak and two systems of FRP (Fiber reinforced plastic) composites. The goals of this study are to 1) evaluate the ability of differentiating materials, such as thermal properties estimate for composite materials, for our current calorimetry bench scale apparatus; 2) make an initial attempt to standardize uncertainty analysis for calorimetry bench scale apparatus. The uncertainty analysis was conducted on a cone calorimeter in the Fire Science Laboratory at WPI.

The thesis is divided into two sections. The first section (Appendix A) describes the methodology of uncertainty analysis for each component instrument (direct measurement) of cone calorimeter. The uncertainties of the indirect measured quantities, such as HRR, extinction coefficient, etc, are also estimated.

This Section of the thesis provides the motivation to estimate the uncertainty of the calorimetry bench scale apparatus. Previous works are reviewed. It also examines the standardization history of ISO and NIST for measurement uncertainty. ISO Guide<sup>1,2</sup> and NIST Guide<sup>3</sup> on measurement uncertainty analysis and instrument calibration are introduced and performed in this Section. Some of the knowledge on statistical techniques is also briefly reviewed.

It looks at the operational principles of each component instrument, such as load cell, oxygen analyzer, laser photodiodes, etc, and describes the methodology for uncertainty analysis based on corresponding standards of ISO and NIST.

Load cell and laser are calibrated based on ISO 11095<sup>1</sup>. Before apply the guide, four assumptions should be examined: 1) there is no error in the accepted values of the reference materials (RMs); 2) calibration function is linear; 3) repeated measurements of a given reference material are independent and normally distributed; and 4) the residual standard deviation is either constant or proportional to the accepted value of the reference material. Following the steps introduced by the guide, the four assumptions are tenable for load cell and laser. The residual standard deviation of load cell is constant, and the residual standard deviation of laser is proportional to the accepted value of the reference obscuration. The 95% confidence intervals are estimated for load cell and laser respectively. The estimated uncertainty of load cell is 0.38g, which is consistent with the manufacturer's value 0.5g. Due to the existence of the power cycle phenomenon, the uncertainty of laser is "big". It is 1.6% (relative) for main photodiode and 2% (relative) for compensation photodiode.

ISO 11095<sup>1</sup> is not applicable to oxygen analyzer, since 1) there are errors in RM values (99.9% nitrogen for zero gas and dry air for span gas); 2) only two RMs are available (at least three RMs are required). Fortunately, the paramagnetic oxygen analyzer is inherently linear by design based on its transducer and the function can be represented by

$$O_2 \% = mV + b$$

where m is slope determined by

$$m = \frac{O_{2span} \% - O_{2zero} \%}{V_{span} - V_{zero}}$$

b is intercept determined by

$$b = \frac{O_{2zero} \% V_{span} - O_{2span} \% V_{zero}}{V_{span} - V_{zero}}$$

$O_{2zero} \%$  and  $O_{2span} \%$  are accepted values of the reference materials at zero and span point,  $V_{zero}$  and  $V_{span}$  are corresponding oxygen analyzer voltage output at zero and span point. The standard uncertainty of m ( $\delta m$ ) and b ( $\delta b$ ) are estimated by the Law of Propagation of Uncertainty according to ISO<sup>2</sup> and NIST<sup>3</sup> Guide. The uncertainty of oxygen measurement result can be represented as

$$U(O_2 \%) = k_p (\delta m V + \delta b)$$

$k_p$  is the coverage factor of the expanded uncertainty ( $U = k_p u_c(y)$ ), which defines an interval having p level of confidence (p is selected to be 95%).  $k_p$  was defined by Student's t

distribution based on  $\nu_{eff}$  number of effective degrees of freedom. The effective degrees of freedom were estimated by Welch-Satterthwaite formula. The estimated coverage factor  $k_p$  of oxygen analyzer was two. A typical calculation of  $\delta m$  was 0.000036 volume fraction of oxygen per volt, and  $\delta b$  was zero. At about 20% oxygen, the uncertainty was 0.06% oxygen. The manufacturer value was 0.1% oxygen.

Primary standard dead weight, which can generate standard pressure and be used to calibrate pressure transducer, is not available for the bench scale apparatus due to the operational complexity. The manufacturer's value is used for the uncertainty of the pressure transducer. The CO/CO<sub>2</sub> analyzer is inherently non-linear by design based on its transducer. Therefore, the manufacturer's value is used for the uncertainty. Also, the manufacturer specified uncertainty 2.2 K is used for the thermocouples, since 1) thermocouples are relatively accurate and have very complex polynomial functions; 2) temperature uncertainty is insignificant for the indirect measured quantities.

Mass loss rate uncertainty is a special indirect measurement uncertainty. Mass measurement is a time series measurement. The MLR uncertainty was determined experimentally as 1.5 g/sm<sup>2</sup> for 95% confidence. Please note the MLR uncertainty is 4 g/sm<sup>2</sup> for 95% confidence by using different method in Appendix B.

The Law of Propagation of Uncertainty based on ISO<sup>2</sup> and NIST<sup>3</sup> is used to estimate all the other indirect measured parameters of cone calorimeter such as heat release rate, volume flow rate, extinction coefficient, smoke production rate, specific extinction area, and heat of combustion. A full discussion for HRR was conducted in terms of uncertainty as well as sensitivity. Comparisons with both Enright<sup>4</sup> and NIST<sup>5</sup> are shown. The uncertainty and

sensitivity of other quantities were also fully discussed. It was shown that the estimated uncertainties of the smoke obscuration related quantities such as extinction coefficient, smoke production rate, and specific extinction area, are “large”. Our laser doesn’t have the ability to differentiate the obscuration related quantities due to the power cycle phenomenon. A stabilized laser is needed.

All above uncertainty analysis methods (except for MLR uncertainty) are validated by a Monte Carlo Simulation (MCS) technique. Ten thousand random values are generated for each constant (C factor, heat of combustion per unit mass of oxygen) and component instrument based on its inherent variation. Then, 10000 values were estimated for each direct and indirect measured quantity. It was found that 95% of the 10000 values of each quantity are falling in our estimated uncertainty interval with 95% confidence.

At the end of the section, the uncertainties of heat release rate and heat of combustion were estimated based on the manufacturer’s value. It was shown that the manufacturer’s uncertainty was conservative and tended to overestimate the uncertainty.

The second section (Appendix B) of the thesis focuses on composite material thermal property estimation. How measurement uncertainty influences the thermal property variation is shown. In this section, previous works on material property estimation are reviewed. A FDM pyrolysis model is introduced and performed to estimate the properties for composites. The properties of a natural composite--red oak and two FRP (fiber reinforced plastic) composite systems are estimated. The time to ignition and mass loss rate history measured in the apparatuses, Cone and FPA, are used to estimate material properties. The best estimate properties make the pyrolysis model simulations agree with the experiment for both the time

to ignition and the subsequent transient mass loss rate of the material for different applied heat fluxes. For red oak time to ignition is measured by using cone, mass loss rate is measured by using cone in air and FPA in nitrogen. For the FRP composite all the measurements are conducted by using cone in air. The estimated properties are: Density of virgin and char, thermal conductivity of virgin and char, specific heat of virgin and char, pyrolysis temperature, pre-exponential coefficient, vaporization heat, and surface emissivity, etc.

The properties of red oak were estimated by using the pyrolysis model at different conditions, i.e., thermally “thin” and “thick” specimens tested in both air and nitrogen environments. It is found that most of the estimated properties are consistent between the different conditions and with literature values (maximum 25% variation). The exceptions are pre-exponential coefficient and vaporization heat. There are no literature values for these properties. Across the various conditions the pre-exponential coefficient varies by a factor of 3.5 and the vaporization heat varies by a factor of 6.8. Given the consistency of the vast majority of the properties for red oak the model is considered to be working properly with an uncertainty of 25% or as noted above for pre-exponential coefficient and vaporization heat.

Since two standard deviations don't work for the pyrolysis model, one standard deviation of mass loss rate is introduced to the model as the measurement uncertainty. Variations of four “key” properties, i.e., thermal conductivity of virgin and char, pre-exponential coefficient, and pyrolysis heat, are investigated. Based on red oak and the FRP composite, the variations of the four “key” properties are within the model uncertainty estimates.

## CONCLUSIONS

1) The measurement uncertainties of component instruments (direct measurement), load cell, oxygen analyzer, and laser were estimated based on ISO<sup>2</sup> and NIST<sup>3</sup> Guide. Pressure transducer, CO/CO<sub>2</sub> analyzer, and thermocouples measurement uncertainties were determined by using manufacturer's specification. The uncertainties of load cell, oxygen analyzer, and laser were expressed by 95% confidence interval and the uncertainties of load cell and oxygen analyzer were smaller than those specified by manufacturers (there was no manufacturer specifications for laser.). The study initially standardized measurement uncertainty analysis for calorimetry apparatus measurement.

Based on the uncertainties of component instruments, indirect measured parameter uncertainties were estimated. They are heat release rate, extinction coefficient, volume flow rate, specific extinction area, smoke production rate, and heat of combustion. Uncertainty interval of 95% confidence was determined.

All the uncertainty bands of direct and indirect measurement were validated by using Monte Carlo Simulation technique for sampling size of 10,000. It demonstrated that our uncertainty analysis methods were appropriate.

The measurement uncertainty analysis showed that our laser doesn't have the ability to differentiate obscuration related quantities. The theoretical approach for MLR uncertainty estimate is not available. The uncertainty is determined experimentally and statistically, and expressed by 95% confidence interval.

R value analysis showed that, for our case, HRR uncertainty depends not only on oxygen concentration uncertainty, but also on C factor and heat of combustion per mass of oxygen.

The HRR uncertainty and its normalized uncertainty were compared at different HRR levels among the current analysis, Enright et al<sup>4</sup>, manufacturer value, and NIST<sup>5</sup>. Current results are higher than that of Enright et al<sup>4</sup> because different methods were used to estimate oxygen concentration uncertainty. Current method is basically the same with NIST<sup>5</sup>. It also showed that the normalized HRR uncertainty is decreasing as the HRR increasing. The normalized uncertainty of current analysis at higher HRR level is consistent with NIST<sup>5</sup>.

The data analysis for the HRR calibration at 1, 3, and 5 kW showed that the normalized HRR uncertainty based on component instrument calibration is consistency with the normalized HRR based on day-to-day variation.

2) An important characteristic of composite materials is the ability to “custom design” the system. To be able to properly measure the properties of the material, sufficiently accurate and precise instruments and models are needed. In this work the Cone and FPA along with a current ignition and pyrolysis model were evaluated. The evaluation considered a natural composite, red oak, and two FRP composites. The measurement systems (apparatuses and model) were able to estimate properties of the red oak that were consistent with literature values as well as estimate reasonable properties for the two composites. An important aspect of simulating fires for design is to know the uncertainties of the material properties. Consideration of the measured mass loss rate uncertainty at the one standard deviation level showed that the current model could estimate properties and that their uncertainties were consistent with those inherent of the model. Considering the two standard deviation level of

mass loss rate uncertainty (recommended by ISO<sup>2</sup> and NIST<sup>3</sup>) stable and reasonable property sets could not be estimated. Future work needs to focus on either lowering the mass loss rate uncertainty or development of more robust models so that property uncertainties can be more reliably estimated.

### 3) Recommendations for Future Work

a) A robust method should be figured out to estimate mass loss rate uncertainty so that the MLR uncertainty can be obtained for different level of MLR.

b) For material property estimation, it needs a more robust and easy-to-use pyrolysis model.

c) The cone calorimeter in the Fire Science Laboratory at WPI needs a stabilized laser.

## **REFERENCES**

1. International Organization for Standardization, Linear Calibration Using Reference Materials, ISO 11095:1996(E).
2. International Organization for Standardization, Guide to the expression of Uncertainty in Measurement, ISBN 92-67-10188-9, ISO, Geneva, 1995.
3. Taylor, B. N., and Kuyatt, C. E., Guidelines for Evaluating and Expressing the Uncertainty of NIST Measurement Results, NIST Technical Note 1297, NIST, Gaithersburg, MD, Sept. 1994.
4. Enright, P., and Fleischmann, C., "Uncertainty of Heat Release Rate Calculation of the ISO5660-1 Cone Calorimeter Standard Test Method", Fire Technology, 35:2 (1999) 153-169

5. Bryant, Rodney A., Ohlemiller, Thomas J., Johnsson, Erik L., Hammins, Anthony, Grove, Brian S., Guthrie, William F., Maranghides, Alexander, and Mulholland George W., "The NIST 3 Megawatt Quantitative Heat Release Rate Facility", NIST Special Publication 1007, December 2003.

# **APPENDIX A MEASUREMENT UNCERTAINTY ANALYSIS FOR CALORIMETRY APPARATUSES**

Lei Zhao and Nicholas A. Dembsey  
Worcester Polytechnic Institute

## **ABSTRACT**

The authors applied traditional probability and statistics methodologies recommended by ISO and NIST to standardize measurement uncertainty analysis on bench scale apparatuses. The analysis was conducted for each component instrument (direct measurement) and each related physics quantity measured indirectly. There were many sources contributing to the ultimate uncertainty, however, initially, we dealt with the intrinsic uncertainty of each measuring instrument and the uncertainty from calibration. All other sources of uncertainty i.e., drift, data acquisition, data reduction (round off, truncation, and curve smoothing), and personal operation were assumed to be negligible. Results were expressed as an interval having 95% confidence that the “true” value would fall within. A Monte Carlo Simulation technique with sampling size of 10000 was conducted to model the experiments. It showed that at least 95% of the modeled experiment results were inside the estimate interval. The consistency validated our analysis method. The comparison showed that current uncertainties (for heat release rate and average heat of combustion) were smaller than those estimated from manufacturer’s values.

## **INTRODUCTION**

This paper focuses on the measurement uncertainty analysis for calorimetry apparatuses. There are bench scale, intermediate scale and large scale calorimetry material flammability test methods. The bench scale ones, such as Cone Calorimeter<sup>1,2</sup> and Fire Propagation Apparatus<sup>3</sup>, are intended to be applied to material components or composite materials. The intermediate and large scale tests, such as intermediate scale calorimeter (ICAL)<sup>4</sup>, parallel panel apparatus (intermediate scale)<sup>5</sup> and room corner test (large scale) specified by ASTM<sup>6</sup> and FM Global<sup>7</sup>, can deal with complete products: upholstered furniture, mattresses, stacking chairs, textile wall coverings, other interior finish, foam plastic insulation, foam displays, electrical cables and electro-technical products<sup>8</sup>. In the thesis, the uncertainty analysis examples were conducted on the Cone Calorimeter in the Fire Science Laboratory at Worcester Polytechnic Institute.

Measurement is the process of finding the value of a physical quantity experimentally with the help of special technical means called measuring instruments<sup>9</sup>. It has been recognized to be the most important means in science and engineering. However, the experimental data will be meaningless until the appropriate uncertainties are known. Intervals with a certain high percentage of confidence should be provided to the measured results. Then, one knows how good are the measurements, i.e., he/she has a certain high percentage of confidence that the “true” values will fall in the intervals.

Manufacturers define the uncertainty for one type of instrument (usually, there are several types for one kind of instrument) by the original plan of design. The uncertainty is always

defined conservatively. The experimenter could do additional work to know more characteristics about the instrument, hence, to obtain more exact measurement and uncertainty estimates. However, the absence of an standardized uncertainty analysis methodology for calorimetry apparatus made not only significant comparison of test results between fire laboratories difficult, but also could not provide a common means for people to estimate the uncertainty of the test, further, people didn't know if the apparatus had the ability to differentiate materials. This study focused on standardizing uncertainty analysis method, on which cone calorimeter evaluation was based. The measurement uncertainty analysis was implemented in a Cone VI software (LabView).

The measurement uncertainty analysis was conducted for both direct and indirect measurements. In the case of direct measurements the object of study is made to interact with the measuring instrument, and the value of the measurand is read from the indications of the latter. The measurands of temperature, pressure and oxygen concentration, etc are examples of direct measurements. In the case of indirect measurements, the value of the measurand  $y$  is related to the values of arguments  $x_i$  by a known function  $f$ . This relationship can be represented in a general form as  $y = f(x_1, \dots, x_n)$ . The measurands of heat release rate, smoke production rate, etc are examples of indirect measurements.

Measurement uncertainty is made up of two components: Type A and Type B evaluation of uncertainty. While Type A uncertainty is obtained by the statistical analysis of series of observations, Type B uncertainty is obtained by means other than the statistical analysis of series of observations<sup>10</sup>. In this paper, both Type A and Type B uncertainties were considered.

Many sources of uncertainty could contribute to the ultimate result. For present, we only dealt with the intrinsic uncertainty of measuring instruments and the uncertainty from calibration. All other sources of uncertainty i.e., drift, data acquisition, data reduction (round off, truncation, and curve smoothing), and personal operation were assumed to be negligible.

The measurement uncertainty analysis methodology used was recommended in NIST<sup>10</sup> and ISO<sup>11</sup> Guide. These methodologies were based on traditional probability and statistics theory. The results were compared with those from a Monte Carlo Simulation technique modeling experiments. The consistency validated the theory.

Mass loss rate uncertainty analysis was an exception since the weight measurement in burning test was identified as time series procedure. For now, MLR uncertainty was determined experimentally and statistically.

## **BACKGROUND**

For over 20 years, people have done a lot of research related to, and using Cone Calorimeter and FPA. A few studies exist which address the uncertainty of heat release rate measurements by oxygen consumption calorimetry. One of the works by Patrick A. Enright and Charles M. Fleischmann<sup>12</sup> focused on the uncertainty associated with the heat release rate calculation for the cone calorimeter. In their study, the component uncertainties were taken from the manufacturer's specification in the cases of the temperature and differential pressures. The component uncertainty of the oxygen analyzer is assumed to be  $\pm 100$ ppm, which is the maximum linear response and drift that ASTM E 1354<sup>2</sup> accepts. The normalized HRR

uncertainty (uncertainty of HRR/HRR) was reported as about 5.5% for the HRR in the range of 200 kW/m<sup>2</sup> to 500 kW/m<sup>2</sup>. It was also demonstrated that the relative uncertainty was very high at low HRR. The greatest sources of uncertainty identified were the heat of combustion factor, the combustion expansion factor, and oxygen measurement.

Rodney A. Bryant et al<sup>13</sup> built a 3 MW quantitative heat release rate facility at NIST. In calculating HRR, they used the most basic measurement inputs of instrument voltages, thermocouple temperatures, and constant parameters (universal, empirical and calibration). It showed that the normalized uncertainties (uncertainty of HRR/HRR) were 7.5%, 5.3%, and 5.3% for the HRR at 0.05 MW, 0.65 MW, and 2.7 MW respectively. The average HRR and its standard deviation were calculated from the measured gas flow of the calibration burner. For the same time intervals, the average and standard deviation for the HRR were calculated from the hood system measured parameters (oxygen level, hood flow, etc.). Plot the two results versus each other as “Actual HRR” for the natural gas calibration burner output on the x-axis and “Apparent HRR” for the oxygen consumption calorimetry calculated result on the y-axis. Perform a linear least squares fit of the data using a graphing package or spreadsheet statistics. Compare the results to previous such data for the system. The slopes typically agree within 1% to 2%.

Alston<sup>14</sup> estimated material properties or fire growth model parameters for two GRP composite systems, an eight-layer glass and a one-layer glass over 1-inch balsa core sandwich system both vacuum infused with vinyl ester resin. Instrument and calculation uncertainty were investigated to explore their impact on the determination of material properties and model parameters used in screening tools and models for evaluating material systems. Manufacturer specified uncertainties were used in estimating the measurement uncertainty.

The cone test uncertainty analysis only focused on heat released rate and the calibration uncertainty was not included in the ultimate uncertainty. He concluded that: “Although the techniques each showed differing results for effective thermal inertia for each material, the calculation uncertainties are too large to fully and accurately differentiate the two systems. It is unlikely that the techniques could differentiate between more subtle variations in material or skin thickness.”

## **UNCERTAINTY ANALYSIS OF COMPONENT INSTRUMENT (DIRECT MEASUREMENT)**

The measurement uncertainty analysis was conducted for each component instrument of calorimetry bench scale apparatus. In the thesis, the component instruments were chosen from Cone calorimeter in the Fire Science Laboratory at Worcester Polytechnic Institute.

### **1. Load Cell**

The load cell was Type 6005D manufactured by Automatic Timing & Control. The accuracy was specified as 0.5g (0.1% of full scale) by the manufacturer<sup>15</sup>. The linear calibration function provided by manufacturer is  $y = 29.1x$ .  $y$  is mass in gram, and  $x$  is voltage output in volt.

The measurement uncertainty analysis for load cell is based on ISO 11095<sup>16</sup>. Four assumptions are made: 1) there is no error in the accepted values of the reference materials (RMs); 2) calibration function is linear; 3) repeated measurements of a given reference material are independent and normally distributed; and 4) the residual standard deviation is

either constant or proportional to the accepted value of the reference material. The estimation of the linear calibration function under the assumption of constant residual standard deviation is captured by the model

$$y_{nk} = \beta_0 + \beta_1 x_n + \varepsilon_{nk}$$

where

$x_n$  is the accepted value of the  $n^{\text{th}}$  RM ( $n=1, \dots, N$ );

$y_{nk}$  is the  $k^{\text{th}}$  measurement of the  $n^{\text{th}}$  RM ( $k=1, \dots, K$ ), and determined based on measured voltage and manufacturer's calibration factor;

$\beta_0 + \beta_1 x_n$  represents the expected value of the measurements of the  $n^{\text{th}}$  RM,  $\beta_0$  is the intercept and  $\beta_1$  is the slope;

$\varepsilon_{nk}$  is the deviation between  $y_{nk}$  and the expected value of the measurement of the  $n^{\text{th}}$  RM.

Estimates of the parameters  $\beta_0$  and  $\beta_1$  can be obtained by using the formulae below.

Estimates of parameters in this paper have a hat above the symbol to differentiate them from the parameters themselves which are unknown.

$$\hat{\beta}_1 = \frac{\sum_1^6 (x_n - \bar{x})(y_n - \bar{y})}{\sum_1^6 (x_n - \bar{x})^2}$$

$$\hat{\beta}_0 = \bar{y} - \hat{\beta}_1 \bar{x}$$

where

$\bar{x} = \sum_1^N x_n / N$  is the average of the accepted value of the reference material;

$y_n = \sum_1^K y_{nk} / K$  is the average of the measurement values of a accepted value of reference

material;

$\bar{y} = \sum_1^N y_n / N$  is the average of  $y_n$ .

$$\hat{y}_n = \hat{\beta}_0 + \hat{\beta}_1 x_n$$

where

$\hat{y}_n$  is the fitted value of an accepted value of a reference material;

$\hat{\beta}_0$  is an estimate of  $\beta_0$ , for a “perfect” instrument  $\hat{\beta}_0$  should be zero;

$\hat{\beta}_1$  is an estimate of  $\beta_1$ , for a “perfect” instrument  $\hat{\beta}_1$  should be one;

Assumption 1) was appropriate because the reference material were test weights. Since the response time of the load cell system was in the range of 0.4s to 0.6s (see Appendix I) and voltage output was recorded once per second, the measurements were independent. Also, based on the Guide<sup>10,11</sup> the voltage output of a reference material was normally distributed. Assumption 3) was, therefore, satisfied. Assumption 2) and 4) will be examined.

In the day-to-day calibration, load cell is calibrated at 6 different RM levels, i.e., 0g, 50g, 100g, 150g, 200g, and 230g. At each point the data are collected 60 times at the scan rate of once per second. As such, the linear function of load cell was estimated as

$$\hat{y}_n = \hat{\beta}_0 + \hat{\beta}_1 x_n = -0.00179 + 1.00008 x_n$$

The residuals are calculated as

$$e_{nk} = y_{nk} - \hat{y}_n$$

The relationship of  $e_{nk}$  (residuals) and  $\hat{y}$  (fitted value) is shown in Figure A-1. As seen in Figure A-1, the dispersion of the residuals for any fitted value is almost constant throughout, except for a few outliers at 230g. Therefore, the assumption, of constant residual standard deviation is tenable for the load cell.

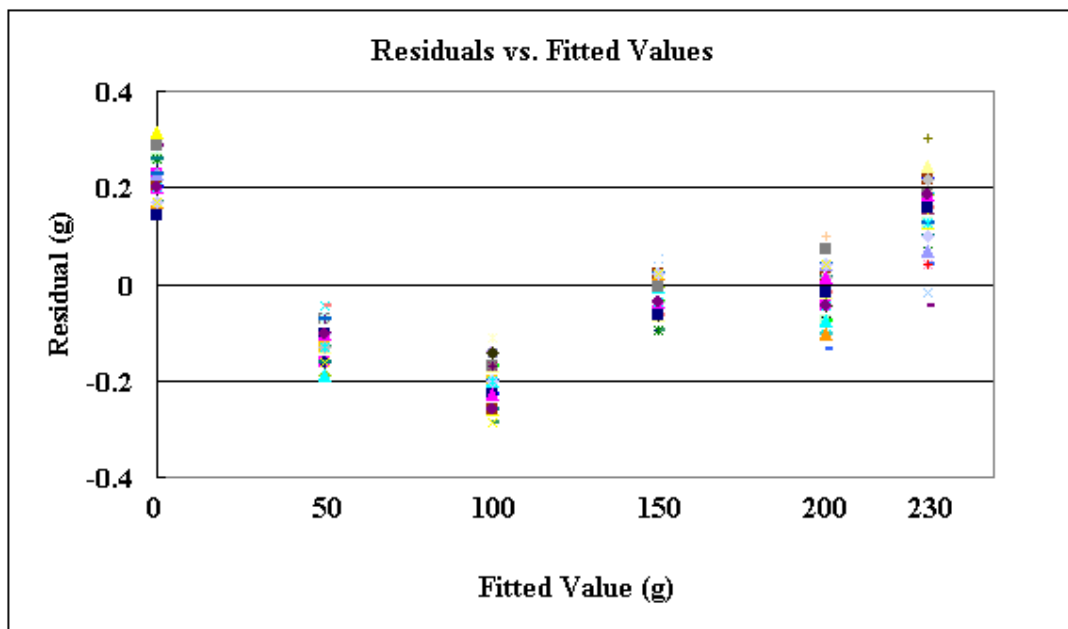


**Figure A-1 Load Cell Residual Dispersion**

The linearity of load cell can be visualized from Figure A-2.

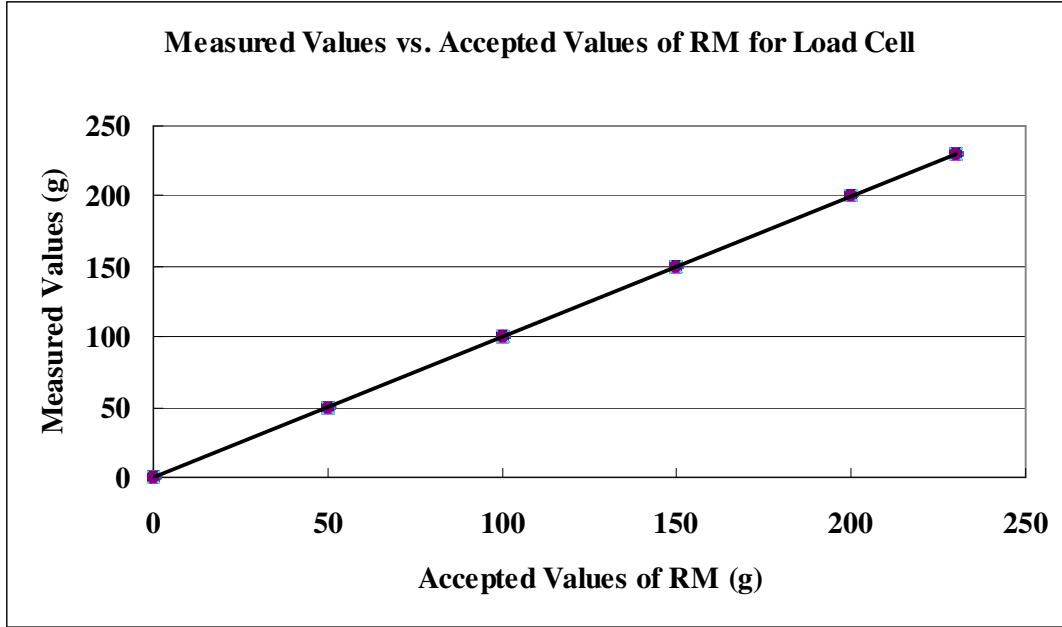


**Figure A-2 Load Cell Measured Values vs. Accepted Values of Reference Materials**

Since the measurement uncertainties (at magnitude of 0.1g) are too small comparing to the measurement range (at magnitude of 100g), load cell cannot be concluded to be linear only from the visualization inspection of Figure A-2. ISO 11095<sup>16</sup> recommends the Analysis of

Variance (ANOVA) to check the linearity. If F ratio ( $= \frac{\hat{\delta}_1^2}{\hat{\delta}_p^2}$ ) is not larger than

$F_{(1-\alpha)}(N-2, NK-N)$ , then there is no evidence to reject the linear model. A sum of squares divided by its associated degrees of freedom is called a mean square.

Where

$SSP = \sum_{n=1}^N \sum_{k=1}^K (y_{nk} - y_n)^2$  is the sum of the squared deviations between  $y_{nk}$  and  $y_n$ ;

$SSE = \sum_{n=1}^N \sum_{k=1}^K (e_{nk})^2$  is the sum of the squared residuals;

$\hat{\sigma}_1^2 = \frac{SSE - SSP}{N - 2}$  is the mean square of the deviation of SSE and SSP;

$\hat{\sigma}_p^2 = \frac{SSP}{NK - N}$  is the mean square of SSP.

$F_{(1-\alpha)}(N - 2, NK - N)$  is the  $(1 - \alpha)$  -quantile of the F distribution with numerator degrees of freedom  $N-2$  and denominator degrees of freedom  $NK-N$ ;

$\alpha$  is the significance level, the probability to reject the linear model if the model is true.

We select  $\alpha = 0.05$ .

Since the load cell is calibrated by using 6 RMs in day-to-day activity,  $N$  equals 6. At each RM 60 measurements are taken, therefore,  $K$  equals 60. The load cell turned out to be nonlinear. At  $K=60$  F test maybe too sensitive. Due to the “small” error the non-linearity of the load cell can be mapped.

For the load cell measurement uncertainty analysis, we assume that the device is essentially stationary throughout the day. Our focus then is on the linearity of the instrument given that we know there will be some perturbation of the stationary assumption as we move from reference value to reference value -- arguing that we need to remove the mass and replace it for each measurement. Assuming essentially stationary is consistent with the fact that we appear to have during any 60 scans period minimal disturbance of the measurement from the environment. Checking linearity then makes sense based on perturbations of stationary at 2 measurements per 60 scans where we are comparing the non-linearity of our instrument to our perturbations due to operation of the instrument given an assumed stationary

environment. Since ISO 11095<sup>16</sup> recommends at least 2 measurements for a RM, the averages

of the first 30 and last 30 scans are used. Then, we have  $\frac{\hat{\delta}_1^2}{\hat{\delta}_p^2} = 4.26 \leq F_{0.95}(4,6) = 4.53$ .

Based on the statistical test and our assumptions of 2 measurements per RM we have demonstrated that the instrument is *effectively* linear. Effectively linear indicates that load cell uncertainty is primarily composed of instrument non-linearity not measurement error. Therefore, for practical purpose, the load cell is assumed to be linear.

Since the load cell is linear, a single measurement  $y_0$  of an unknown weight will lead to a reported weight value of

$$x^* = \frac{y_0 - \hat{\beta}_0}{\hat{\beta}_1} = \frac{y_0 - (-0.00179)}{1.00008}$$

$x^*$  is transformed value. According to ISO 11095<sup>16</sup>, two reference weights are selected for the control method. These weights are selected in such a way that they cover as large a range as possible of values encountered during normal operating conditions. 0g and 230g are selected. The control values at 0g and 230g are calculated respectively

$$d_i = x_i^* - x_i$$

where  $x_i$  is the accepted value of RM<sub>i</sub>

The upper control limit  $U_d$  and the lower control limit  $L_d$  are estimated as

$$U_d = \frac{\hat{\delta}}{\hat{\beta}_1} t_{(1-\xi/2)}(NK-2) = 0.41g$$

$$L_d = -0.41g$$

where

$$\hat{\delta} = \sqrt{\frac{SEE}{(NK-2)}} \text{ is standard deviation of residual;}$$

$t_{(1-\xi/2)}(NK-2)$  is the  $(1-\xi/2)$ -quantile of the t-distribution with NK-2 (258) degrees of freedom.  $\xi$  is the significance level associated with each individual RM and with the limits

$U_d$  and  $L_d$  such that the overall significance of  $\alpha$  is obtained for all the  $m$  ( $m=2$ ) RMs

simultaneously  $\xi = \frac{\alpha}{m}$ .  $\alpha$  is the significance level selected for the control chart as seen in

Figure A-3. In our case  $\alpha$  is taken to be 5%.  $m$  is the number of RMs selected for the control method. In our case  $m$  is taken to be 2, i.e., 0g and 230g. Select  $m$  RMs such that their accepted values cover the range of values encountered under normal operating conditions. Five day's control values  $d_i$  at 0g and 230g are calculated. The control values and the upper and lower limit are plotted in Figure A-3. As seen in Figure A-3, all the control values are between the upper and lower limit. Based on ISO 11095<sup>16</sup>, the load cell system is declared in-control.

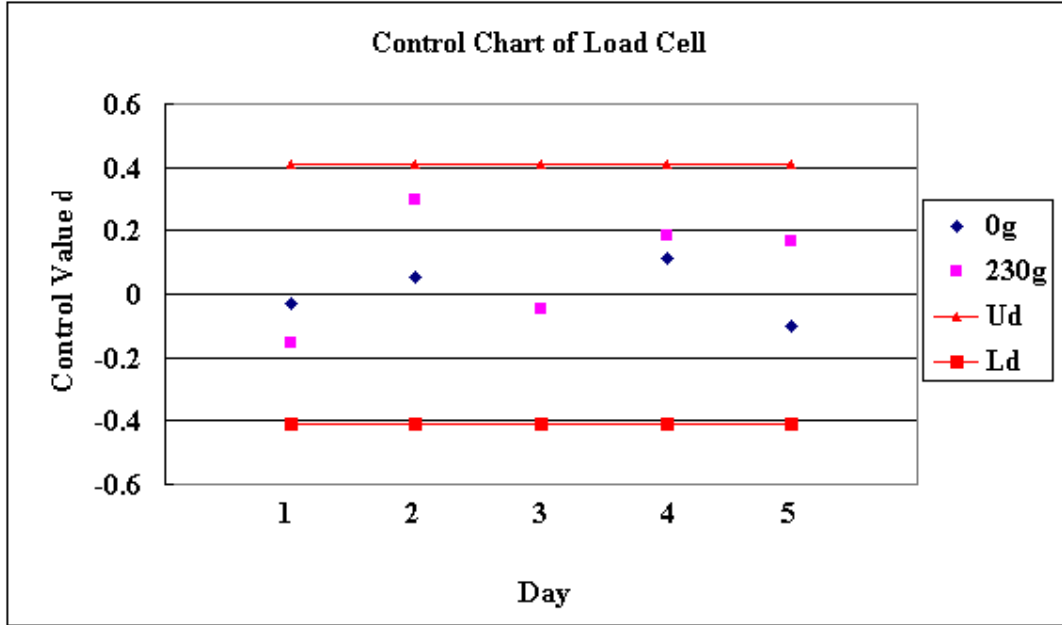


Figure A-3 Schematic Diagram of a Control Chart for Load Cell

Based on ISO 11095<sup>16</sup>, the standard uncertainty of load cell is calculated as

$$\hat{\delta}_{cal} = \sqrt{\frac{\sum_{j=1}^J (d_{lj}^2 + d_{hj}^2)}{2J}}$$

where

J represents the time at which the measurements were made, our case  $J = 60$ .

$d_{lj}$  and  $d_{hj}$  are the corresponding residuals at lowest (0g) and highest (230g) accepted values of reference material respectively.

Two were taken as the coverage factor for the interval of 95% confidence according to the Student's t-distribution with degrees of freedom 2J (120). Then the result can be represented by:

$$x^* \pm 2 \hat{\delta}_{cal}$$

A typical calculation showed that  $\delta$  is approximated as 0.19g. Then,  $\delta(95\%)=0.38g$ . If this uncertainty value is deemed to be too large based on the indirect measurement results then the effective linearity demonstrated above is not adequate. To lower the uncertainty the non-linear nature of the load cell would have to be taken into account.

## 2. Laser

As being custom designed, laser doesn't have the calibration factors provided by manufacturer. The calibration factor of laser is determined by ourselves. The linear functions of the main and compensation photodiodes are  $y = 0.29x + 0.001$  and  $y = 0.15x + 0.002$  respectively.  $y$  is the obscuration in obscuration,  $x$  is the voltage output in volt.

The measurement uncertainty analysis for laser was based on ISO 11095<sup>16</sup>. The same four assumptions have to hold. Assumptions 1) and 3) were examined in Load Cell Section. The situation is the same for laser. The estimation of the linear calibration function under the assumption of proportional residual standard deviation is captured by the model

$$y_{nk} = \gamma_0 + \gamma_1 x_n + \eta_{nk}$$

where

$\gamma_0 + \gamma_1 x_n$  represents the expected value of the measurement of the  $n^{\text{th}}$  RM;

$\eta_{nk}$  is the deviation between  $y_{nk}$  and the expected measurement of the  $n^{\text{th}}$  RM,  $y_{nk}$  is determined based on measured voltage and calibration factor;

This model can be transformed into a model equivalent to the one given in Load Cell Section, i.e., with errors having constant variance. The transformation consists of dividing by  $x_n$  both on both sides. This gives

$$z_{nk} = \gamma_1 + \gamma_0 w_n + \varepsilon_{nk}$$

where

$z_{nk} = y_{nk} / x_n$  is normalized measured value at  $n^{\text{th}}$  RM;

$w_n = 1 / x_n$  is reciprocal at  $n^{\text{th}}$  RM;

$\varepsilon_{nk} = \eta_{nk} / x_n$  is normalized residual at  $n^{\text{th}}$  RM.

Estimates of the parameters  $\gamma_0$  and  $\gamma_1$  can be obtained by using the formulae below.

Estimates of parameters in this paper have a hat above the symbol to differentiate them from the parameters themselves which are unknown.

$$\hat{\gamma}_0 = \frac{\sum_1^N (w_n - \bar{w})(z_n - \bar{z})}{\sum_1^N (w_n - \bar{w})^2}$$

is an estimate of  $\hat{\gamma}_0$ , for a “perfect” instrument  $\hat{\gamma}_0$  should be zero;

$\hat{\gamma}_1 = \bar{z} - \hat{\gamma}_0 \bar{w}$  is an estimate of  $\hat{\gamma}_1$ , for a “perfect” instrument  $\hat{\gamma}_1$  should be one;

where

$$NK = N \times K ;$$

$$\bar{w} = \sum_1^N w_n / N \text{ is the average of } w_n ;$$

$$z_n = \sum_1^K z_{nk} / K \text{ is the average of normalized measured value at } n^{\text{th}} \text{ RM};$$

$$\bar{z} = \sum_1^N z_n / N \text{ is the average of } z_n ;$$

$$\hat{z}_n = \hat{\gamma}_1 + \hat{\gamma}_0 w_n \text{ is normalized fitted value;}$$

$$u_{nk} = z_{nk} - \hat{z}_n \text{ is normalized residual at } n^{\text{th}} \text{ RM};$$

$$WSSE = \sum_1^N \sum_1^K (u_{nk})^2 \text{ is sum of squared normalized residual at } n^{\text{th}} \text{ RM};$$

$$\hat{\sigma}^2 = \frac{WSSE}{NK - 2} \text{ is the mean square of WSSE.}$$

In the day-to-day calibration, laser is calibrated at 4 different RM levels, i.e., 0%, 16%, 48%, and 100% obscuration. At each point the data are collected 60 times at the scan rate of once per second. Since the normalized value at 0% reference obscuration cannot be obtained, the other three points will be used for laser uncertainty analysis.

As such, the linear function of laser was estimated as

$$\text{Main photodiode: } \hat{z}_n = \hat{\gamma}_1 + \hat{\gamma}_0 w_n = 0.9919 - 0.0003w_n$$

$$\text{Compensation photodiode: } \hat{z}_n = \hat{\gamma}_1 + \hat{\gamma}_0 w_n = 1.0041 - 0.0030w_n$$

The relationship of  $u_{nk}$  (normalized residuals) and  $\hat{z}$  (normalized fitted value) is shown in Figure A-4 and Figure A-5. As seen in Figure A-4 and Figure A-5, the dispersion of the normalized residuals for any normalized fitted value is almost constant through, except for a few outliers at 16% and 100% obscuration for compensation photodiode. Therefore, the assumption, of proportional residual standard deviation is tenable for both main and compensation photodiodes.

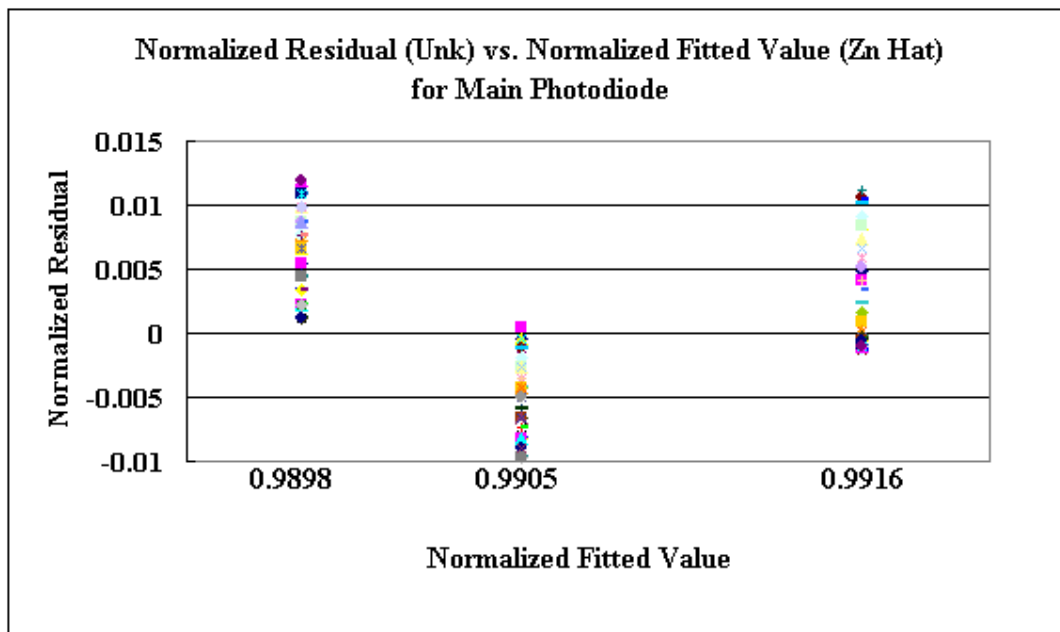


**Figure A-4 Laser Main Photodiode Normalized Residual Dispersion**

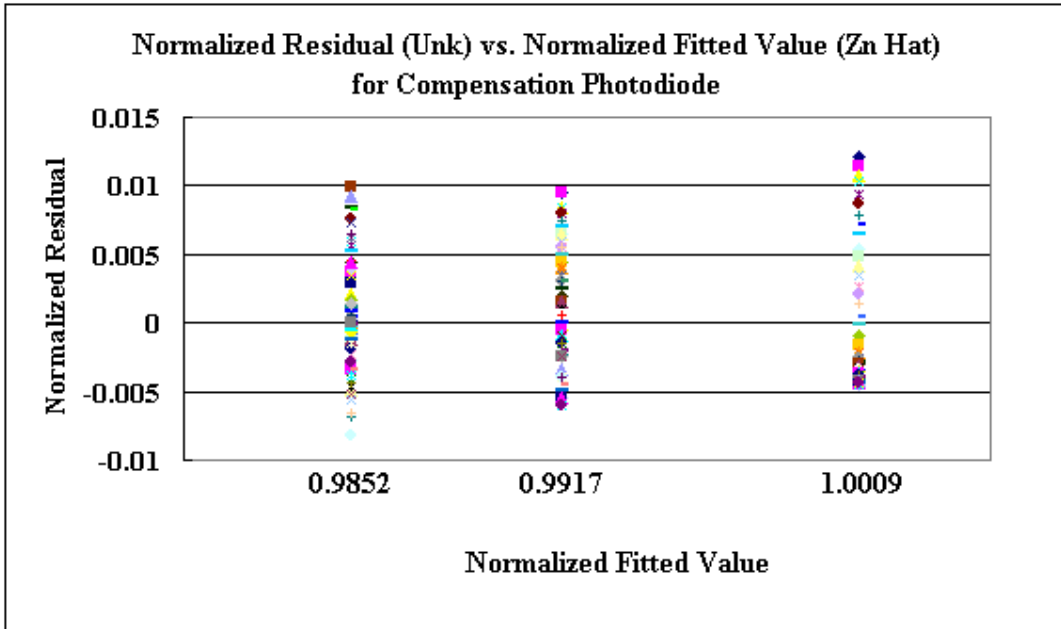


**Figure A-5 Laser Compensation Photodiodes Normalized Residual Dispersion**

The linearity of laser main and compensation photodiodes can be visualized from Figure A-6 and Figure A-7.

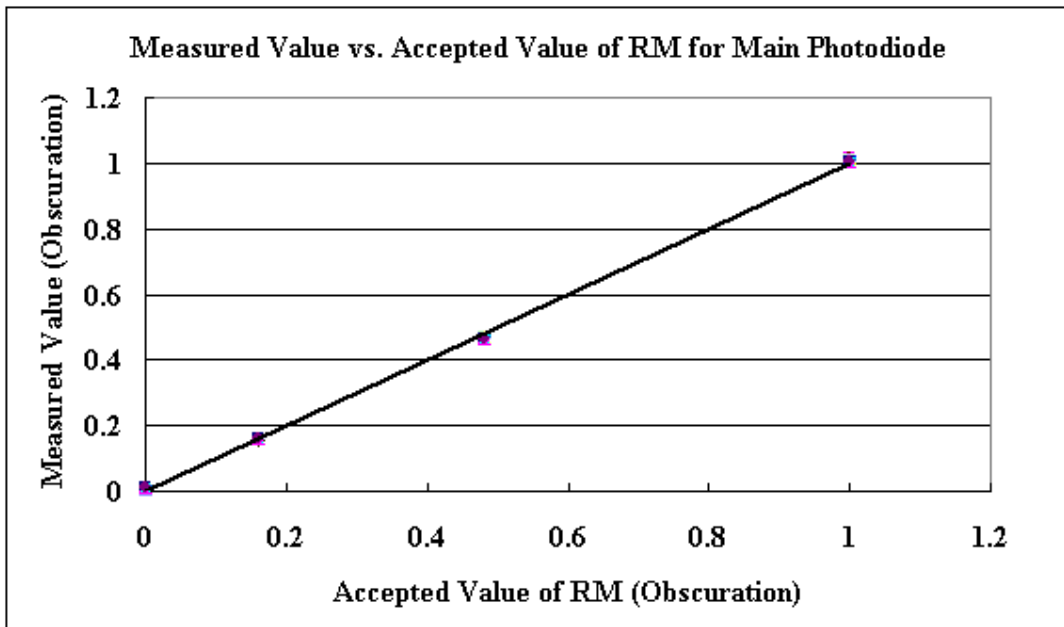


**Figure A-6 Measured Values vs. Accepted Values of Reference Materials for Main Photodiode**

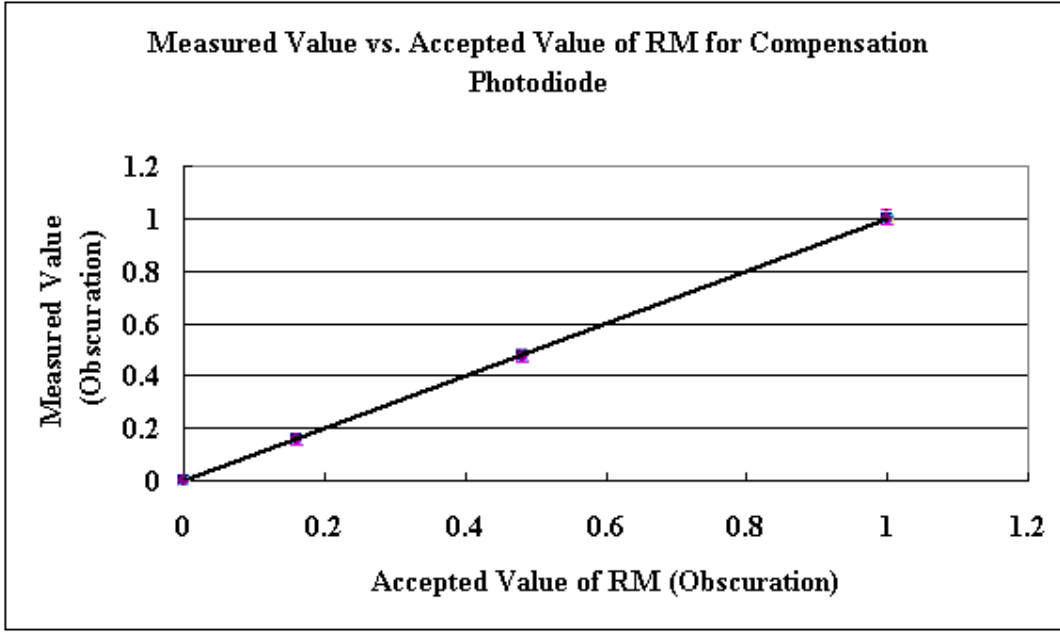


**Figure A-7 Measured Values vs. Accepted Values of Reference Materials for Compensation Photodiode**

However, the linearity should be confirmed by using Analysis of Variance method (ANOVA)

recommended by ISO 11095<sup>16</sup>. If F Ratio ( $= \frac{\hat{\tau}_1^2}{\hat{\tau}_p^2}$ ) is not larger than  $F_{(1-\alpha)}(N-2, NK-N)$ ,

then there is no evidence to reject the linear model.

Where

$WSSP = \sum_{n=1}^N \sum_{k=1}^K (z_{nk} - z_n)^2$  is the sum of squared deviations between  $z_{nk}$  and  $z_n$ ;

$\hat{\tau}_1^2 = \frac{WSSE - WSSP}{N-2}$  is the mean square of the deviation of WSSE and WSSP;

$\hat{\tau}_p^2 = \frac{WSSP}{NK-N}$  is the mean square of the WSSP.

For 60 measurements, the compensation photodiode is linear, while the main photodiode is nonlinear. At K=60 F test maybe too sensitive. Due to the “small” error the non-linearity of the main photodiode can be mapped.

For the laser measurement uncertainty analysis, we assume that the device is essentially stationary throughout the day. With the same reason as described for the load cell, we use 2 measurements to check the linearity. The 2 measurements are the averages of the first and last 30 scans.  $F_{(1-\alpha)}(N-2, NK-N)$  is the F distribution with numerator degrees of freedom N-2 and denominator degrees of freedom NK-N, and confidence level of  $1-\alpha$ .  $\alpha$  is the significance level, the probability to reject the linear model if the model is true. For the laser main and compensation photodiode, let  $\alpha=0.05$ , we have

For main photodiode,  $\frac{\hat{\tau}_1^2}{\hat{\tau}_p^2} = 6.1 \leq F_{0.95}(1,3) = 10.1$ , therefore, it is linear.

For compensation photodiode,  $\frac{\hat{\tau}_1^2}{\hat{\tau}_p^2} = 0.25 \leq F_{0.95}(1,3) = 10.1$ , therefore, it is linear also.

Based on the statistical test and our assumptions of 2 measurements per RM we have demonstrated that the main photodiode is *effectively* linear. Effectively linear indicates that the main photodiode uncertainty is primarily composed of instrument non-linearity not measurement error. Therefore, for practical purpose, the main photodiode is assumed to be linear.

Since the laser is linear, a single measurement  $y_0$  of an unknown obscuration will lead to a reported obscuration value of

$$\text{Main photodiode: } x^* = \frac{y_0 - \hat{\gamma}_0}{\hat{\gamma}_1} = \frac{y_0 - (-0.0003)}{0.9919}$$

$$\text{Compensation photodiode: } x^* = \frac{y_0 - \hat{\gamma}_0}{\hat{\gamma}_1} = \frac{y_0 - (-0.003)}{1.0041}$$

According to ISO 11095<sup>16</sup>, two reference obscurations are selected for the control method. These obscurations are selected in such a way that they cover as large a range as possible of values encountered during normal operating condition. 16% and 100% are selected. The control values at 16% and 100% are calculated respectively

$$c_i = \frac{x_i^* - x_i}{x_i}$$

where  $x_i$  is the accepted value of  $RM_i$

The upper control limit  $U_c$  and the lower control limit  $L_c$  are estimated as

Main Photodiode

$$U_c = \frac{\hat{\tau}}{\hat{\gamma}_1} t_{(1-\xi/2)}(NK - 2) = 0.037$$

$$L_c = -0.037$$

Compensation photodiode

$$U_c = \frac{\hat{\tau}}{\hat{\gamma}_1} t_{(1-\xi/2)}(NK - 2) = 0.009$$

$$L_c = -0.009$$

where

$t_{(1-\xi/2)}(NK - 2)$  is the  $(1 - \xi/2)$ -quantile of the t-distribution with  $NK-2$  (358) degrees of freedom.  $\xi$  is the significance level associated with each individual RM and with the limits  $U_c$  and  $L_c$  such that the overall significance of  $\alpha$  is obtained for all the  $m$  ( $m=2$ ) RMs simultaneously  $\xi = \frac{\alpha}{m}$ .  $\alpha$  is the significance level selected for the control chart as seen in

Figure A-8 and A-9. In our case  $\alpha$  is taken to be 5%.  $m$  is the number of RMs selected for the control method. In our case  $m$  is taken to be 2, i.e., 16% and 100% obscuration. Select  $m$  RMs such that their accepted values cover the range of values encountered under normal operating conditions. Five day's control values  $c_i$  at 16% and 100% obscuration are calculated. The control values and the upper and lower limit are plotted in Figure A-8 and Figure A-9. As seen in Figure A-8 and Figure A-9, all the control values are between the upper and lower limit. Based on ISO 11095<sup>16</sup>, the laser system is declared in-control.

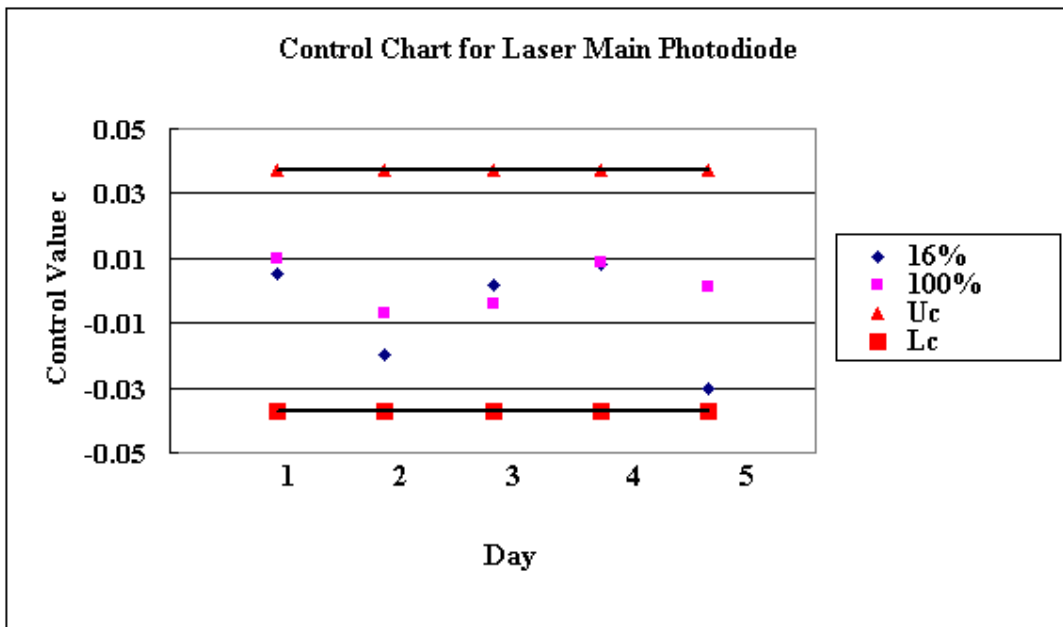


Figure A-8 Schematic Diagram of a Control Chart for Laser Main Photodiode

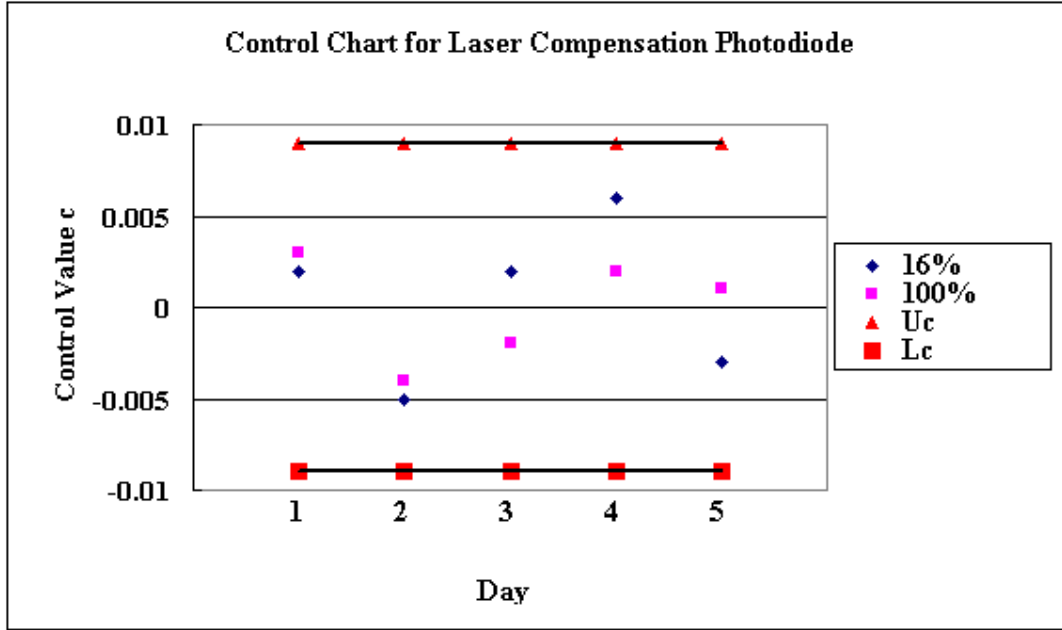


Figure A-9 Schematic Diagram of a Control Chart for Laser Compensation Photodiode

Based on ISO 11095<sup>16</sup>, the standard uncertainty of laser is calculated as

$$\hat{\tau}_{cal} = \sqrt{\frac{\sum_{j=1}^J (c_{lj}^2 + c_{hj}^2)}{2J}}$$

where

J represents the time at which the measurements were made, our case  $J = 60$ .

$c_{lj}$  and  $c_{hj}$  are the corresponding control values at 16% and 100% obscuration respectively.

Two were taken as the coverage factor for the interval of 95% confidence according to the Student's t-distribution with degrees of freedom 2J (120). Then the result can be represented by:

$$x^* \pm 2\hat{\tau}_{cal} * x^*$$

A typical calculation showed that  $\tau$  is approximated as 0.012 (obscurtion/obscurtion) for main photodiode, and 0.004 (obscurtion/obscurtion) for compensation photodiode. Then, the 95% confidence interval for main photodiode is “measured value \* 0.024”, and for compensation photodiode is “measured value \* 0.008”. If this uncertainty value is deemed to be too large based on the indirect measurement results then the effective linearity demonstrated above is not adequate. To lower the uncertainty the non-linear nature of the laser would have to be taken into account.

### 3. Oxygen Analyzer

The oxygen analyzer was Type X1420 manufactured by Servomex. The accuracy was specified as 0.1% of oxygen for the full scale (0-25%) by the manufacturer<sup>17</sup>. The linear function provide by the manufacturer is  $y = 0.025x$ .  $y$  is the oxygen volume fraction,  $x$  is the voltage output in volt.

For oxygen analyzer calibration, we would like to use the same calibration approaches for load cell and laser. Unfortunately, we only had zero gas and span gas. Any standard oxygen concentration source was not available between zero and span gas. Zero gas was 99.99% nitrogen. The volume fraction of oxygen can be assumed to be in the range of 0% to 0.01%, therefore, it was approximated as  $0.005\% \pm 0.005\%$ . Span gas was supplied by breathing dry air that had an oxygen volume fraction of  $20.9\% \pm 0.05\%$ <sup>13</sup>. The relative humidity of the laboratory is about 15%. The oxygen concentration at this relative humidity in air is about 20.85%. Considering the oxygen concentration in dry air is 20.95%, we assume the oxygen

concentration after removing water from the incoming air to be in the range of 20.9%±0.05% oxygen. Assuming equal probabilities for the “true” oxygen concentrations lie anywhere within the intervals for both zero and span gas, that is, modeled them by a uniform distribution<sup>10</sup>. Therefore, the standard uncertainty was calculated to be  $0.005\% / \sqrt{3} = 0.003\%$  , and  $0.05\% / \sqrt{3} = 0.03\%$  <sup>10,11</sup> for zero and span gas. Since the oxygen concentration and the standard uncertainty of zero gas was too small to have obvious effect on the uncertainty calculation, therefore, the values were assumed to be zero. Since only two standards were available, we could not check the behavior of the residuals, i.e., if they are constant or proportional to reference materials. ISO 11095<sup>16</sup> was not applicable to this case. Fortunately, the paramagnetic oxygen analyzer was inherently linear by design based on its transducer and the function was represented by

$$O_2 \% = mV + b$$

where m is slope determined by

$$m = \frac{O_{2span} \% - O_{2zero} \%}{V_{span} - V_{zero}}$$

b is intercept determined by

$$b = \frac{O_{2zero} \% V_{span} - O_{2span} \% V_{zero}}{V_{span} - V_{zero}}$$

$O_{2zero} \%$  and  $O_{2span} \%$  are accepted value of the reference materials at zero and span point,

$V_{zero}$  and  $V_{span}$  are corresponding oxygen analyzer voltage output at zero and span point. The

standard uncertainty of m and b is estimated according to the Law of Propagation of Uncertainty in NIST Guide<sup>10</sup> and ISO Guidelines<sup>11</sup>.

$$u_c^2(y) = \sum \left(\frac{\partial y}{\partial x_i}\right)^2 u^2(x_i)$$

The covariance terms were eliminated since the error sources were uncorrelated, i.e., the measurements didn't share errors from identical sources<sup>18</sup>. Each  $u(x_i)$  was a standard uncertainty of above four direct measured quantities. Standard uncertainty is the uncertainty of the result of a measurement expressed as a standard deviation<sup>10,11</sup>. The standard uncertainty of voltage output was estimated as

$$u(V) = \sqrt{\frac{1}{n-1} \sum_1^n (V_i - \bar{V})^2}$$

Where: n was times the voltage output recorded (60 for our case)

$$\bar{V} = \frac{V_1 + \dots + V_n}{n}$$

Since the uncertainty of each variable is known, i.e.,  $u(V_{zero}) = 0$  and  $u(V_{span}) = 3.8 \times 10^{-4}$  were oxygen analyzer voltage output standard uncertainty at zero and span point respectively; the data were from a typical day-to-day calibration case.  $u(O_{2zero} \%) = 0\%$  and  $u(O_{2span} \%) = 0.03\%$  were oxygen concentration standard uncertainty at zero and span point respectively. The standard uncertainty of m and b was estimated as

$$\delta m = \sqrt{\left(\frac{(O_{2zero} \% - O_{2span} \%)}{(V_{span} - V_{zero})^2} u(V_{zero})\right)^2 + \left(\frac{(O_{2span} \% - O_{2zero} \%)}{(V_{span} - V_{zero})^2} u(V_{span})\right)^2 + \left(\frac{-1}{V_{span} - V_{zero}} u(O_{2zero} \%)\right)^2 + \left(\frac{1}{V_{span} - V_{zero}} u(O_{2span} \%)\right)^2}$$

$$\delta b = \sqrt{\left(\frac{V_{span} (O_{2zero} \% - O_{2span} \%)}{(V_{span} - V_{zero})^2} u(V_{zero})\right)^2 + \left(\frac{V_{zero} (O_{2span} \% - O_{2zero} \%)}{(V_{span} - V_{zero})^2} u(V_{span})\right)^2 + \left(\frac{V_{span}}{V_{span} - V_{zero}} u(O_{2zero} \%)\right)^2 + \left(\frac{-V_{zero}}{V_{span} - V_{zero}} u(O_{2span} \%)\right)^2}$$

The uncertainty of oxygen measurement result can be represented as

$$u(O_2 \%) = k_p (\delta m V + \delta b)$$

A typical calculation showed that  $\delta m$  was approximated as 0.000036 volume fraction of oxygen per volt, and  $\delta b$  as 0 for standard uncertainty. In our day-to-day calibration, the sampling size is 60 at both of zero and span point.

If a physics quantity  $y$  (for now,  $y$  is  $m$  or  $b$ ) is not measured directly, but is determined from  $n$  other statistically independent quantities  $x_1, \dots, x_n$  through a functional relationship  $f$  :

$$y = f(x_1, \dots, x_n),$$

based on NIST<sup>10</sup> and ISO<sup>11</sup>, the coverage factor  $k_p$  of the expanded uncertainty

( $U = k_p u_c(y)$ ), which defines an interval having  $p$  level of confidence ( $p$  is usually selected

to be 95%).  $k_p$  was defined by Student's  $t$  distribution based on  $\nu_{eff}$  number of effective

degrees of freedom. The effective degrees of freedom was estimated by Welch-Satterthwaite formula

$$v_{eff} = \frac{u_c^4(y)}{\sum_{i=1}^n \frac{(\partial f / \partial x_i)^4 u^4(x_i)}{v_i}}$$

Where  $v_i$  is the degrees of freedom of  $u(x_i)$  and usually  $v_i = n - 1$ ,  $n$  is the sampling size of component parameter  $x_i$ .

The effective degrees of freedom calculated by using Welch-Satterthwaite formula was about 60 for both of  $m$  and  $b$ . Then, 2 was taken as the coverage factor for interval of 95% confidence, the uncertainty was expressed as

$$u(O_2 \%) = 2 \times (0.000036V)$$

The comparison of manufacturer specified uncertainty and current uncertainty is shown Figure A-10.

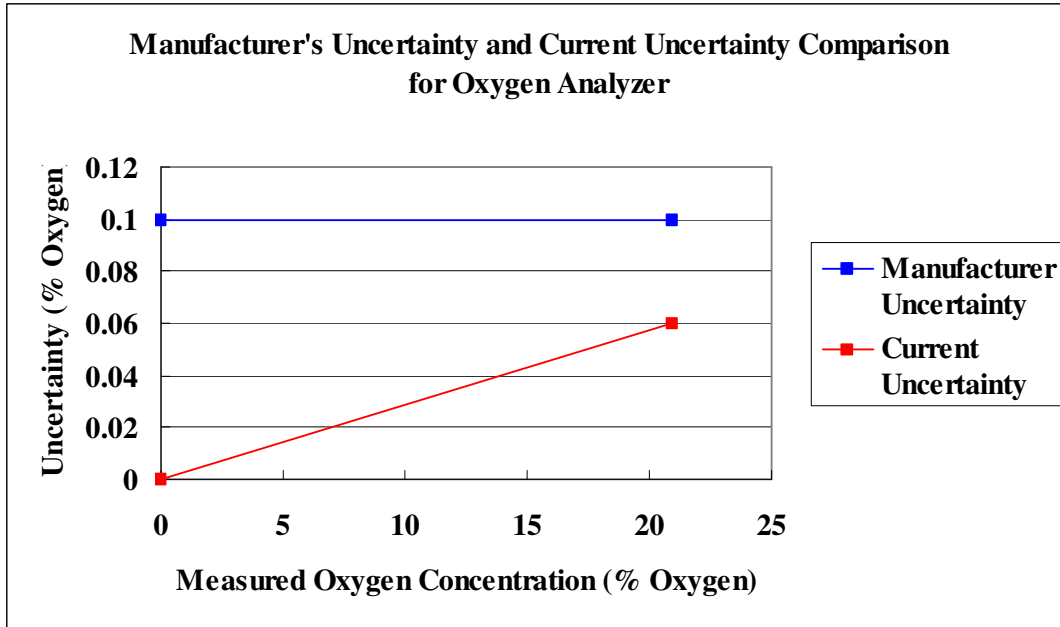


**Figure A-10 Manufacturer's Uncertainty and Current Uncertainty Comparison for Oxygen Analyzer**

The above uncertainty analysis approach for oxygen analyzer was essentially the same with that conducted by NIST<sup>13</sup>. In the current approach, the uncertainty analysis for oxygen analyzer was separated from that of HRR uncertainty analysis. In NIST<sup>13</sup>, the uncertainties of all the most basic measurement quantities were directly used to calculate the HRR uncertainty, the uncertainty of the oxygen analyzer was not estimated.

#### **4. Pressure Transducer**

The pressure transducer was Type 223 manufactured by MKS. The voltage output was linear with pressure and the uncertainty was 2.5 Pa in the full scale (500 Pa)<sup>19</sup>. The linear function provided by the manufacturer is  $y = 100x$ .  $y$  is pressure in Pa,  $x$  is voltage output in volt.

Since the deadweight primary standard (which can be used as standard pressure to calibrate pressure transducer) was not available, the uncertainty was estimated by using the

manufacturer's specification. In day-to-day test activities, pressure transducer's working condition is checked by zero and span pressure. Zero pressure was obtained by covering the duct, and span pressure obtained by turning on exhaust fan and hood.

## **5. Thermocouple**

The thermocouples used to measure stack and smoke temperature were type K and manufactured by Omega Engineering INC. According to the manufacturer, these thermocouples had fundamental error limits of  $2.2K^{20}$ . Assuming a uniform distribution, the standard uncertainty was computed by dividing the limit by  $\sqrt{3}^{10,11}$ .

## **6. CO/CO<sub>2</sub> Analyzer**

CO/CO<sub>2</sub> analyzer was Type ULTRAMAT 22 manufactured by Siemens. The accuracy was specified by the manufacturer as 30 ppm of CO for the full scale (0-3000 ppm) and 0.1% of CO<sub>2</sub> for the full scale (0-10%)<sup>21</sup>. The linear function provided by the manufacturer is  $y = 1500x$  for CO.  $y$  is the CO concentration in ppm.  $x$  is the voltage output in volt. The linear function of CO<sub>2</sub> provided by manufacturer is  $y = 0.05x$ .  $y$  is the CO<sub>2</sub> volume fraction.  $x$  is the voltage output in volt. The instrument operates on the non-dispersive infrared absorption principle using the single-beam method with opto-pneumatic double-layer detector. The detector has a filter in front of it, which eliminates all light except the 4.26  $\mu\text{m}$  wavelength that CO<sub>2</sub> molecules can absorb and 4.75 $\mu\text{m}$  wavelength that CO molecules can absorb. The intensity of 4.26  $\mu\text{m}$  and 4.75 $\mu\text{m}$  light that reaches the detector is inversely related to the concentration of CO<sub>2</sub> and CO respectively. The intensity of light striking the

detector is described by Beer's Law, which is an exponential function and makes the instrument highly non-linear. Since CO/CO<sub>2</sub> analyzer behaved highly non-linear, and only zero and span gases were available, the uncertainty cannot be estimated using ISO 11095<sup>16</sup> and the uncertainty analysis method for oxygen analyzer is not applicable also. In day-to-day test activities, CO/CO<sub>2</sub> analyzer's working condition is checked by zero and span gases. Zero gas was 99.99% nitrogen, and span gases were 8.9% of CO<sub>2</sub> and 2210 ppm of CO.

### UNCERTAINTY ANALYSIS OF INDIRECT MEASUREMENT

Some of the important physics quantities such as heat release rate (HRR), extinction coefficient, specific extinction area (SEA), and heat of combustion (HOC), etc could not be measured directly but were instead found in two distinct steps. First, we measured quantities, such as oxygen concentration, stack/smoke temperature, pressure difference across the orifice, mass loss, and beam intensity of smoke, etc that could be measured directly and from which the interested physics quantities could be calculated. Second, we used the measured values of these quantities to calculate the interested physics quantities by using equations in ASTM E1354<sup>2</sup>. In general, based on NIST<sup>10</sup> and ISO<sup>11</sup>, if a physics quantity  $y$  is not measured directly, but is determined from  $n$  other statistically independent quantities  $x_1, \dots, x_n$  through a functional relationship  $f : y = f(x_1, \dots, x_n)$ , the combined standard uncertainty  $u_c(y)$  is the positive square root of the combined variance  $u_c^2(y)$ , which is given by the Law of Propagation of Uncertainty (if the covariance of each pair of variables is zero.)

$$u_c^2(y) = \sum \left( \frac{\partial f}{\partial x_i} \right)^2 u^2(x_i) \quad (1)$$

Each  $u(x_i)$  is a standard uncertainty of the direct measured quantity, which was already estimated in direct measurement. The degrees of freedom can be estimated by using Welch-Satterthwaite formula and the coverage factor  $k_p$  be obtained by using Student t distribution table.

In Cone test, single measurement was taken for each direct measured quantity every second. Technically there would be no Type A uncertainty for a single measurement. However, if the measurement is supposed to represent a larger sampling size process, and if one has some previous knowledge of the process precision (Type A) uncertainty (at a 95% confidence level), then this information can be used<sup>22</sup>. In the calibration procedure, each instrument precision (Type A) uncertainty was within 95% confidence level with effective degrees of freedom about 60. Since the Type B uncertainty was obtained from experiences or general knowledge, and the lower and upper limits were chosen in such a way that the probability of the quantity in question lying outside these limits is in fact extremely small, the effective degrees of freedom may be taken to be  $\infty$ <sup>10,11</sup>. For Example, the relative humidity of the laboratory is about 15%. The oxygen concentration at this relative humidity in air is about 20.85%. Considering the oxygen concentration in dry air is 20.95%, we assume the oxygen concentration after removing water to be in the range of 20.9%±0.05% oxygen.

The degrees of freedom of the combination of those Type A and B uncertainties for all the indirect measured quantities were approximated (by using Welch-Satterthwaite formula) to be sufficiently large enough so that  $k_p$  can be taken to be 2 (obtained by using Student t distribution table) for the expanded uncertainty with 95% confidence.

## 1. Heat Release Rate

### 1.1 Uncertainty Estimation

HRR is calculated by using equation (4) in ASTM E 1354<sup>2</sup>

$$\dot{Q}(t) = \left(\frac{\Delta h_c}{r_0}\right) 1.10C \sqrt{\frac{\Delta P}{T}} \frac{X_{O_2}^0 - X_{O_2}(t)}{1.105 - 1.5X_{O_2}(t)} \quad (2)$$

where:  $\left(\frac{\Delta h_c}{r_0}\right) = 13100$  kJ/kg unless exact value is known for the test material.

Then the uncertainty of heat release rate can be calculated as following:

$$\frac{\partial \dot{Q}(t)}{\partial \left(\frac{\Delta h_c}{r_0}\right)} = 1.10C \sqrt{\frac{\Delta P(t)}{T(t)}} \frac{X_{O_2}^0 - X_{O_2}(t)}{1.105 - 1.5X_{O_2}(t)} \quad (3)$$

$$\frac{\partial \dot{Q}(t)}{\partial C} = \left(\frac{\Delta h_c}{r_0}\right) 1.10 \sqrt{\frac{\Delta P(t)}{T(t)}} \frac{X_{O_2}^0 - X_{O_2}(t)}{1.105 - 1.5X_{O_2}(t)} \quad (4)$$

$$\frac{\partial \dot{Q}(t)}{\partial \Delta P} = 0.5 \left(\frac{\Delta h_c}{r_0}\right) 1.10C \sqrt{\frac{1}{\Delta P(t)T(t)}} \frac{X_{O_2}^0 - X_{O_2}(t)}{1.105 - 1.5X_{O_2}(t)} \quad (5)$$

$$\frac{\partial \dot{Q}(t)}{\partial T} = -0.5 \left(\frac{\Delta h_c}{r_0}\right) 1.10C \sqrt{\frac{\Delta P(t)}{T(t)^3}} \frac{X_{O_2}^0 - X_{O_2}(t)}{1.105 - 1.5X_{O_2}(t)} \quad (6)$$

$$\frac{\partial \dot{Q}(t)}{\partial X_{O_2}^0(t)} = \left(\frac{\Delta h_c}{r_0}\right) 1.10C \sqrt{\frac{\Delta P(t)}{T(t)}} \frac{1}{1.105 - 1.5X_{O_2}(t)} \quad (7)$$

$$\frac{\partial \dot{Q}(t)}{\partial X_{O_2}(t)} = \left(\frac{\Delta h_c}{r_0}\right) 1.10C \sqrt{\frac{\Delta P(t)}{T(t)}} \frac{1.5X_{O_2}^0 - 1.105}{[1.105 - 1.5X_{O_2}(t)]^2} \quad (8)$$

Temperature (T) was assumed to be uniformly distributed<sup>13</sup>. If the quantity  $\left(\frac{\Delta h_c}{r_0}\right)$  was known (such as methane 12540 kJ/kg), there was no uncertainty contribution to the HRR. Otherwise, 5% of the generic value (13100 kJ/kg) was taken<sup>2</sup> as the uncertainty. C factor, i.e., the flow coefficient, is the relative measure of the fluid flow ability of the orifice in the exhaust duct. The flow coefficient is determined by the volume flow rate through the orifice and the pressure difference across the orifice (See Appendix D). It has 5% of uncertainty<sup>2</sup>. C factor value was taken as 0.043<sup>23</sup>. The upper and lower limits for C-factor and  $\left(\frac{\Delta h_c}{r_0}\right)$  were chosen in such a way that the probability of the “true” values of the quantities were lying outside these limits was extremely small. The quantities were treated as if it is equal probable for them to lie within the intervals, therefore, they were assumed to be uniformly distributed. The uncertainty of  $X_{O_2}(t)$  was determined by the uncertainty of oxygen analyzer, which was discussed in the previous Section. Since there was water vapor in the incoming air, the volume fraction of oxygen should be corrected as  $X_{O_2}^0 = 0.2095(1 - X_{H_2O}^0)$ , where  $X_{H_2O}^0 = \frac{P_{H_2O}}{760} \frac{H}{100}$ <sup>24</sup>.  $P_{H_2O}$  was the vapor pressure of water in mm Hg at the ambient temperature and  $H$  was the relative humidity in percent.  $P_{H_2O}$  could be found in CRC Handbook<sup>25</sup>. The uncertainty of corrected oxygen volume fraction in the incoming air was

assumed to be zero. Substitute equations (3)-(8) into (1) to estimate HRR standard uncertainty  $u_c(HRR)$  and HRR can be reported as

$$HRR \pm 2u_c(HRR)$$

Typical HRR calculations for 38mm red oak at 40 kW/m<sup>2</sup> external heat flux and 2mm red oak at 70 kW/m<sup>2</sup> external heat flux in cone test are shown in Figure A-11 and Figure A-12 respectively. We have 95% confidence of the uncertainty intervals.

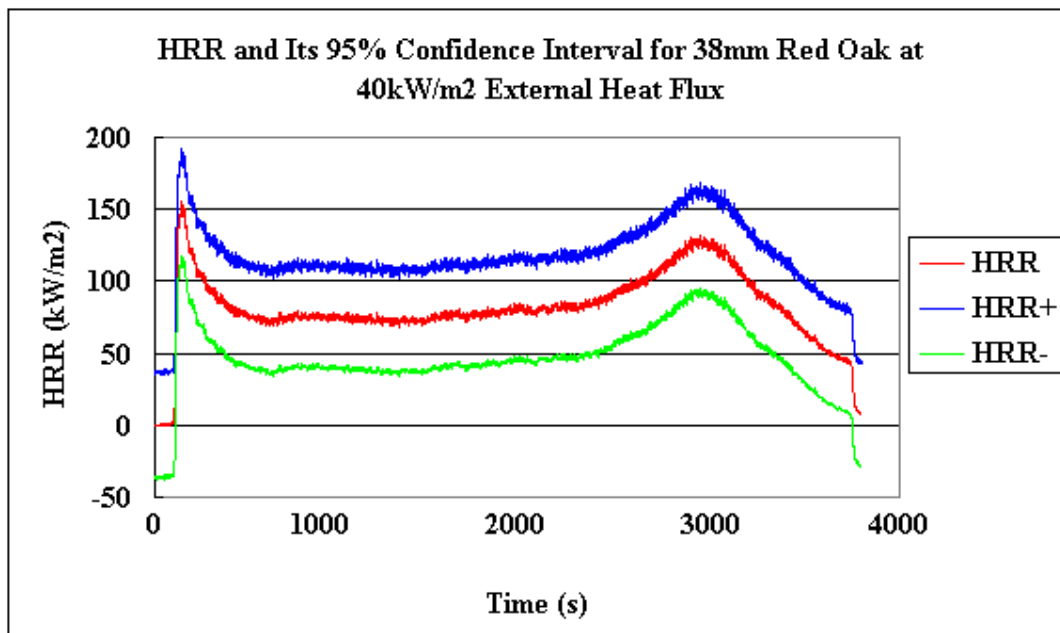


**Figure A-11 Heat Release Rate and Its 95% Confidence Interval for 38mm Red Oak at 40 kW/m<sup>2</sup> External Heat Flux in Cone Test**

As seen in Figure A-11, when HRR was at around 75 kW/m<sup>2</sup> (1000s to 2000s), the uncertainty was about 35 kW/m<sup>2</sup>, which was 45% of the HRR; when HRR was 100 kW/m<sup>2</sup> (the second peak), the uncertainty was still about 35 kW/m<sup>2</sup>, which was 35% of the HRR. As seen in Figure A-12, when HRR was at 300 kW/m<sup>2</sup>, the uncertainty was 41 kW/m<sup>2</sup>, which

was 13.6% of the HRR; when HRR was at 500 kW/m<sup>2</sup> (near peak), the uncertainty was 51 kW/m<sup>2</sup>, which was 10% of the HRR.

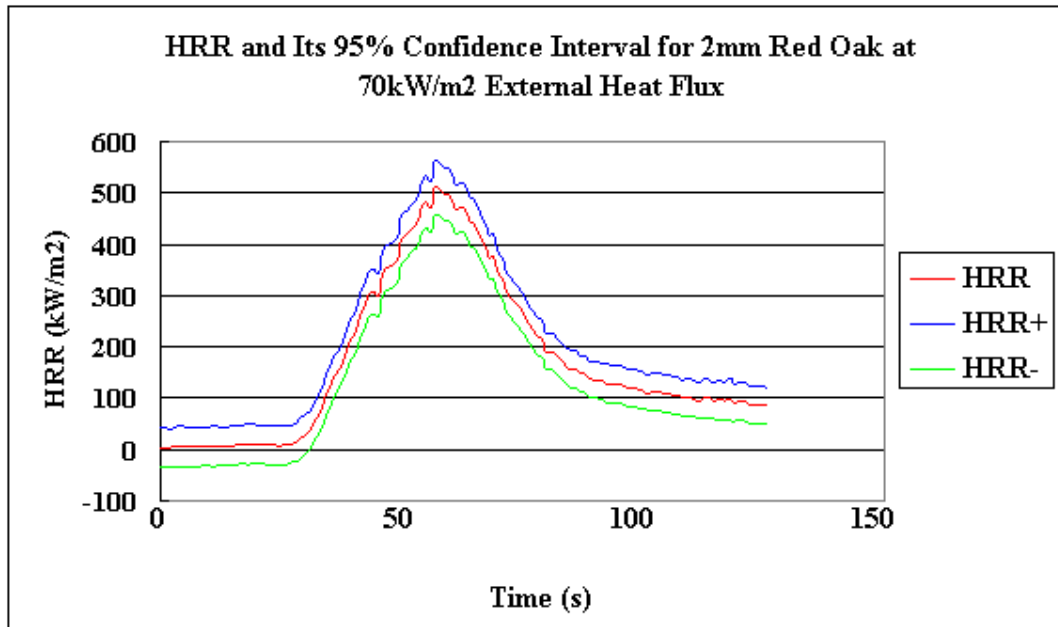


Figure A-12 Heat Release Rate and Its 95% Confidence Interval of 2mm Red Oak at 40 kW/m<sup>2</sup> External Heat Flux in Cone Test

## 1.2 HRR Uncertainty Comparison

Table A-1 shows the HRR uncertainty comparison of current results, Enright and Fleischmann's results<sup>12</sup>, and NIST results<sup>13</sup>. NIST results<sup>13</sup> are listed just as a reference since the HRR measured was much larger than the other two cases. As seen in Table A-1, the HRR uncertainty and the normalized HRR uncertainty of Enright and Fleischmann<sup>12</sup> was less than the current results, especially at lower HRR level such as 1 kW, since their uncertainty of oxygen analyzer was assumed to be 0.01%, which is the maximum drift value of oxygen analyzer the ASTM standard<sup>2</sup> accepts. However, in the current work, the uncertainty of oxygen was estimated based on two-point calibration method introduced in the Oxygen Analyzer Section. The uncertainty is in the range of 0.048% to 0.058% based on different

oxygen concentration level, which is 5 to 6 times bigger than theirs. Drift uncertainty is not included in the uncertainty analysis in the current work.

**Table A-1 HRR Uncertainty Estimation Comparison**

	Current Results			Enright and Fleischmann			NIST
	1 kW (100 kW/m <sup>2</sup> )	3 kW (300 kW/m <sup>2</sup> )	5 kW (500 kW/m <sup>2</sup> )	1 kW (100 kW/m <sup>2</sup> )	3 kW (300 kW/m <sup>2</sup> )	5 kW (500 kW/m <sup>2</sup> )	50 kW
Uncer.	0.35 kW	0.41 kW	0.51 kW	0.06 kW	0.17 kW	0.27 kW	3.75 kW
Norm. Uncer.	35%	13.6%	10%	6%	5.5%	5.5%	7.5%

To verify our HRR uncertainty, three similar thick PMMA (23mm) burning tests were replicated. The average HRR and the standard deviation of the average HRR were calculated based on the data of steady burning duration of each test, see Table A-2. As seen in Table A-2, the average HRRs at steady burning duration were 526 kW/m<sup>2</sup>, 502 kW/m<sup>2</sup>, and 536 kW/m<sup>2</sup> respectively. The standard deviation of the three average HRRs was 18 kW/m<sup>2</sup>. The uncertainty of 95% confidence is, therefore, 57 kW/m<sup>2</sup> with 3 degrees of freedom. Our estimate showed that the uncertainty of 95% confidence was 53 kW/m<sup>2</sup> for HRR at the level of 510 kW/m<sup>2</sup>. The test result and the estimate were similar.

**Table A-2 Average HRR and the Standard Deviation of HRR at Steady State Burning Duration of Thick PMMA**

	Average HRR (kW/m <sup>2</sup> )	SD of HRR (kW/m <sup>2</sup> )	95% Confidence Uncer (kW/m <sup>2</sup> )
Test 1	526	18	57
Test 2	502		
Test 3	536		

### 1.3 HRR Uncertainty and Methane HRR Calibration

In day-to-day calibration, methane is used to generate 1, 3, and 5 kW of HRR. At each HRR level, data are collected for 120s at the rate of one scan per second. The measured quantities are voltage output of methane flow meter, oxygen analyzer, and pressure transducer. The stack temperature is reported as degree C. Data sets for each HRR level in ten different days are selected. By using the collected data and oxygen consumption method (Equation (2)) recommended by ASTM E 1354<sup>2</sup>, 120 HRRs are calculated and averaged at each HRR level for each day. The standard deviation of the ten means for each HRR level is estimated and the 95% confidence interval can be approximated. Also, 120 HRR uncertainties with 95% confidence and their averages can be calculated by using the Law of Propagation of Uncertainty at each HRR level for each day. Please note that the uncertainty of the heat of combustion per mass of oxygen for methane is assumed to be negligible since the exact value is known. The results are shown in Table A-3. The values in column 2, 4, and 6 from “Day1” row to “Day10” row in Table A-3 are HRR averages of 1, 3, and 5 kW at each day. HRR is calculated based on oxygen consumption method (Equation (2)) recommended by ASTM E 1354<sup>2</sup>. C factor is taken as a fixed value 0.043<sup>23</sup>. The values in the last row of column 2, 4, and 6 in Table A-3 are HRR uncertainty with 95% confidence based on the day-to-day variation. The ten HRR averages at each level are assumed to be in a normally distributed population respectively, and the standard deviation  $u(HRR)$  for each HRR level can be calculated by using the following equations

$$u(HRR) = \sqrt{\frac{1}{10-1} \sum_1^{10} (HRR_i - [HRR])^2}$$

$$[HRR] = \frac{HRR_1 + \dots + HRR_{10}}{10}$$

where: [HRR] represents the average of ten HRR averages.

The uncertainties of 95% confidence for day-to-day variation at each level (values in the last row of column 2, 4, and 6 in Table A-3) are estimated as  $2.26u(HRR)$ , where 2.26 is the coverage factor obtained from 95%-quantile of t distribution with 9 (10-1) degrees of freedom.

**Table A-3 HRR Uncertainty Based on Day-to-Day Variation and HRR Uncertainty Based on Component Instrument Calibration**

	1 (unit: kW)		3 (unit: kW)		5 (unit: kW)	
	Avg. HRR	Avg. Uncer.	Avg. HRR	Avg Uncer	Avg. HRR	Avg. Uncer.
Day 1	0.92	0.37	1.94	0.32	4.28	0.36
Day 2	1.57	0.22	2.78	0.33	4.93	0.39
Day 3	1.33	0.28	3.35	0.34	4.79	0.39
Day 4	1.17	0.32	3.22	0.32	5.05	0.38
Day 5	1.07	0.30	2.92	0.31	4.76	0.36
Day 6	1.36	0.33	3.40	0.34	5.00	0.4
Day 7	1.11	0.32	3.08	0.31	4.78	0.36
Day 8	1.21	0.30	3.14	0.32	5.31	0.38
Day 9	1.35	0.32	3.34	0.32	5.05	0.39
Day 10	1.17	0.32	3.19	0.33	4.96	0.39
95% Conf. Uncer.	0.42	0.31 (avg. above)	0.98	0.32 (avg. above)	0.60	0.38 (avg. above)

The values in column 3, 5, and 7 from “Day1” row to “Day10” row in Table A-3 are HRR uncertainty averages of 1, 3, and 5 kW at each day. HRR uncertainty is calculated by using the Law of Propagation of Uncertainty recommended by NIST<sup>10</sup> and ISO<sup>11</sup> (as introduced in the beginning of HRR Section). The uncertainty of C factor is based on 5% of the fixed value 0.043<sup>23</sup>. The uncertainty of oxygen concentration is based on the calibration of oxygen analyzer as introduced in the Section of “Oxygen Analyzer”. The values in the last row of column 3, 5, and 7 in Table A-3 are averages of HRR uncertainty based on ten day’s uncertainty averages.

As seen in Table A-3, the uncertainty based on day-to-day variation is much bigger than that by using the Law of Propagation of Uncertainty. In day-to-day calibration, the operator cannot set the HRR (based on methane) exactly to 1, 3 or 5 kW based on the poor control of the needle valve. Since the study of the needle valve is out of our scope, normalization will be needed to meaningfully compare the HRR (based on oxygen) day-to-day variation to the calibration based uncertainty as seen Table A-4.

Basically, the values in Table A-4 are the normalized values of Table A-3. The values in column 2, 4, and 6 from “Day1” row to “Day10” row in Table A-4 are normalized HRR averages of 1, 3, and 5 kW at each day. Normalized HRR is calculated as the ratio of HRR based on oxygen consumption method recommended by ASTM E 1354<sup>2</sup> and HRR based on methane flow rate (see Appendix K). The values in the last row of column 2, 4, and 6 in Table A-4 are the uncertainties with 95% confidence based on day-to-day variation of normalized HRR averages at each HRR level for ten days. The ten normalized HRR averages at each level are assumed to be in a normally distributed population respectively, and the standard deviation  $u(NorHRR)$  can be calculated by using the following equations

$$u(NorHRR) = \sqrt{\frac{1}{10-1} \sum_1^{10} (NorHRR_i - [NorHRR])^2}$$

$$[NorHRR] = \frac{NorHRR_1 + \dots + NorHRR_{10}}{10}$$

where: [NorHRR] represents the average of ten normalized HRR averages.

The uncertainties of 95% confidence for day-to-day variation at each level (values in the last row of column 2, 4, and 6 in Table A-4) are estimated as  $2.26u(NorHRR)$ , where 2.26 is the coverage factor obtained from 95%-quantile of t distribution with 9 (10-1) degrees of freedom.

The values in column 3, 5, and 7 from “Day1” row to “Day10” row in Table A-4 are normalized HRR uncertainty averages of 1, 3, and 5 kW at each day. HRR uncertainty is calculated by using the Law of Propagation of Uncertainty recommended by NIST<sup>10</sup> and ISO<sup>11</sup> (as introduced in the beginning of “HRR” Section). The uncertainty of C factor is based on 5% of the fixed value 0.043<sup>23</sup>. The uncertainty of oxygen concentration is based on the calibration of oxygen analyzer as introduced in the Section of “Oxygen Analyzer”.

Normalized HRR uncertainty is the ratio of HRR uncertainty and the HRR based on methane flow rate (see Appendix K).

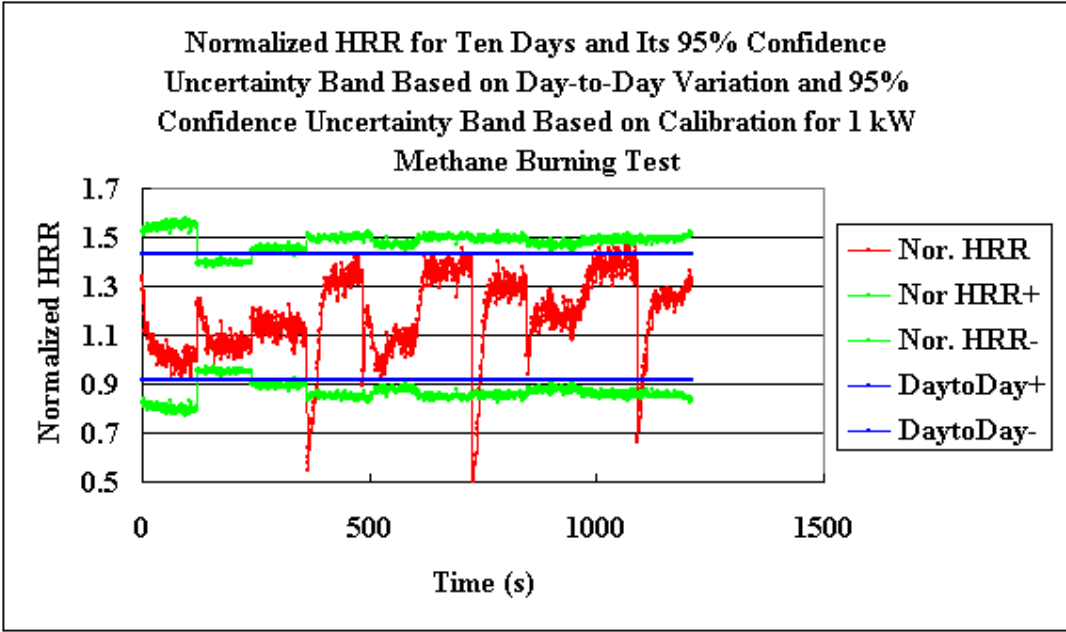
As seen in Table A-4, our estimated normalized uncertainty averages are consistency with the uncertainties based on day-to-day variation at each HRR level. Therefore, the methane calibration is under control in terms of our uncertainty estimation based on the uncertainty of component instrument calibration. This is also shown in Figure A-13, Figure A-14, and

Figure A-15. As seen in Figure A-13, the red line demonstrates the normalized HRRs at 1 kW for ten days. There are 120 normalized HRRs for each day. Therefore, there are total 1200 HRRs as shown in Figure A-13. Then, the 1200 normalized HRRs are averaged. The “green band” is the averaged value plus and minus the normalized HRR uncertainty dynamically. The “blue band” is the average value plus and minus the 95% confidence uncertainty based on day-to-day variation, i.e., the last value in column 2 of Table A-4. Figure A-14 and Figure A-15 are constructed in the similar way with Figure A-13.

**Table A-4 Normalized HRR Uncertainty based on Day-to-Day Variation and Normalized HRR Uncertainty Based on Component Instrument Calibration**

	1 (unit: kW)		3 (unit: kW)		5 (unit: kW)	
	Avg. Nor.	Avg. Nor.	Nor. Avg.	Avg. Nor.	Nor. Avg.	Avg. Nor.
	HRR	Uncer.	HRR	Uncer.	HRR	Uncer.
Day 1	1.03	0.37	0.99	0.17	0.94	0.08
Day 2	1.08	0.22	1.11	0.13	1.03	0.08
Day 3	1.13	0.28	1.08	0.11	0.95	0.08
Day 4	1.19	0.32	1.07	0.11	1.03	0.08
Day 5	1.06	0.30	0.98	0.11	0.95	0.07
Day 6	1.35	0.33	1.14	0.11	1.00	0.08
Day 7	1.17	0.32	1.02	0.10	0.95	0.07
Day 8	1.17	0.30	1.04	0.10	1.06	0.08
Day 9	1.37	0.32	1.13	0.11	1.00	0.08
Day 10	1.17	0.32	1.09	0.11	0.98	0.08
95% Conf. Uncer.	0.26	0.31	0.12	0.12	0.09	0.08

As seen in these three Figures, our estimated bands (green bands) are almost the same with the day-to-day variation bands (blue bands), i.e., our methane calibration is under control, which is the same conclusion drawn above from Table A-4.



**Figure A-13 Normalized HRR for Ten Days and Its 95% Confidence Uncertainty Band Based on Day-to-Day Variation and 95% Confidence Uncertainty Band based on Calibration for 1 kW Methane Burning Test**

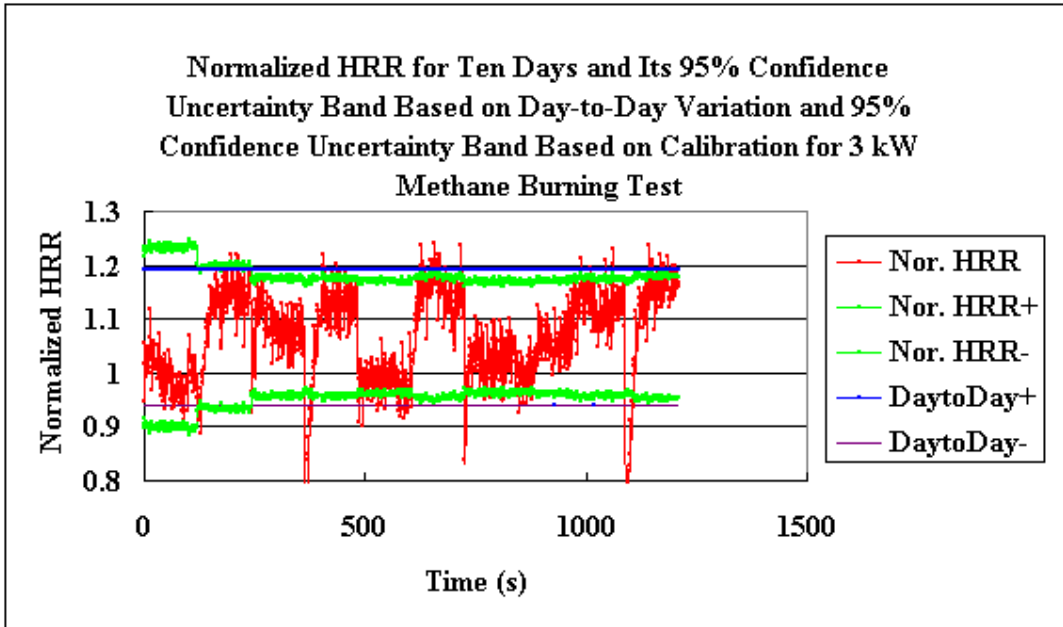


**Figure A-14 Normalized HRR for Ten Days and Its 95% Confidence Uncertainty Band Based on Day-to-Day Variation and 95% Confidence Uncertainty Band based on Calibration for 3 kW Methane Burning Test**

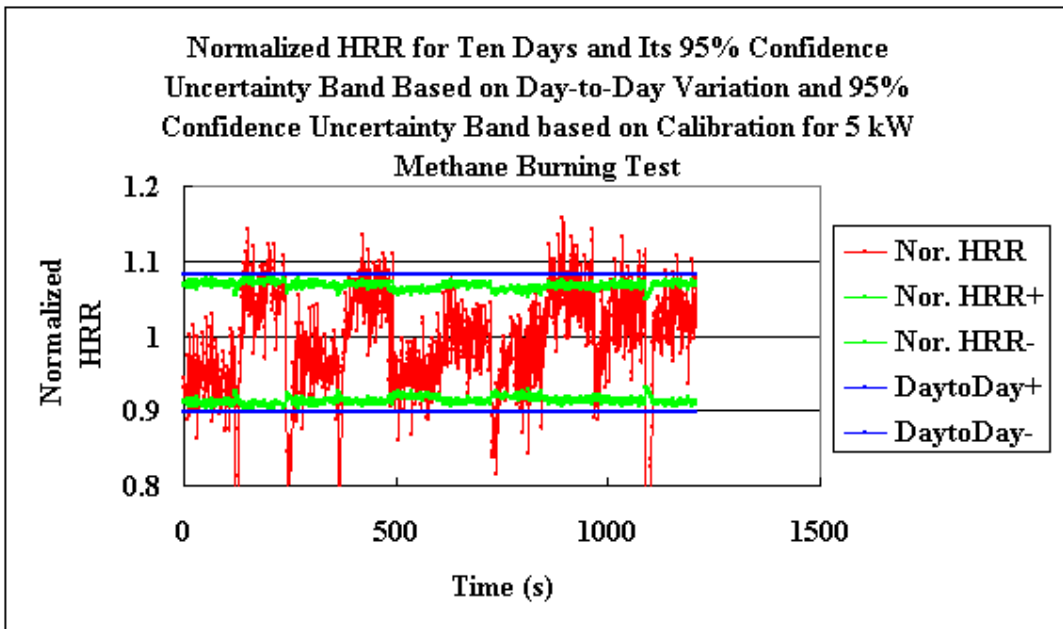


**Figure A-15 Normalized HRR for Ten Days and Its 95% Confidence Uncertainty Band Based on Day-to-Day Variation and 95% Confidence Uncertainty Band based on Calibration for 5 kW Methane Burning Test**

**1.4 HRR Uncertainty and Normalized HRR Uncertainty**

In current study, the normalized HRR uncertainty was decreasing as the HRR increasing. The reason for this is observed in Figure A-16 and Figure A-17. The data for these two Figures are of the 2mm red oak burn test at external heat flux of 70 kW/m<sup>2</sup>. The Y-axis on the left is the HRR uncertainty. The Y-axis on the right is the normalized HRR uncertainty, which is the ratio of HRR uncertainty and HRR. The X-axis is the HRR. As seen in Figure A-16, at lower HRR level (4 to 30 kW/m<sup>2</sup>) the HRR uncertainty is in the range of 30 to 34 kW/m<sup>2</sup>, while the normalized HRR uncertainty is in the range of 110% to 800%. As seen in Figure A-17, at higher HRR level (40 to 500 kW/m<sup>2</sup>) the HRR uncertainty is in the range of 30 to 50 kW/m<sup>2</sup>, while the normalized HRR uncertainty is in the range of 8% to 76%. It is found that at higher HRR level the normalized HRR uncertainty is lower. As seen in Figure A-19 again, when the HRR is in the range of 200 to 500 kW/m<sup>2</sup>, the normalized HRR uncertainty is in the range of 10% to 20%.

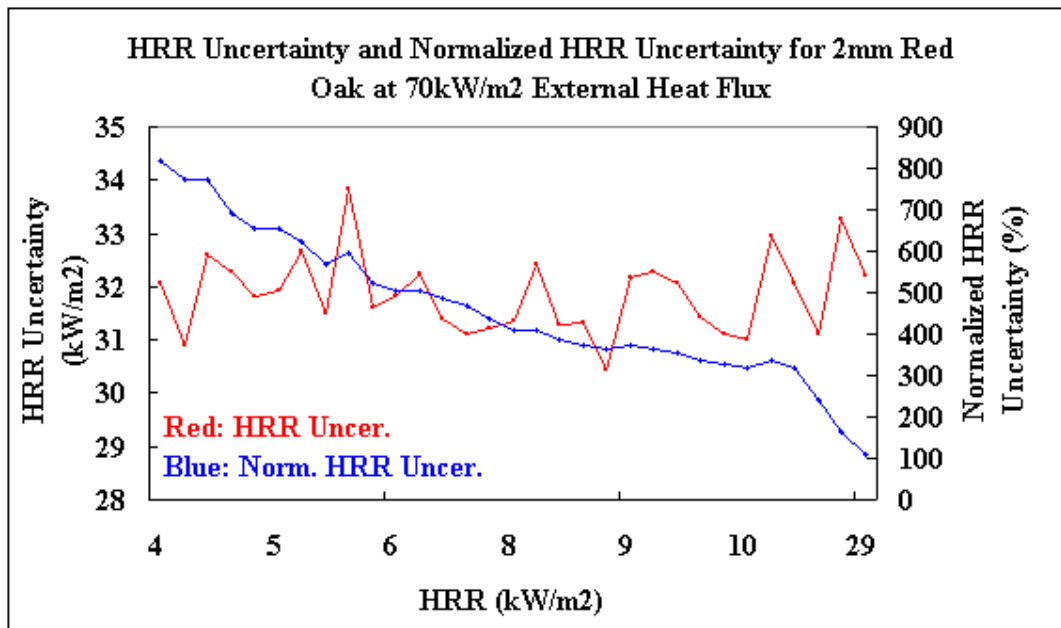
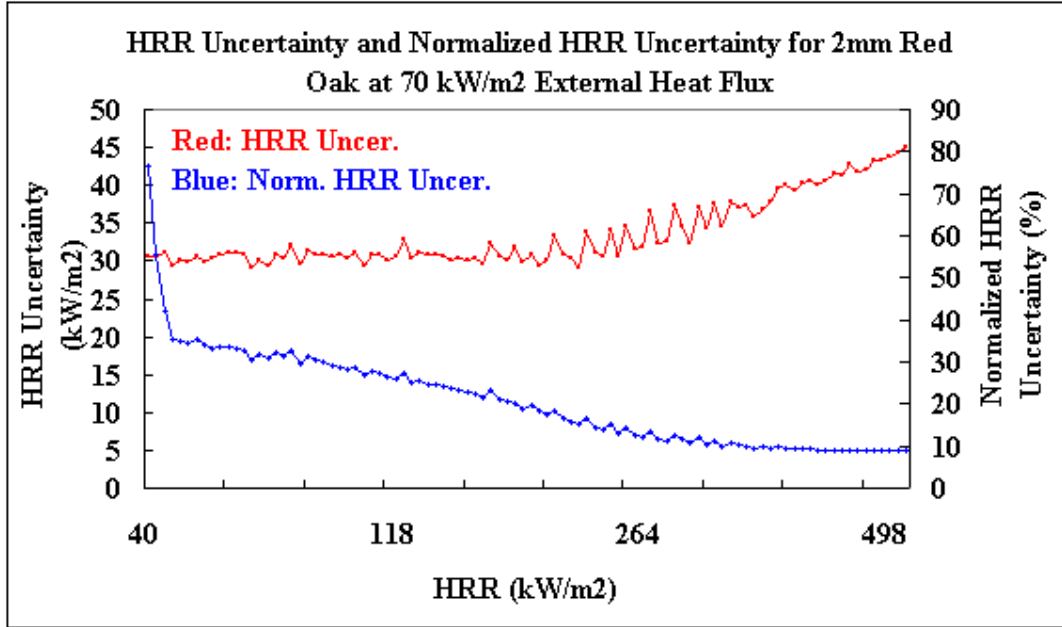


Figure A-16 HRR Uncertainty and the Normalized HRR Uncertainty (above 100%) of 2mm Red Oak at 70 kW/m<sup>2</sup> External Heat Flux in Cone Test



**Figure A-17 HRR Uncertainty and the Normalized HRR Uncertainty (below 100%) of 2mm Red Oak at 70 kW/m<sup>2</sup> External Heat Flux in Cone Test**

### 1.5 Uncertainty Contribution from Component Parameters

In order to investigate the uncertainty contribution of each component variable to the total uncertainty, R value was introduced. Based on the uncertainty of day-to-day calibration, we define  $UN_i$  as the variance of the indirect measured quantity (HRR for this case) calculated from only one of the component variables, and  $UN_t$  as the total variance of indirect measured quantity calculated from all of the component variables, then,  $R_i = 100 * (UN_i / UN_t) %$ .

Based on the definition, it is obvious  $\sum_i UN_i = UN_t$  and  $\sum_i R_i = 1$ .

Figure A-18 showed R value for each component variable. As seen in Figure A-18, R values of temperature and pressure were always small, i.e., HRR was not sensitive to pressure and temperature. At lower HRR, oxygen uncertainty dominated the uncertainty of HRR. However, as the HRR was going up, R value of oxygen was going down and those of C factor and heat

of combustion per unit mass of oxygen were going up. Eventually, R values of Oxygen concentration, C factor, and heat of combustion per mass of oxygen are 36%, 32%, and 32% respectively when HRR reached about 500 kW/m<sup>2</sup>. The R values of these three parameters are similar. For our case, HRR is not only sensitive to oxygen concentration, but also sensitive to C factor and HOC per unit mass of oxygen, especially at higher HRR level. The reasons for this are 1) the oxygen depletion term increases as oxygen concentration decreases, which will result in bigger values for equation (3) and (4); 2) uncertainty (% of oxygen) of oxygen concentration measurement decreases as oxygen concentration decreases. Considering the two reasons and equation (1), (3), (4), and (8), the trend in Figure A-18 is obvious.

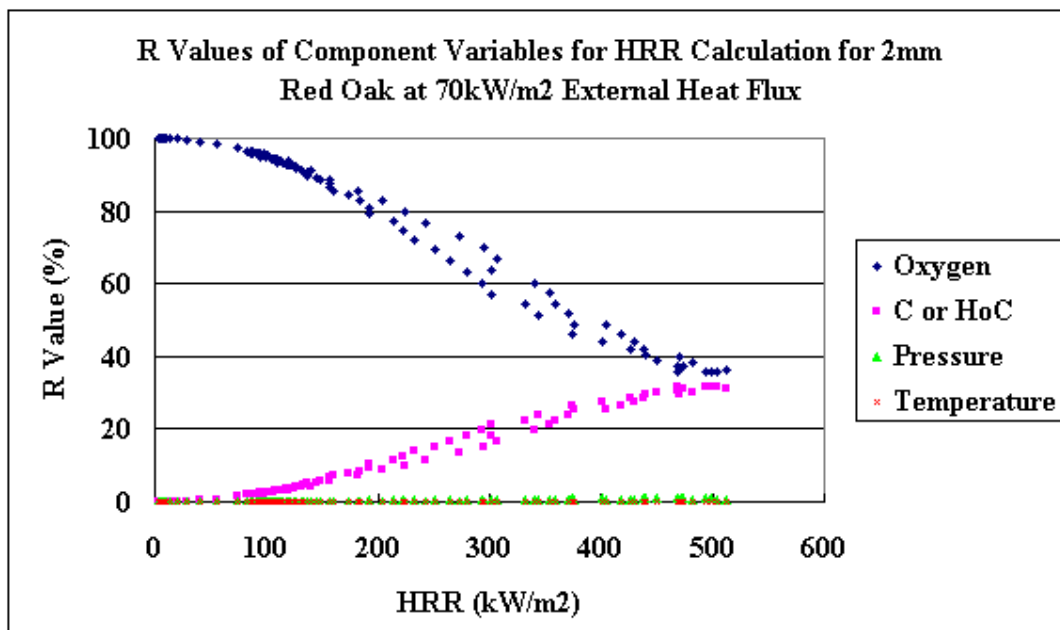


**Figure A-18 R Values of the Component Variables for Heat Release Rate Calculation for 2mm Red Oak at 70 kW/m<sup>2</sup> External Heat Flux in Cone Test**

Generally speaking, HRR is most sensitive to oxygen concentration. However, for a specific oxygen analyzer with certain uncertainty, there is a specific HRR point, around which HRR is

sensitive not only to oxygen concentration, but also to C factor and HOC per unit mass of oxygen.

## 2. Extinction Coefficient

Extinction coefficient is calculated by using equation (14) in ASTM E 1354<sup>2</sup>

$$k = \left(\frac{1}{L}\right) \ln \frac{I_0}{I}$$

Then the uncertainty of extinction coefficient can be calculated as following

$$\frac{\partial k}{\partial I_0} = \frac{1}{LI_0} \quad (9)$$

$$\frac{\partial k}{\partial I} = -\frac{1}{LI} \quad (10)$$

Substitute equations (9)-(10) into (1) to estimate  $k$  standard uncertainty  $u_c(k)$  and  $k$  can be reported as

$$k \pm 2u_c(k)$$

A typical  $k$  calculation for 38mm red oak at 40 kW/m<sup>2</sup> external heat flux is shown in Figure A-19. We have 95% confidence of the uncertainty.

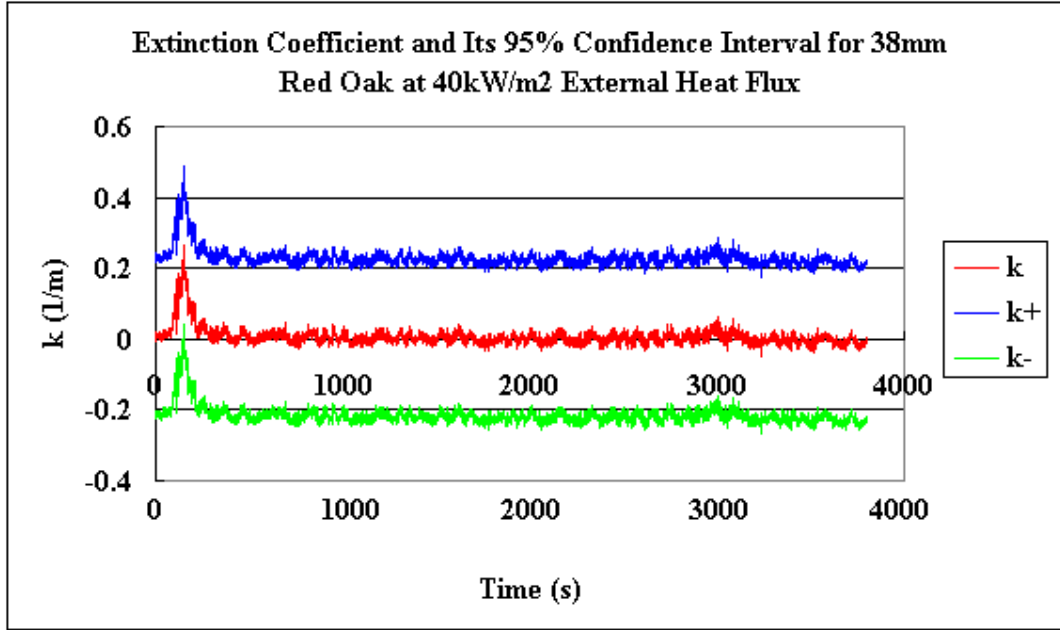


**Figure A-19** Extinction Coefficient and Its 95% Confidence Interval of 38mm Red Oak at 40 kW/m<sup>2</sup> External Heat Flux in Cone Test

The uncertainty analysis of extinction coefficient showed that the uncertainty was a constant - $0.2 \frac{1}{m}$ . As seen in Figure A-19, during 500s to 3800s, the extinction coefficient is around zero, which is much less than the estimated uncertainty. Around the peak value of the extinction coefficient, the normalized uncertainty (k uncertainty/k value) is about 100%. Therefore, the uncertainty is too big relative to the measured extinction coefficient. Since the photodiode uncertainty is proportional to the measured value, the extinction coefficient uncertainty is a constant. This constant is “too big” because the photodiode can only be calibrated to 0.024 of measured value of uncertainty for main photodiode and 0.008 of measured value of uncertainty for compensation photodiode. The reason for this is because of the power variation of the laser.

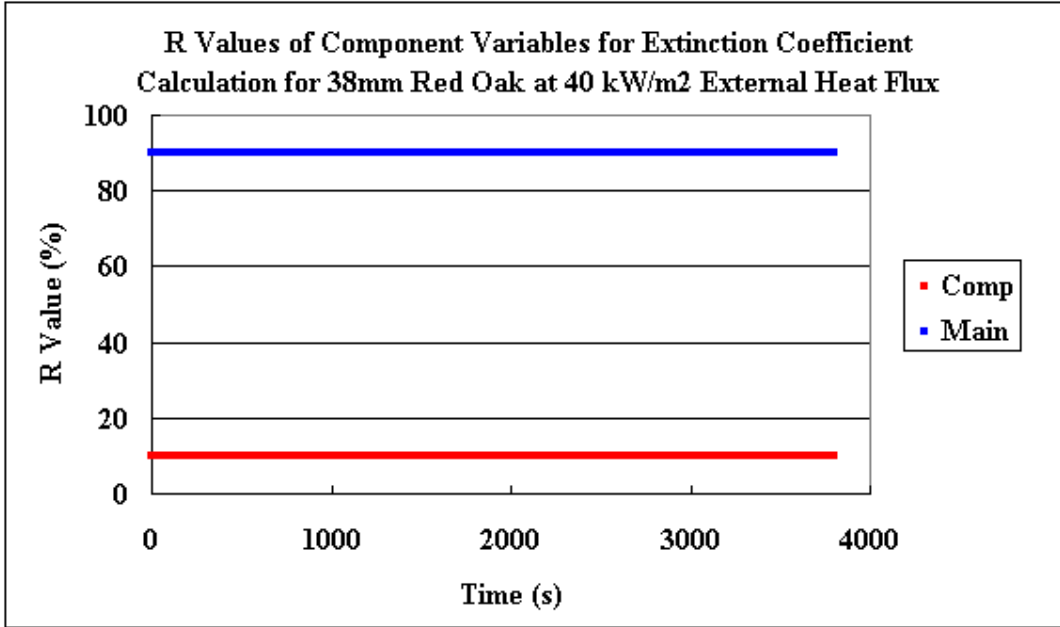


**Figure A-20 R Values of the Component Variables for Extinction Coefficient Calculation for 38mm Red Oak at 40 kW/m<sup>2</sup> External Heat Flux in Cone Test**

Since the uncertainty of main photodiodes is larger than that of compensation photodiode (from the typical calculation), the R value is also larger, see Figure A-20. Apparent difference in photodiodes and / or circuits used to produce voltage response. Each photodiode has different amplification in its circuits to make the voltages similar. This effectively indicates that compensation photodiode is not working.

### 3. Average Specific Extinction Area

Average specific extinction area is calculated by using equation (15) in ASTM E 1354<sup>2</sup>

$$SEA = \frac{\sum_1^n (VFR)_i (k)_i \Delta t_i}{m_1 - m_2} = \frac{\sum_1^n \frac{C\sqrt{P_i T_i}}{353} \frac{1}{L} \ln\left(\frac{I_{0i}}{I_i}\right) \Delta t_i}{m_1 - m_2}$$

where  $\Delta t_i$  is 1 second and assumed to be no error.  $m_1$  and  $m_2$  are initial and final mass respectively. Then the uncertainty of SEA can be calculated as following

$$\frac{\partial(SEA)}{\partial(C_i)} = \frac{\sqrt{P_i T_i} \frac{1}{L} \ln\left(\frac{I_{0i}}{I_i}\right) \Delta t_i}{m_1 - m_2} \quad (11)$$

$$\frac{\partial(SEA)}{\partial(I_{0i})} = \frac{C \sqrt{P_i T_i} \Delta t_i}{353 L I_{0i} (m_1 - m_2)} \quad (12)$$

$$\frac{\partial(SEA)}{\partial(I_i)} = \frac{C \sqrt{P_i T_i} \Delta t_i}{353 L I_i (m_1 - m_2)} \quad (13)$$

$$\frac{\partial(SEA)}{\partial(P_i)} = \frac{C \ln\left(\frac{I_{0i}}{I_i}\right) \sqrt{\frac{T_i}{P_i}} \Delta t_i}{706 L (m_1 - m_2)} \quad (14)$$

$$\frac{\partial(SEA)}{\partial(T_i)} = \frac{C \ln\left(\frac{I_{0i}}{I_i}\right) \sqrt{\frac{P_i}{T_i}} \Delta t_i}{706 L (m_1 - m_2)} \quad (15)$$

$$\frac{\partial(SEA)}{\partial(m_1)} = \frac{-\sum_1^n \frac{C \sqrt{P_i T_i}}{353} \frac{1}{L} \ln\left(\frac{I_{0i}}{I_i}\right) \Delta t_i}{(m_1 - m_2)^2} \quad (16)$$

$$\frac{\partial(SEA)}{\partial(m_2)} = \frac{\sum_1^n \frac{C\sqrt{P_i T_i}}{353} \frac{1}{L} \ln\left(\frac{I_{0i}}{I_i}\right) \Delta t_i}{(m_1 - m_2)^2} \quad (17)$$

Substitute equations (11)-(17) into (1), we obtain

$$u_c(SEA) = \sqrt{\sum (\delta I_i \frac{\partial(SEA)}{\partial I_i})^2 + (\delta m \frac{\partial(SEA)}{\partial m_1})^2 + (\delta m \frac{\partial(SEA)}{\partial m_2})^2 + \sum (\delta I_{0i} \frac{\partial(SEA)}{\partial I_{0i}})^2 + \sum (\delta C \frac{\partial(SEA)}{\partial C_i})^2 + \sum (\delta P \frac{\partial(SEA)}{\partial P_i})^2 + \sum (\delta T \frac{\partial(SEA)}{\partial T_i})^2}$$

to estimate SEA standard uncertainty  $u_c(SEA)$  and SEA can be reported as

$$SEA \pm 2u_c(SEA)$$

A typical average SEA calculation for 38mm red oak at 40 kW/m<sup>2</sup> external heat flux is 0.003 ±0.002 m<sup>2</sup>/g. We have 95% confidence of the uncertainty. The R values of the parameters of average SEA calculation are listed in Table A-5. As seen in Table A-5, average SEA is most sensitive to main photodiode. Compensation photodiode also has significant effect on average SEA. Theoretically, the average SEA should be equally sensitive to main and compensation photodiode, which can be seen from equation (21) and (22). Apparent difference in photodiodes and / or circuits used to produce voltage response. Each photodiode has different amplification in its circuits to make the voltages similar. This effectively indicates that compensation photodiode is not working. Since the uncertainty of main photodiodes is larger than that of compensation (from the analysis of typical test data), the R value is also larger.

The other parameters such as C factor, pressure, temperature, and mass, are insignificant for average SEA calculation.

**Table A-5 R Values of C Factor, Pressure, Temperature, Main Photodiode, compensation Photodiode, and Mass for Average SEA Calculation**

	C Factor	Pressure	Temperature	Compensation	Main	Mass ( $m_1$ and $m_2$ )
R Value (%)	0.0005	0.0001	$2 \times 10^{-5}$	10	90	$1.7 \times 10^{-11}$

#### 4. Average Heat of Combustion

Average effective heat of combustion (HOC) is calculated by using equation (12) in ASTM E 1354<sup>2</sup>

$$HOC = \frac{\sum_{i=1}^n \dot{q}_i(t) \Delta t}{m_1 - m_2}$$

where  $\Delta t$  is 1 second and assumed to be no error.  $m_1$  and  $m_2$  are initial and final mass respectively.

Then the uncertainty of average HOC can be calculated as following

$$\frac{\partial(HOC)}{\partial(\dot{q}_i(t))} = \frac{\Delta t}{m_1 - m_2} \quad (18)$$

$$\frac{\partial(HOC)}{\partial(m_1)} = \frac{-\sum_1^n \dot{q}_i(t)\Delta t}{(m_1 - m_2)^2} \quad (19)$$

$$\frac{\partial(HOC)}{\partial(m_2)} = \frac{\sum_1^n \dot{q}_i(t)\Delta t}{(m_1 - m_2)^2} \quad (20)$$

Substitute equations (18)-(20) into (1) , we obtain

$$u_c(HOC) = \sqrt{\sum (\delta(\dot{q}_i(t)) \frac{\partial(HOC)}{\partial(\dot{q}_i(t))})^2 + (\delta m_1 \frac{\partial(HOC)}{\partial(m_1)})^2 + (\delta m_2 \frac{\partial(HOC)}{\partial(m_2)})^2}$$

to estimate HOC standard uncertainty  $u_c(HOC)$  and HOC can be reported as

$$HOC \pm 2u_c(HOC)$$

A typical average HOC calculation for 38mm red oak at 40 kW/m<sup>2</sup> external heat flux is 13.4±0.1 kJ/g. The normalized uncertainty is about 0.8%. We have 95% confidence of the uncertainty. The calculation shows that the R value of HRR is 99.8% and the R value of initial and final mass is 0.1% respectively. Therefore, most of the average HOC uncertainty comes from HRR uncertainty contribution. Mass uncertainty has insignificant effect on average HOC for our case.

## UNCERTAINTY ANALYSIS METHODS VALIDATION BY MONTE CARLO SIMULATION (MCS)

All of the methods recommended by ISO and NIST can be expected to work well in many circumstances. However, it is generally difficult to quantify the effects of the approximations involved, namely, linearization (GUM<sup>11</sup> 5.1.2), the Welch-Satterthwaite formula for the effective degrees of freedom<sup>11</sup> (GUM G.4.2) and that assumption that the probability distribution for the output quantity value is normal (GUM<sup>11</sup> G.2.1, G.6.6). Linearization approximation was based on the assumption that the indirect measured quantity was approximated by a first order Taylor expansion.

$$Y = c_1 X_1 + c_2 X_2 + \dots + c_n X_n$$

Even if the distributions of  $X_i$  are not normal, the distribution of Y may often be approximated by a normal distribution because of the Central Limit Theorem<sup>11</sup>. The approximation of Welch-Satterthwaite formula can be found in Appendix C. Since these circumstances cannot readily be tested, MCS technique is the one can be used to validate our method<sup>26</sup>. The uncertainty intervals with 95% of confidence of all the physics quantities measured directly and indirectly were validated. The example of HRR was introduced.

First, hypothetical true values for the variables were assigned along with their standard uncertainties for normal distributions and half width for uniform distributions. The values used in the example are given in Table A-6. With the information given in Table A-6 and a assumed voltage output for a specific transient oxygen concentration, the uncertainty interval

(band),  $HRR_{true} \pm 2u_c(HRR)$ , with 95% confidence was estimated by using the method introduced in “HRR Section”.

**Table A-6 Hypothetical True Values for HRR Variables**

Variables	True Value	Distribution
$(\frac{\Delta h_c}{r_0})$ (kJ/kg)	13100	Uniform Distribution, half width=665
C-factor	0.043	Uniform Distribution, half width=0.002
Pressure (Pa)	150.0	Normal Distribution, Standard Uncertainty=1.25
Temperature (K)	323.0	Normal Distribution, Standard Uncertainty=1.1
O <sub>2</sub> analyzer slope m	0.025	Normal Distribution, Standard Uncertainty=0.000036 1/v

Suppose above assumptions (linearity, Welch-Satterthwaite formula and normal distribution of output quantity) are hold for our HRR case. We can safely conclude that if a large number of HRR was calculated at specific pressure, temperature, and oxygen concentration, and if all the related parameters for HRR calculation vary based on the population that we estimated in the previous sections, 95% of calculated HRR will fall in the estimated uncertainty interval. The hypothetical true values were assumed to be the means of the corresponding parent populations. Then, 10000 values (experiments) were generated for each variable according to its mean and standard deviation of normal distribution or half width of uniform distribution. We take C factor case as an example. C factor is assumed to be in a uniformly distributed population. As seen in Table A-6, the mean value (true value as indicated) is 0.043<sup>23</sup>, the half width is 0.002. The generated 10000 values are expected to be uniformly distributed in the

range of 0.041 to 0.045. As a built in function, the random variable generator can be found in Excel and MatLab. Ten thousand HRR were calculated by using the values of each parameter randomly. For example, one value from each population (10000 numbers) is picked as, C factor: 0.042, HoC: 12600 kJ/kg, slope of oxygen analyzer: 0.024982, temperature: 323.87K, and pressure: 149.62Pa. Suppose the ambient oxygen concentration is known, the HRR is calculated to be 500.5 kW/m<sup>2</sup> when the voltage output for oxygen analyzer is 8v. For each of the 10000 HRRs, a check was made for the interval to determine if the band  $HRR_{true} \pm 2u_c(HRR)$  contained the HRR. If the band contained the HRR, a counter was increased by one. This technique allowed the determination of the coverage fraction for the estimated band. This kind of simulation was conducted for all of the direct and indirect measurements. The results can be found in Table A-7.

**Table A-7 Monte Carlo Simulation Results**

	Interval Coverage Fraction for MC Simulated Values
Load Cell	96%
Main Photodiode	99%
Compensation Photodiode	96%
Oxygen Analyzer	95%
HRR	96%
Volume Flow Rate	99%
Extinction Coefficient	96%
Smoke Production Rate	95%
Specific Extinction Area	95%
Heat of Combustion	95%

The results demonstrated that the appropriate interval with 95% confidence can be obtained by using our uncertainty analysis methods.

### **MANUFACTURER VALUE VS. CURRENT ANALYSIS**

The uncertainty of direct measurement has direct effects on the uncertainty of indirect measurement. For Example, the uncertainty of oxygen analyzer has effects on the uncertainty estimate of heat release rate and heat of combustion, and the uncertainty of load cell has effects on the uncertainty estimate of heat of combustion, specific extinction area etc.

As seen in Figure A-21, when the HRR was 75 kW/m<sup>2</sup> from 1000s to 2000s, the uncertainty interval was -40 kW/m<sup>2</sup> to 200 kW/m<sup>2</sup> based on the manufacturer's specification. The normalized HRR uncertainty is as high as 160%. It was obvious that the interval was too big. Also as seen in Figure A-21, the current uncertainty analysis narrowed down the range of 95% confidence interval, which is about 40 kW/m<sup>2</sup> to 110 kW/m<sup>2</sup>. The normalized HRR uncertainty decreased to 47%. Figure A-22 shows the comparison between manufacturer's and current analysis for higher level of HRR. At 300 kW/m<sup>2</sup> of HRR, the uncertainty is 60 kW/m<sup>2</sup> based on manufacturer value. The normalized uncertainty is 20%. At 500 kW/m<sup>2</sup> of HRR, the uncertainty is 68 kW/m<sup>2</sup> based on the manufacturer value. The normalized uncertainty is 14%.

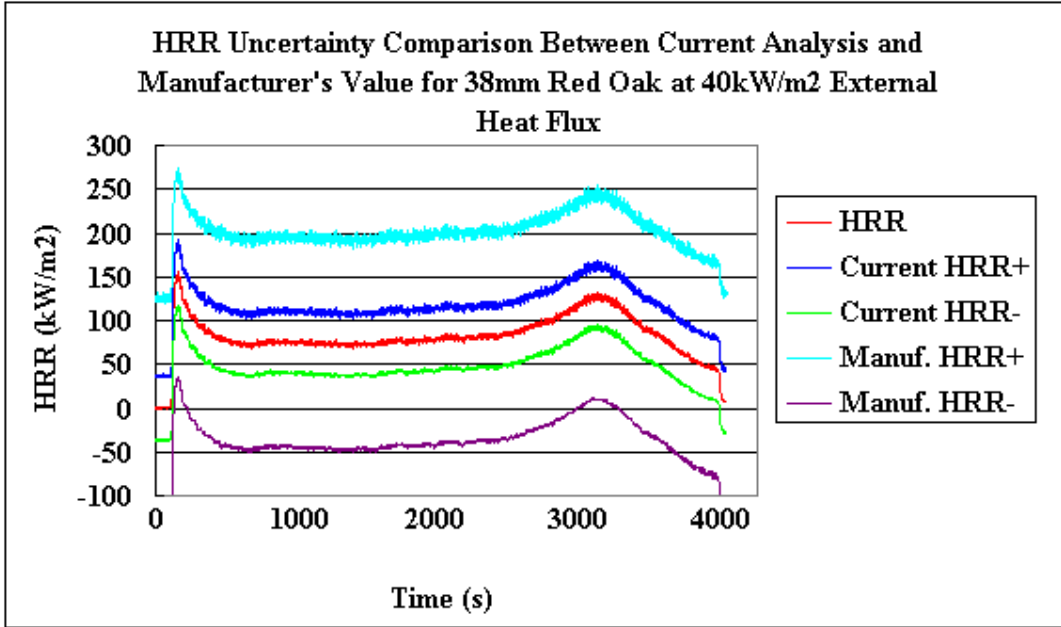


Figure A-21 HRR Uncertainty Comparison Between Current Analysis and Manufacturer's Value for 38mm Red Oak at 40 kW/m<sup>2</sup> External Heat Flux in Cone Test

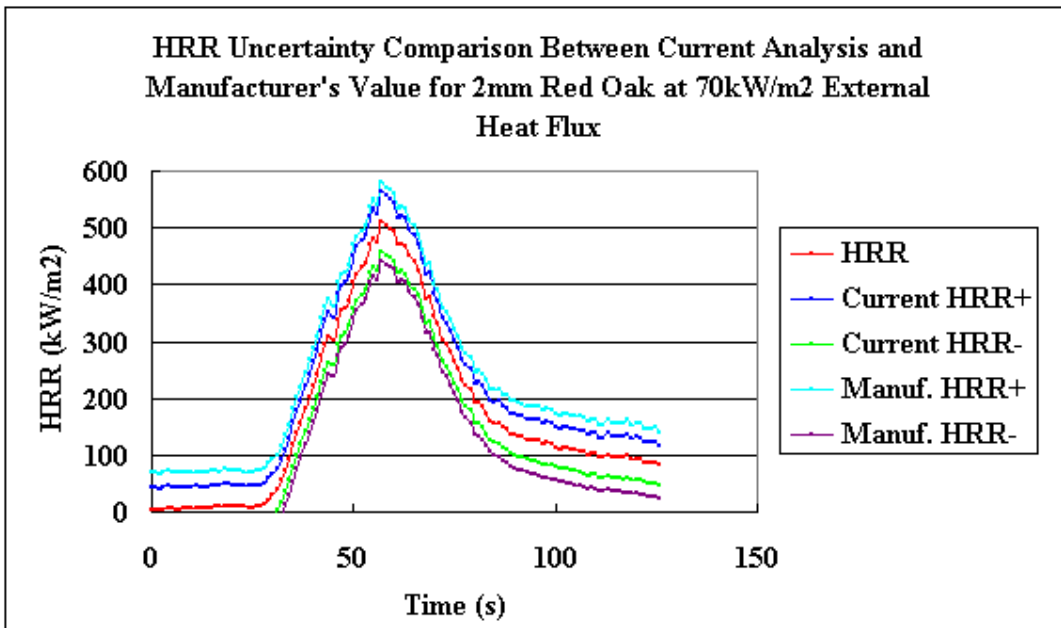


Figure A-22 HRR Uncertainty Comparison Between Current Analysis and Manufacturer's Value for 38mm Red Oak at 40 kW/m<sup>2</sup> External Heat Flux in Cone Test

Table A-8 shows the HRR uncertainty comparison among current analysis, Enright et al<sup>12</sup>, Manufacturer Value (of Cone in WPI), and NIST<sup>13</sup>. The HRR uncertainty and its normalized uncertainty at different HRR level are listed. From Table A-8, we found that the HRR uncertainty at various HRR levels based on our instrument manufacturer value is bigger than the others, i.e., our current analysis, Enright et al<sup>12</sup>, and NIST<sup>13</sup>. Enright et al<sup>12</sup> showed smallest HRR uncertainty at all three levels of HRR. The normalized uncertainty of current analysis at higher HRR level is consistent with NIST<sup>13</sup>.

**Table A-8 HRR Uncertainty and Its Normalized Uncertainty Comparison among Current Analysis, Enright et al<sup>12</sup>, Manufacturer Value, and NIST<sup>13</sup>**

	HRR Level	Uncertainty	Normalized Uncertainty
Current Uncertainty	1 kW	0.35 kW	35%
	3 kW	0.35 kW	11.7%
	5 kW	0.45 kW	9%
Enright et al	1 kW	0.06 kW	6%
	3 kW	0.17 kW	5.5%
	5 kW	0.27 kW	5.5%
Manufacturer	1 kW	1.3 kW	130%
	3 kW	0.6 kW	20%
	5 kW	0.68 kW	14%
NIST	50 kW	3.75 kW	7.5%

The information in Table A-8 is also shown in Figure A-23. As seen in Figure A-23, the normalized HRR uncertainty is decreasing as the HRR increasing.

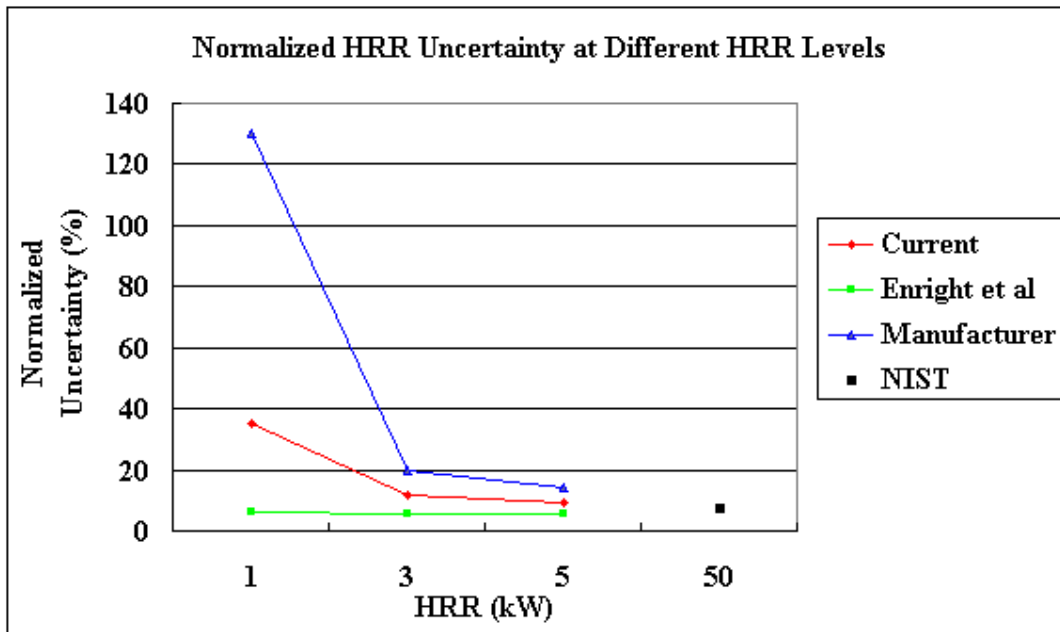


Figure A-23 Normalized HRR Comparison at Different HRR Levels among Current Analysis, Enright et al<sup>12</sup>, Manufacturer Values (of Cone in WPI), and NIST<sup>13</sup>

Uncertainty of average heat of combustion is calculated by using the manufacturer's value (oxygen analyzer and load cell) for a cone calorimeter test of 38mm red oak at 40 kW/m<sup>2</sup> external heat flux. The uncertainty is 0.32 kJ/g, which is 3 times bigger than that (0.1 kJ/g) based on our calibration uncertainty. Since the average heat of combustion is the same, the normalized average heat of combustion uncertainty of manufacturer is also 3 times bigger than that based on our calibration uncertainty.

## CONCLUSIONS

The measurement uncertainties of component instruments (direct measurement), load cell, oxygen analyzer, and laser were estimated based on NIST<sup>10</sup> and ISO<sup>11</sup> Guide. Pressure transducer, CO/CO<sub>2</sub> analyzer, and thermocouples measurement uncertainties were determined by using manufacturer's specification. The uncertainties of load cell, oxygen analyzer, and

laser were expressed by 95% confidence interval and the uncertainties of load cell and oxygen analyzer were smaller than those specified by manufacturers (there was no manufacturer specifications for laser.). The study initially standardized measurement uncertainty analysis for calorimetry apparatus measurement.

Based on the uncertainties of component instruments, indirect measured parameter uncertainties were estimated. They are heat release rate, extinction coefficient, volume flow rate, extinction coefficient, smoke production rate, and heat of combustion. Uncertainty interval of 95% confidence was determined.

All the uncertainty bands of direct and indirect measurement were validated by using Monte Carlo Simulation technique for sampling size of 10,000. It demonstrated that our uncertainty analysis methods were appropriate.

The measurement uncertainty analysis showed that our laser doesn't have the ability to differentiate obscuration related quantities. The theoretical approach for MLR uncertainty estimate is not available. The uncertainty is determined experimentally and statistically, and expressed by 95% confidence interval.

R value analysis showed that, for our case, HRR uncertainty depend not only on oxygen concentration uncertainty, but also on C factor and heat of combustion per mass of oxygen.

The HRR uncertainty and its normalized uncertainty were compared at different HRR levels among the current analysis, Enright et al<sup>12</sup>, manufacturer value, and NIST<sup>13</sup>. Current results are higher than that of Enright et al<sup>12</sup> because different methods were used to estimate oxygen

concentration uncertainty. Current method is basically the same with NIST<sup>13</sup>. It also showed that the normalized HRR uncertainty is decreasing as the HRR increasing. The normalized uncertainty of current analysis at higher HRR level is consistent with NIST<sup>13</sup>.

The data analysis for the HRR calibration at 1, 3, and 5 kW showed that the normalized HRR uncertainty based on component instrument calibration is consistency with the normalized HRR based on day-to-day variation.

## **REFERENCES**

1. ISO 5660-1:1993, "Fire Tests-Reaction to Fire-Part 1: Rate of Heat Releases from Building Products (Cone Calorimeter Method)", International Organization for Standardization, Geneva, Switzerland, 1993.
2. ASTM E 1354, "Standard Test Method for Heat and Visible Smoke Release Rates for Materials and Products Using an Oxygen Consumption Calorimeter", Annual Book of ASTM Standards, American Society for Testing Materials, Philadelphia, PA. 2002.
3. ASTM E 2058-01, "Standard Test Methods for Measurement of Synthetic Polymer Material Flammability Using a Fire Propagation Apparatus (FPA)", Annual Book of ASTM Standards, Vol. 04.07. American Society for Testing Materials, Philadelphia, PA.
4. ASTM E-1623-04, Test Method for Determination of Fire and Thermal Parameters of Materials, Products, and Systems Using an Intermediate Scale Calorimeter ICAL, Annual Book of ASTM Standards, Vol. 04.07. American Society for Testing Materials, Philadelphia, PA.
5. Wu, Peter K., and Bill, Robert G., "Laboratory Test for Flammability Using Enhanced Oxygen", Fire Safety Journal 38 (2003) 203-217.

6. ASTM E603-04, Standard Guide for Room Fire Experiments, Annual Book of ASTM Standards, Vol. 04.07. American Society for Testing Materials, Philadelphia, PA.
7. “Approval Standard for Class 1 (A) Insulated Wall or Wall & Roof/Ceiling Panels (B) Plastic Interior Finish Materials (C) Plastic Exterior Building Panels (D) Wall/Ceiling Coating Systems (E) Interior or Exterior Finish Systems”, Class No. 4880, FM Global, Norwood, MA, August 1994.
8. Hirschler, Marcelo M., Use of Heat Release Measurements and/or Fire Hazard Assessment in Codes and Standards in the USA, GBH International.
9. Semyon G. Rabinovich, “Measurement Errors and Uncertainties-Theory and Practice” 2<sup>nd</sup> Edition, 1999
10. Taylor, B. N., and Kuyatt, C. E., Guidelines for Evaluating and Expressing the Uncertainty of NIST Measurement Results, NIST Technical Note 1297, NIST, Gaithersburg, MD, 1994.
11. International Organization for Standardization, “Guide to the Expression of Uncertainty in Measurement”, ISBN 92-67-10188-9, 1995.
12. Enright, P., and Fleischmann, C., "Uncertainty of Heat Release Rate Calculation of the ISO5660-1 Cone Calorimeter Standard Test Method", Fire Technology, 35:2 (1999) 153-169.
13. Bryant, Rodney A., Ohlemiller, Thomas J., Johnsson, Erik L., Hammins, Anthony, Grove, Brian S., Guthrie, William F., Maranghides, Alexander, and Mulholland George W., “The NIST 3 Megawatt Quantitative Heat Release Rate Facility”, NIST Special Publication 1007, December 2003.
14. Alston, J. J., “Methods for Determining Material Fire Properties and Uncertainty”, Thesis, 2004
15. 6005D Weight Cell Manual, “Automatic Timing & Controls”

16. International Organization for Standardization, “Linear Calibration Using Reference Materials”.
17. Servomex, “Oxygen Analyzer (X1420) Manual”.
18. Coleman, H. W. and Steele, W. G., “Experimentation and Uncertainty Analysis for Engineers” 2<sup>nd</sup> Edition, 1998.
19. MKS, “Type 223—Baratron General Purpose Differential Pressure Transducer”, Bulletin 223DIFF-9/02, MKS Instruments, Inc., 2002
20. Omega Engineering, Inc., “The Omega Temperature Handbook and Encyclopedia” Vol. MMV, 5<sup>th</sup> Edition, 2005.
21. Siemens, “Double Channel IR Analyzer—ULTRAMAT 22 Manual”, Siemens.
22. Steele, W. G., Taylor, R. P., Burrell R. E. and Coleman H. W., “Use of Previous Experience to Estimate Precision Uncertainty of Small Sample Experiments”, AIAA Journal, Vol 31, 10, October 1993.
23. Babrauskas, V., “Development of the Cone Calorimeter—A Bench-Scale Heat Release Rate Apparatus Based on Oxygen Consumption”, Technical Report NBSIR82-2611, NIST, Gaithersburg, MD, 1982.
24. Parker, W. J., “Calculations of the Heat Release Rate by Oxygen Consumption for Various Applications”, NBSIR 81-2427, 1982
25. David R. Lide, ed., CRC Handbook of Chemistry and Physics, Internet Version 2005, <http://www.hbcpnetbase.com>, CRC Press, Boca Raton, FL, 2005.
26. International Organization for Standardization, “Guide to the Expression of Uncertainty in Measurement (GUM)—Supplement 1: Numerical Methods for the Propagation of Distributions”, ISO GUM Suppl. 1 (IDGUIDE 99998), 2004

# **APPENDIX B UNCERTAINTY EFFECTS ON MEASUREMENT OF FIRE CHARACTERISTICS OF MATERIAL SYSTEMS**

Lei Zhao & Nicholas A. Dembsey  
Worcester Polytechnic Institute, USA

## **ABSTRACT**

An important characteristic of composite material systems is the ability to “custom design” the system to meet performance criteria such as cost, durability, strength and / or reaction to fire. To determine whether a new system is an improvement over previous ones and can meet required performance criteria, sufficiently accurate and precise instruments are needed to measure the system’s material properties in bench scale testing. Commonly used bench scale apparatuses are the cone calorimeter (Cone) and the FMGR fire propagation apparatus (FPA). For this paper, thermally “thin” and “thick” specimens of a natural composite, red oak, were tested in the Cone in an air environment and in the FPA in a nitrogen environment. Cone test data of two FRP composite systems from the previous work of Alston are also considered. The material reaction to fire properties were estimated considering both ignition and pyrolysis measurements made via the Cone and FPA. Investigation of the ultimate uncertainty of these material fire properties based on the intrinsic uncertainty of the component instruments (e.g. load cell) as well as the uncertainty introduced via use of a current ignition and pyrolysis model are considered.

## **INTRODUCTION**

How a material reacts to the thermal insult from fire depends on properties of the material, such as: density of the virgin material and the char, heat conductivity of the virgin material and the char, heat capacity of the virgin material and the char, etc. Material reaction to fire is usually measured as heat release rate, mass loss rate, time to ignition, etc. These reactions to fire cannot be simulated for design purposes without knowing the properties of the material. To date there are limited databases of these properties for traditional building materials. For composites there is even less available information on these properties. Since an important aspect of composite material systems is the ability to “custom design” the system to meet performance criteria, the ability to reliably measure the properties of these “custom systems” is of importance. According to Alston and Dembsey<sup>1</sup>, composites are being used in an ever increasing number of applications where reaction to fire is of importance. So, a methodology to estimate properties is critical. There are two steps to obtain the properties of a material: (1) bench scale testing; and (2) estimate properties by use of a pyrolysis model. The most widely used bench scale apparatuses are the cone calorimeter (Cone) and the FMGR fire propagation apparatus (FPA). The Cone test method is regulated in ISO 5660<sup>2</sup> and ASTM E 1354<sup>3</sup> and has the measuring functions of heat release rate, mass loss rate, total heat released, effective heat of combustion, ignitibility, smoke obscuration, smoke production rate, specific extinction area and concentration of CO/CO<sub>2</sub>. The FPA test method is regulated in ASTM E 2058<sup>4</sup> and has measuring functions of chemical heat release rate, convective heat release rate, flame spread, mass loss rate, effective heat of combustion, ignitibility, smoke, soot, toxic gases and total hydrocarbons. The test environment can be from 0% to 40% oxygen balanced with nitrogen.

In this paper, we focus on determining how the test uncertainty causes the estimated properties’ variation. The time to ignition and mass loss rate history measured in the

apparatuses were used to estimate material properties. The best estimate properties make the pyrolysis model simulations agree with the experiment for both the time to ignition and the subsequent transient mass loss rate of the material for different applied heat fluxes.

## **BACKGROUND**

Traditionally, composite material reaction to fire is evaluated by using the “Steiner Tunnel test”, i.e., Standard Test Method for Surface Burning Characteristics of Building Materials, which is regulated as a standard test method in ASTM E 84<sup>5</sup>. The test measures material flammability by using a “flame spread index” and “smoke developed index”. However, it was demonstrated by Dembsey et al<sup>6</sup> that the Steiner Tunnel test is not as good as bench scale apparatuses (Cone or FPA) to characterize the flammability of composites.

An initial attempt to estimate the uncertainty of thermal inertia was conducted by Alston<sup>1</sup>. He used various ignition and pyrolysis models to estimate material properties for both a “thick” and a “thin” composite material. He concluded that: “Although the techniques each showed differing results for effective thermal inertia for each material, the calculation uncertainties are too large to fully and accurately differentiate the two systems. It is unlikely that the techniques could differentiate between more subtle variations in material or skin thickness.”

## **PYROLYSIS MODEL**

The mathematical modeling of charring solids has a long history dating back to the 1950's. Kung<sup>7</sup> formulated and solved the classical mathematical model of wood pyrolysis. He concluded that the pyrolysis rate depends very strongly on the thermal conductivity of char, which has been proven to be a very important practical result. The problems of the model

were 1) not able to handle solids having very narrow pyrolysis fronts with steep density gradients; and 2) very long computation times.

Field modeling based on the CFD methodology is playing a more and more important role in fire research. It has been quite successfully used in many different fire situations over the last two decades. Yan and Holmstedt<sup>8</sup> developed a practical pyrolysis model and implemented it into CFD. The model uses well established physics suitable for engineering applications and achieves its exceptional speed by employing dual spatial meshes—a coarse mesh for the smoothly varying temperature field and a moving fine mesh for the steeply varying density field which moves with the pyrolysis front. It can be used in the complex cases such as those with transient incident heat flux and temperature-dependent material properties. It is generally applicable to charring and non-charring materials. The limitations of Kung's model were overcome.

By using essentially the same pyrolysis model, deRis<sup>9</sup> and Yan<sup>10</sup> developed an equivalent properties optimization program to analyse and fit bench scale test results. The program is able to determine the effective pyrolysis properties of a material which make pyrolysis model predictions agree with experiment for both the time to ignition and the subsequent transient mass loss rate of the material for different external heat fluxes. The algorithm is implemented in a 32-bit digital visual Fortran DLL for access by MS Excel spreadsheet front ends. The program essentially consists of two spreadsheets, i.e., ignition and pyrolysis. A spreadsheet supplies the Fortran program with 1) material properties, such as density of virgin and char, thermal conductivity of virgin and char, specific heat of virgin and char, pyrolysis temperature, pyrolysis rate coefficient, heat of vaporization, etc.; 2) transient external heat flux histories; 3) initial temperature and density profiles; and 4) program parameters. The

ignition spreadsheet returns with the calculated time to ignition at six different external heat fluxes. The pyrolysis spreadsheet returns with the calculated mass loss rate history at three different external heat fluxes. One needs to adjust the material properties so that calculated results agree with test data. The criterion for termination of the property estimation procedure (agreement) is: a) Peak mass loss rate (MLR) matches and; b) MLR residual, see Equation 1, is less than 2 g/m<sup>2</sup>s for n = 100 point interval located evenly throughout test duration.

$$\text{MLR residual} = \sqrt{\frac{\sum_{i=1}^n (MLR_{test}(t) - MLR_{cal}(t))^2}{n}} \quad [1]$$

## **SPECIMEN PREPARATION**

Red Oak (natural composite used for model calibration): Before testing, the red oak samples were conditioned in the laboratory at nominally 12% relative humidity and 23 °C until moisture equilibrium was reached. The moisture content was approximately 3%. The thickness of the samples was 38 mm and 2 mm. The samples were prepared such that the grain was perpendicular to the incident heat flux.

Composite (Alston<sup>1</sup>): The two composite systems tested were chosen based on their thermal behavior and were previously tested at WPI. The typical end use configuration of FRP consists of thin outer skin layer(s) and a core material. The thermally “thick” material consisted of eight layers of 560808 glass with a vinyl ester (VEX) resin. The thermally “thin” specimen, typical of that used in fast ferry construction, consisting of a sandwich panel with one 560808 glass layer with vinyl ester (VEX) resin over a balsa core, was also tested to contrast its fire properties to the “thick”.

In terms of HRR, there are significant differences between the thermally “thin” and thermally “thick” composite systems. In Cone testing the peak HRR was about 400 kW/m<sup>2</sup> for the thermally “thin” composite and 100 kW/m<sup>2</sup> for the thermally “thick” composite. In room corner testing the “thick” and “thin” materials were subjected to a propane source fire of 30 kW. The HRR of the “thick” composite was as low as about 60 kW on average. The HRR of the “thin” composite reached 1200 kW in 190 s, room flashover, such that the test had to be terminated.

## TEST SETUP

An important aspect of the test setup is the sample holder. Theoretical predictions of ignition and pyrolysis in standard flammability apparatuses show that sample holder construction has large effect on the measurements such as time to ignition and mass loss rate especially for thermally thin samples<sup>11</sup>. To minimize the heat loss from the rear surface of the specimens, ceramic fiberboard, which has very low heat conductivity, was used, and, aluminum foil was used to wrap each of the specimens, covering sides and bottom, in order to minimize any mass transfer<sup>3</sup>. In the property estimation procedure two model parameters, rear heat transfer coefficient and rear thermal inertia, are used to represent the heat transfer from the specimens into the ceramic fiberboard. Both of these values were fixed for all property estimations and their values were: rear heat transfer coefficient 5 W/m<sup>2</sup>K, and rear thermal inertia 430 J/m<sup>2</sup>Ks<sup>-0.5</sup>.

For thermally thin specimens and the 2<sup>nd</sup> peak of thermally thick specimens, when the pyrolysis front approaches the rear surface, the insulating effects of the rear boundary allows

the specimen to vaporize with little further addition of heat<sup>10</sup>. Since the sample holder and rear boundary condition was not fully specified, it is unknown if the specimen actually lost or received heat through the sample holder. Thus, there are some uncertainties about MLR data for thermally “thin” and the 2<sup>nd</sup> peak of thermally “thick” specimens. In this paper, we ignore these uncertainties in the following analysis.

Pyrolysis tests (in nitrogen environment) of the same thermally “thin” (2 mm) and “thick” (38 mm) red oak specimens were also tested horizontally using the FPA. In order to make the test results comparable to those of Cone, we used the same sample holder and substrate as we did in Cone and the specimen was wrapped in aluminum foil. The nitrogen was supplied at the flow rate of 100 l/min. The sample is 100×100 mm square and the surface was blackened.

## **PROPERTY ESTIMATION**

The measured reactions to fire of time to ignition and mass loss rate (MLR) at six different external heat fluxes for the “thin” and “thick” red oak, and the “thin” and “thick” composite were used to estimate properties. Since some of the tests were conducted in air environment, the flame heat flux feedback to the surface should be known. It is hard to estimate the heat feedback under lower external heat fluxes for thermally “thick” specimens because the flame is very small and not stable. Higher external heat fluxes (50 kW/m<sup>2</sup> and above) were selected for thermally “thick” specimens so that the flames were observed above the cone heater and stable, i.e., flame feedback to the surface can be estimated to be 30 kW/m<sup>2</sup> according to Quintiere and Rhodes<sup>12</sup>. For the thermally “thin” specimens, both high and low external heat fluxes can be selected since the flame is high and stable so that the flame feed back can be estimated as 30 kW/m<sup>2</sup>. The estimated properties make pyrolysis

model predictions agree with experiment for both the time to ignition and the subsequent transient mass loss rate for different applied heat fluxes.

## **1. ESTIMATION OF BASELINE PROPERTIES**

Baseline properties were estimated by using the test data without mass loss rate uncertainties. Red oak from the same tree should have a set of unique properties no matter whether the specimen is thermally “thick” or “thin”, and, no matter whether the specimen is tested in air or nitrogen environment. Thermally “thick” and “thin” red oak specimens were tested in both the Cone and FPA in air and nitrogen environment respectively. The properties of red oak were then estimated by using the pyrolysis model and compared with the literature values. The purpose is to calibrate the pyrolysis model since it was not tested extensively. It should be noted that the model takes the surface regression into account. The model is more suitable to apply to red oak. Surface regression was not obvious for the composite systems.

### **1.1 Red Oak Tested in Air Environment Using Cone**

38 mm thickness red oak (which was identified as thermally “thick”) and 2 mm thickness red oak (which was identified as thermally “thin”) specimens were tested by using the Cone in air environment. Time to ignition tests were conducted at 30, 40, 50, 60, 70 and 80 kW/m<sup>2</sup>, and, mass loss rate tests were conducted at 60, 70 and 80 kW/m<sup>2</sup> for the thermally “thick” specimens. Similar to thermally “thick” red oak, thermally “thin” red oak were tested at 20, 22, 40, 60, 65, and 70 kW/m<sup>2</sup> for time to ignition, and, also were tested at 60, 65 and 70 kW/m<sup>2</sup> for mass loss rate. The properties of thermally “thin” and “thick” red oak were estimated by using the pyrolysis model. These estimated properties make the calculated time to ignition and mass loss rate data agree with the test data. Figure B-1 shows the comparison of experimental mass loss rate history with the estimated one for thermally “thick” red oak

specimen subject to  $60 \text{ kW/m}^2$  external heat flux. Figure B-2 shows the comparison of experimental mass loss rate history with the estimated one for thermally “thin” red oak specimen subject to  $20 \text{ kW/m}^2$  external heat flux. Table B-1 shows the comparison of estimated properties (from thermally “thin” and “thick” red oak) with the literature values.

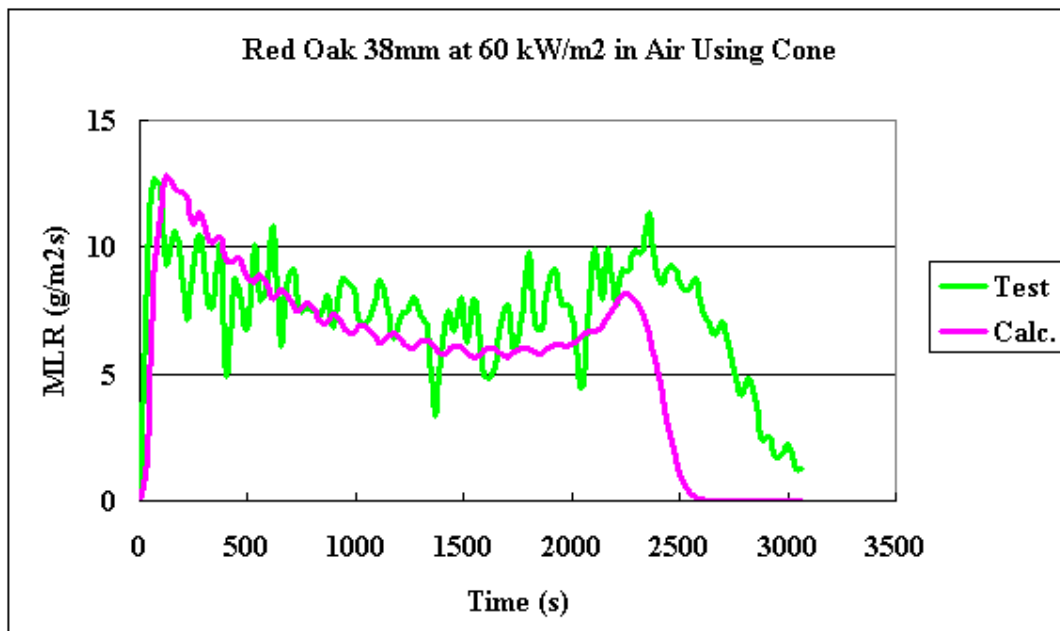


**Figure B-1 Measured and Calculated MLR Comparison for Thermally “Thick” Red Oak at  $60 \text{ kW/m}^2$  External Heat Flux in Air Using Cone**

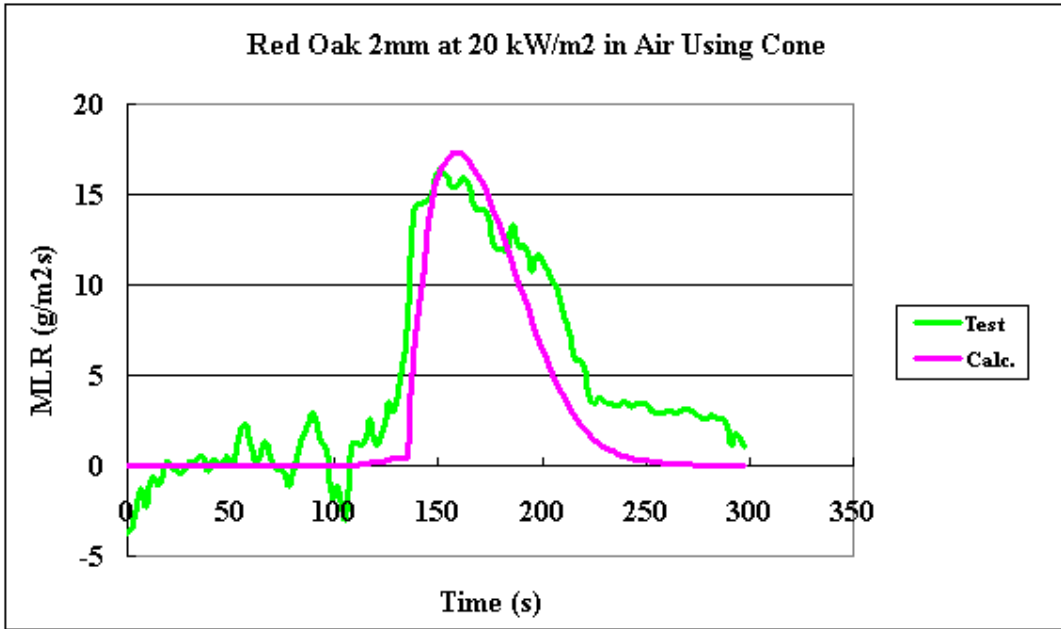


**Figure B-2 Measured and Calculated MLR Comparison for Thermally “Thin” Red Oak at 20 kW/m<sup>2</sup> External Heat Flux in Air Using Cone**

**Table B-1 Comparison of Estimated Properties (Using Cone Data in Air without Uncertainties) and Literature<sup>13, 14, 15, 0</sup> Values of Red Oak.**

Properties	38mm	2mm	Liter.
Virgin Density (kg/m <sup>3</sup> )	675	675	660
Char Density (kg/m <sup>3</sup> )	200	200	170
Pyro. T (K)	720	720	600
Pre-exponential coeff. (1/Ks)	0.00017	0.0003	N/A
Vaporization Heat (kJ/kg)	680	600	N/A
Surface Emmissivity	1	1	0.88-1
Arrheniud E/R*T	20	20	N/A
Critical Ign. MLR (g/sm <sup>2</sup> )	2	2	2-4
Virgin Conductivity (W/mK)	0.16	0.16	0.15-0.21
Virgin specific heat (J/kgK)	1500	1580	1400-1700
Char conductivity (W/mK)	0.26	0.27	0.23
Char specific heat (J/kgK)	3000	3000	2500

### 1.2 Red Oak Tested in Nitrogen Environment Using FPA

Pyrolysis tests (in nitrogen environment) for the same thermally “thin” (2 mm) and “thick” (38 mm) red oak specimens were also tested horizontally using the FPA. Three pyrolysis tests were conducted at 25, 35 and 50 kW/m<sup>2</sup> for the thermally “thick” specimens. Ignition data from the Cone was also needed and taken at 20, 30, 40, 45, 50 and 60 kW/m<sup>2</sup>. Similar to thermally “thick” red oak, thermally “thin” red oak were tested at 25, 30 and 40 kW/m<sup>2</sup> for the pyrolysis tests. Ignition data from the Cone was also needed and taken at 20, 30, 40, 45, 50 and 60 kW/m<sup>2</sup>. The properties of thermally “thin” and “thick” red oak were estimated by using the pyrolysis model. These estimated properties make the calculated time to ignition

and mass loss rate data agree with the test data. Figure B-3 shows the comparison of experimental mass loss rate history with the estimated one for thermally “thick” red oak specimen subject to  $50 \text{ kW/m}^2$  external heat flux. Figure B-4 shows the comparison of experimental mass loss rate history with the estimated one for thermally “thin” red oak specimen subject to  $25 \text{ kW/m}^2$  external heat flux. Table B-2 shows the comparison of estimated properties with the literature values.

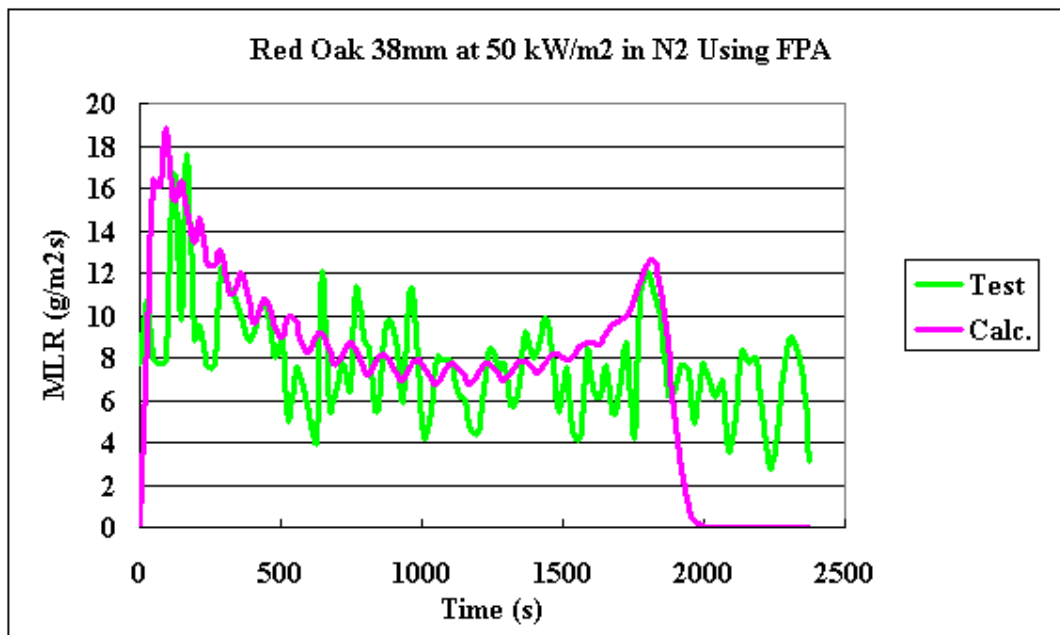


**Figure B-3 Measured and Calculated MLR Comparison for Thermally “Thick” Red Oak at  $50 \text{ kW/m}^2$  External Heat Flux in nitrogen Using FPA.**

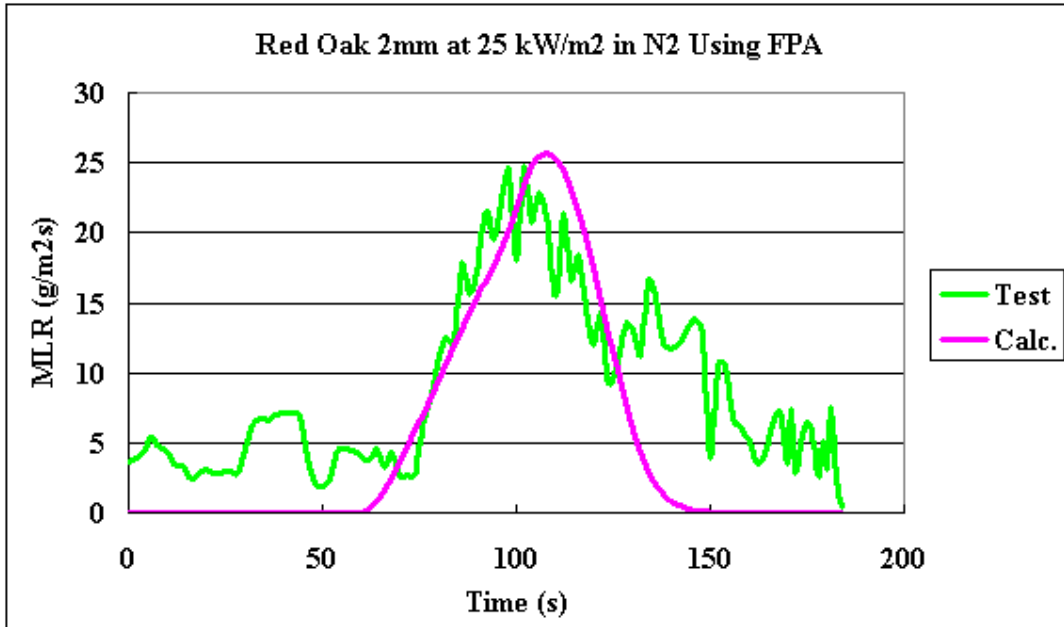


**Figure B-4 Measured and Calculated MLR Comparison for Thermally “Thin” Red Oak at 25 kW/m<sup>2</sup> External Heat Flux in nitrogen Using FPA.**

The properties of red oak were estimated by using the pyrolysis model at different conditions, i.e., thermally “thin” and “thick” specimens tested in both air and nitrogen environments. From Table 1 and 2, it is found that most of the estimated properties are consistent between the different conditions and with literature values (maximum 25% variation). The exceptions are pre-exponential coefficient and vaporization heat. There are no literature values for these properties. Across the various conditions the pre-exponential coefficient varies by a factor of 3.5 and the vaporization heat varies by a factor of 6.8. Given the consistency of the vast majority of the properties for red oak the model is considered to be working properly with an uncertainty of 25% or as noted above for pre-exponential coefficient and vaporization heat.

**Table B-2 Comparison of Estimated Properties (Using FPA Data in nitrogen without Uncertainties) and Literature Values of Red Oak.**

Properties	38mm	2mm	Liter.
Virgin Density (kg/m <sup>3</sup> )	700	675	660
Char Density (kg/m <sup>3</sup> )	200	200	170
Pyro. T (K)	685	675	600
Pre-exponential coeff. (1/Ks)	0.0003	0.0006	N/A
Vaporization Heat (kJ/kg)	100	100	N/A
Surface Emmissivity	1	1	0.88-1
Arrheniud E/R*T	20	20	N/A
Critical Ign. MLR (g/sm <sup>2</sup> )	2	2	2-4
Virgin Conductivity (W/mK)	0.16	0.15	0.15-0.21
Virgin specific heat (J/kgK)	1800	1500	1400-1700
Char conductivity (W/mK)	0.19	0.18	0.23
Char specific heat (J/kgK)	2500	2500	2500

### 1.3 Composites Tested in Air Environment Using Cone

Thermally “thin” and “thick” composite specimens were tested using the Cone in air environment, see Alston<sup>1</sup>. Time to ignition tests were conducted at 20, 35, 40, 50, 75, 85 kW/m<sup>2</sup>, and, mass loss rate tests were conducted at 50, 75 and 85 kW/m<sup>2</sup> for both of the thermally “thin” and “thick” composite specimens. The properties of thermally “thin” and “thick” composites were estimated by using the pyrolysis model. These estimated properties make the calculated time to ignition and mass loss rate data agree with the test data. Figure B-5 shows the comparison of experimental mass loss rate history with the estimated one for thermally “thick” composite specimen subject to 50 kW/m<sup>2</sup> external heat flux. Figure B-6

shows the comparison of experimental mass loss rate history with the estimated one for thermally “thin” composite specimen subject to  $50 \text{ kW/m}^2$  external heat flux.

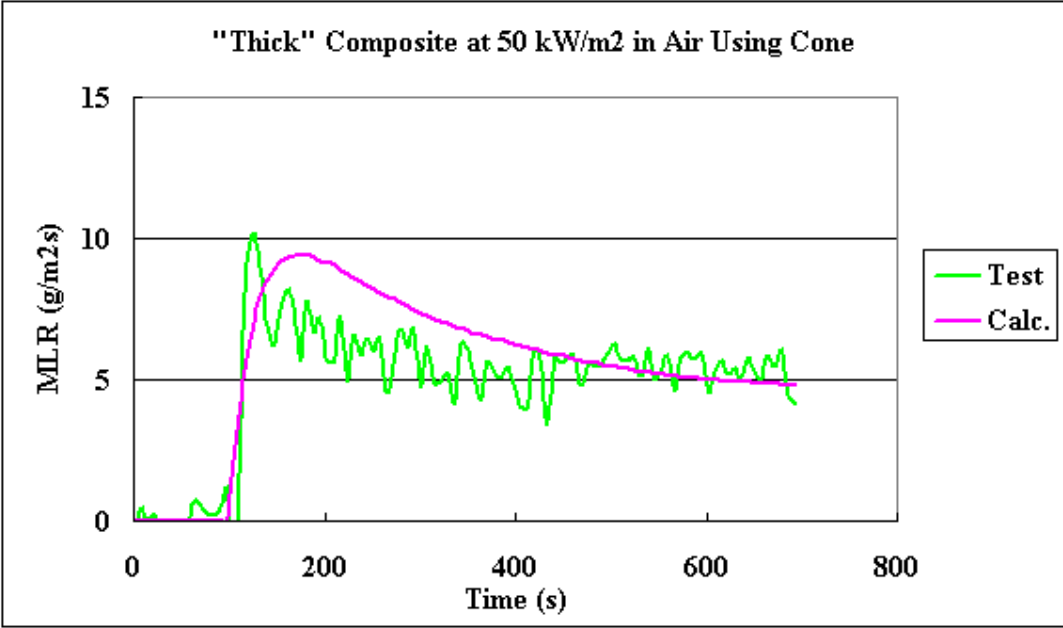


Figure B-5 Measured and Calculated MLR Comparison for Thermally “Thick” Composite at  $50 \text{ kW/m}^2$  External Heat Flux in Air Using Cone.

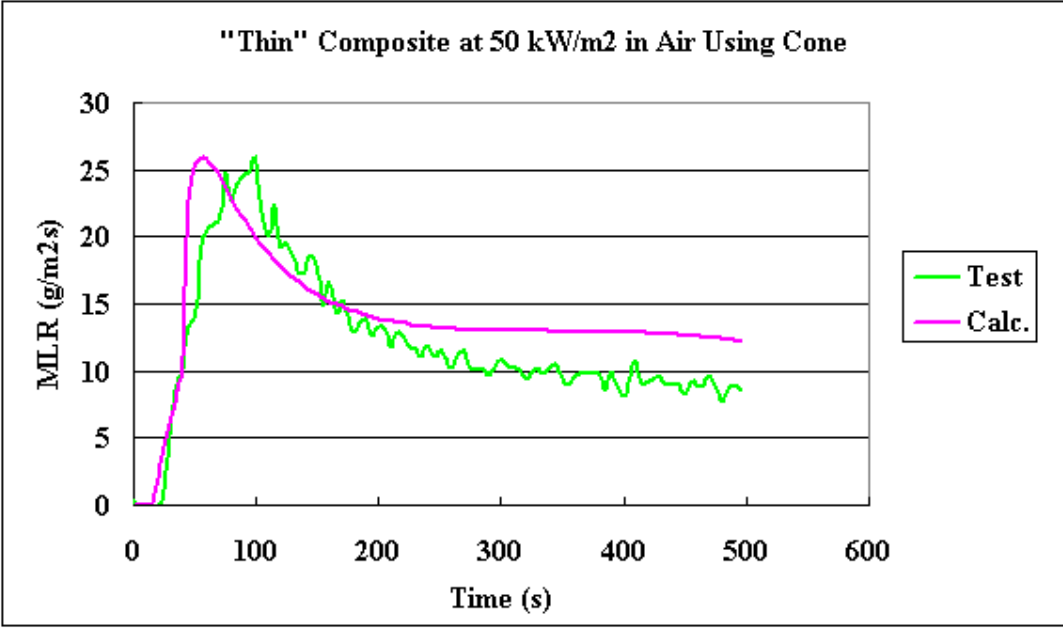


Figure B-6 Measured and Calculated MLR Comparison for Thermally “Thin” Composite at  $50 \text{ kW/m}^2$  External Heat Flux in Air Using Cone.

Table B-3 shows the estimated properties of both thermally “thin” and “thick” composites. Using the model uncertainty estimates noted above, we find that all but one of the properties are consistent with the differences between the material systems or have variations consistent with the model uncertainty. The one exception is the char specific heat which is inconsistent with the virgin material specific heat.

**Table B-3 Comparison of Estimated Properties of Thin and Thick Composites**

Properties	Thin Composite	Thick Composite
Virgin Density (kg/m <sup>3</sup> )	500	2000
Char Density (kg/m <sup>3</sup> )	150	200
Pyro. T (K)	655	825
Pre-exponential coeff. (1/Ks)	0.0003	0.001
Vaporization Heat (kJ/kg)	800	900
Surface Emmissivity	1	1
Arrheniud E/R*T	20	20
Critical Ign. MLR (g/sm <sup>2</sup> )	4	4
Virgin Conductivity (W/mK)	0.3	0.55
Virgin specific heat (J/kgK)	2000	1200
Char conductivity (W/mK)	0.3	0.5
Char specific heat (J/kgK)	1500	2000

## 2. PROPERTY ESTIMATION WITH MLR UNCERTAINTY

In Section 1 (Estimation of Baseline Properties), the baseline properties of red oak were estimated without uncertainty of mass loss rate. Next we will investigate how the estimated thermal properties change according to the uncertainty of mass loss rate and the time to ignition. Please note that the uncertainty of time to ignition is a matter of one second, which

won't cause significant change of the estimated thermal properties. Therefore, we only consider the uncertainty of MLR.

## 2.1 MLR and Its Uncertainty Calculation

### 2.1.1 MLR Calculation

Mass loss rate (MLR) is calculated using 5-point numerical differentiation method recommended by ASTM E-1354<sup>3</sup>:

$$MLR = \frac{-m_{i-2} + 8m_{i-1} - 8m_{i+1} + m_{i+2}}{12\Delta t} \quad [2]$$

where:  $\Delta t$  is 1 second.

### 2.1.2 Uncertainty of MLR Calculation

In the burning test, the mass decreases as the time increases, i.e., it should be identified as a time series measurement. Time series is defined as an ordered sequence of values of a variable at equally spaced time intervals<sup>17</sup>. For now, MLR uncertainty was determined experimentally (statistically). Five similar PMMA burning tests were replicated. We found that the extreme mass loss rate uncertainty of the steady state burning duration is 6 g/m<sup>2</sup>s. Assuming the MLR at steady state burning duration is normally distributed, we conclude that there is 68% confidence of one SD (2 g/m<sup>2</sup>s) interval and 95% confidence of two SD's (4 g/m<sup>2</sup>s) interval. Figure B-7 illustrates two different uncertainty bands of MLR, i.e., one SD band and two SD band.

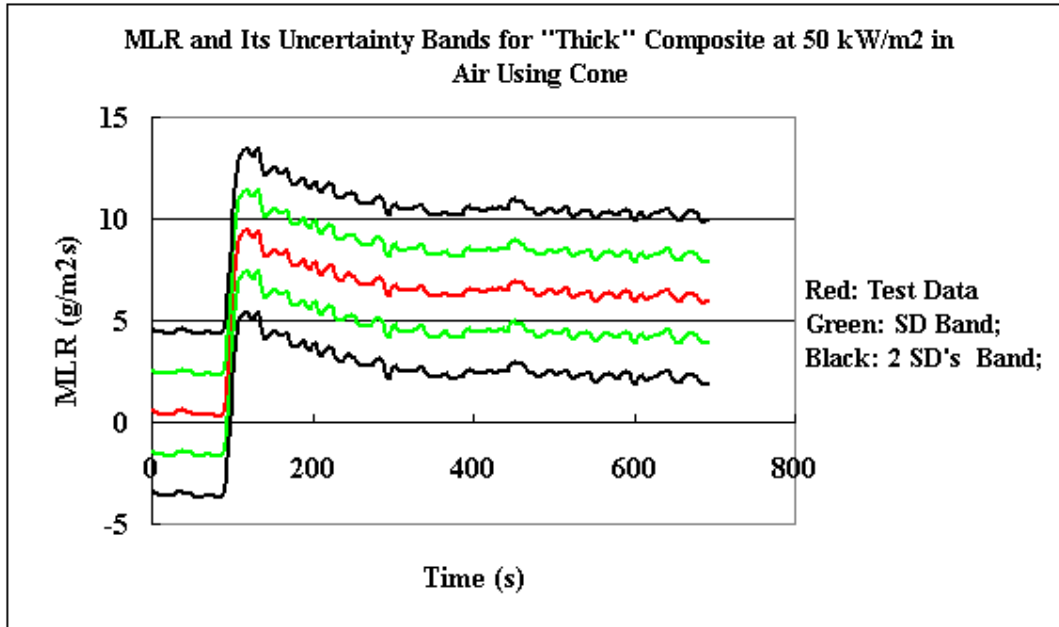


**Figure B-7 MLR and Its Uncertainty Bands for Thermally “Thick” Composite at 50 kW/m<sup>2</sup> External Heat Flux in Air Using Cone Calorimeter.**

The uncertainty of MLR plus the original MLR is the upper limit of the MLR, while the original MLR minus the uncertainty of MLR is the lower limit of the MLR. It was noticed that the average mass loss rate of thermally “thin” red oak and composite were in the range of 10-15 g/m<sup>2</sup>s and that of thermally thick were in the range of 5-10 g/m<sup>2</sup>s. We found that the extreme MLR uncertainty 6 g/m<sup>2</sup>s is too big to implement property estimation for the current pyrolysis model. The estimated properties were totally different from the baseline properties, which was meaningless for the study. In some cases, there was no set of properties that made the calculated results agree with the test data.

As a convention, two SD is used to express an uncertainty in engineering application according to ISO<sup>18</sup> and NIST<sup>19</sup> guide. Therefore, we would like to use 4 g/m<sup>2</sup>s as the uncertainty of MLR and implement the property estimation for the current model. Unfortunately, 4 g/m<sup>2</sup>s still doesn't work. The average MLR of thermally thick red oak and composite is in the range of 5-10 g/m<sup>2</sup>s. Two SD, 4 g/m<sup>2</sup>s, is 40% to 80% of the average

MLR. At this level of uncertainty the model does not work properly. In use of the pyrolysis model, we found that one SD, i.e., 2 g/m<sup>2</sup>s of MLR uncertainty (20% to 40% of the average MLR), can be used to estimate the red oak and composite properties without any problems by using the current pyrolysis model. We will use this mass loss uncertainty to estimate the red oak and composite properties' variation.

## **2.2 Property Estimation with One Standard Deviation of MLR**

In general, the mass loss rate of thermally “thin” material is governed by the pre-exponent coefficient and the pyrolysis heat, while the mass loss rate of thermally “thick” material is governed by the virgin and char thermal conductivities<sup>9</sup>. These four properties are defined as the “key” properties in the current study.

Since the uncertainty of time to ignition is ignored, the original test data will still be used. Mass loss rate uncertainty plus the original mass loss rate is the upper limit mass loss rate. Original mass loss rate minus mass loss rate uncertainty is the lower limit of mass loss rate. The properties of red oak and composite were estimated by using the pyrolysis model. These estimated properties make the calculated time to ignition and mass loss rate data agree with the test data of time to ignition and upper/lower limit of mass loss rate respectively.

### **2.2.1 Red Oak Tested in Air Environment Using Cone and in Nitrogen Environment Using FPA**

When the estimated properties variations are considered based on the upper and lower bounds of the MLR, the comparisons of the “worst” estimations (biggest difference from the baseline values) of the four “key” properties with the baseline values are shown in Table B-4. The

variations of the four “key” properties are within the model uncertainty estimates noted above.

**Table B-4 Comparisons Between the “Worst” Estimations and the Baseline Values for Red Oak.**

		Pre-exponential coeff. (1/Ks)	Pyrolysis Heat (kJ/kg)	Virgin Cond. (W/mK)	Char cond. (W/mK)
Using Cone in Air	Baseline thick	0.00017	680	0.16	0.26
	Worst est.	0.0003	680	0.17	0.23
	Variation	Factor of 1.8	Factor of 0	6%	10%
	Baseline thin	0.0003	600	0.16	0.27
	Worst est.	0.0006	680	0.18	0.29
	Variation	Factor of 2	Factor of 1.1	10%	7%
Using FPA in N2	Baseline thick	0.0003	100	0.16	0.19
	Worst est.	0.0002	200	0.17	0.21
	Variation	Factor of 0.7	Factor of 2	7%	10%
	Baseline thin	0.0006	100	0.15	0.18
	Worst est.	0.0005	150	0.14	0.20
	Variation	Factor of 0.8	Factor of 1.5	7%	11%

### 2.2.2 Composites Tested in Air Environment Using Cone

When the estimated properties variations are considered based on the upper and lower bounds of the MLR, the comparisons of the “worst” estimations of the four “key” properties with the

baseline values are shown in Table B-5. Similar to the red oak the variations of the four “key” properties are within the model uncertainty estimates noted above.

**Table B-5 Comparisons Between the “Worst” Estimations and the Baseline Values for FRP Composite.**

	Pre-exponential coeff. (1/Ks)	Pyrolysis Heat (kJ/kg)	Virgin Cond. (W/mK)	Char cond. (W/mK)
Baseline thick	0.0001	900	0.55	0.5
Worst est.	0.0001	1200	0.6	0.55
Variation	Factor of 0	Factor of 1.3	12%	10%
Baseline thin	0.0003	800	0.3	0.3
Worst est.	0.0005	1000	0.27	0.27
Variation	Factor of 1.7	Factor of 1.2	10%	10%

## CONCLUSIONS

An important characteristic of composite materials is the ability to “custom design” the system. To be able to properly measure the properties of the material, sufficiently accurate and precise instruments and models are needed. In this work the Cone and FPA along with a current ignition and pyrolysis model were evaluated. The evaluation considered a natural composite, red oak, and two FRP composites. The measurement systems (apparatuses and model) were able to estimate properties of the red oak that were consistent with literature values as well as estimate reasonable properties for the two composites. An important aspect of simulating fires for design is to know the uncertainties of the material properties. Consideration of the measured mass loss rate uncertainty at the one standard

deviation level showed that the current model could estimate properties and that their uncertainties were consistent with those inherent of the model. Considering the two standard deviation level of mass loss rate uncertainty (recommended by ISO<sup>18</sup> and NIST<sup>19</sup>) stable and reasonable property sets could not be estimated. Future work needs to focus on either lowering the mass loss rate uncertainty or development of more robust models so that property uncertainties can be more reliably estimated.

## **ACKNOWLEDGEMENTS**

The authors would like to extend their thanks to FM Global Research for their financial support of this study.

## **REFERENCES**

1. Alston, J. J., and N. A. Dembsey, "Marine Composite Material Fire Properties: Implications of Uncertainty", in Proceedings of the 8<sup>th</sup> International Conference on Fire and Materials 2003, San Francisco, CA, USA, 27-28 January, 2003.
2. ISO 5660-1:1993, "Fire Tests-Reaction to Fire-Part 1: Rate of Heat Releases from Building Products (Cone Calorimeter Method)", International Organization for Standardization, Geneva, Switzerland, 1993.
3. ASTM E-1354, "Standard Test Method for Heat and Visible Smoke Release Rates for Materials and Products Using an Oxygen Consumption Calorimeter", Annual Book of ASTM Standards, American Society for Testing Materials, Philadelphia, PA. 2002.
4. ASTM E 2058, "Standard Test Methods for Measurement of Synthetic Polymer Material Flammability Using a Fire Propagation Apparatus (FPA)", Annual Book of ASTM Standards, American Society for Testing Materials, Philadelphia, PA, 2001.

5. ASTM E-84, "Standard Test Method for Surface Burning Characteristics of Building Materials", Annual Book of ASTM Standards, American Society for Testing Materials, Philadelphia, PA. 1998.
6. Dembsey, N. A., C. M. Lee, and S. P. Qureshi, "Fire Growth Evaluation and Mechanical Properties of Seven Thermoset Composites", in Proceedings of SAMPE 2002, Long Beach Convention Center, Long Beach, CA, USA, 12-16 May 2002.
7. Kung, H. C., "A Mathematical model of Wood Pyrolysis", Combustion and Flame 18, 185-195, 1972.
8. Yan, Z., and G. Holmstedt, "CFD and Experimental Studies of Room Fire Growth on Wall Lining Materials", Fire Safety Journal 27 (1996) 201-238.
9. deRis J. L., "A Proposed Methodology for Determining Pyrolysis Properties" FMRC Technical Report, FMRC J.I. 0B1J0.RC, FM Global Research, Norwood, MA, USA, 1997.
10. deRis J. L. and Z. H. Yan, "Modeling Ignition and Pyrolysis of Charring Fuels", Proceedings of the 5<sup>th</sup> International Conference on Fire and Materials 1998, San Antonio, TX, USA, 1998.
11. deRis J. L. and M.M. Khan, "A Sample Holder for Determining Material Properties", Fire and Materials, 24, (2000) 219-226.
12. Rhodes, B. T. and J. G. Quintiere, "Burning Rate and Flame Heat Flux for PMMA in a Cone Calorimeter", Fire Safety Journal, 26 (1996) 221-240.
13. Forest Products Laboratory, Wood Handbook-Wood as an Engineering Material, Gen. Tech. FPL-GTR-113, U.S. Department of Agriculture, Forest Service, Forest Products Laboratory, Madison, WI, 1999.
14. Suuberg, E. M., I. Milosavljevic, and W. D. Lilly, "Behavior of Charring Materials in Simulated Fire Environments", NIST-GCR-94-645, NIST, Gaithersburg, MD, 1992.

15. Atreya, A., Pyrolysis, Ignition and Fire Spread on Horizontal Surfaces of Wood, Dissertation, Harvard University, 1983.
16. Babrauskas, V., Ignition Handbook, Fire Science Publishers, Issaquah, WA, USA, 2003.
17. NIST/SEMATECH e-Handbook of Statistical Methods, <http://www.itl.nist.gov/div898/handbook/>, Dec.1<sup>st</sup>, 2004.
18. International Organization for Standardization, Guide to the expression of Uncertainty in Measurement, ISBN 92-67-10188-9, ISO, Geneva, 1993.
19. Taylor, B. N., and C.E. Kuyatt, Guidelines for Evaluating and Expressing the Uncertainty of NIST Measurement Results, NIST Technical Note 1297, NIST, Gaithersburg, MD, 1994.

# APPENDIX C DERIVATION OF WELCH-SATTERTHWAITE FORMULA<sup>1,2</sup>

## 1. RELATIONSHIP BETWEEN DISTRIBUTIONS

### 1-1 Normal and Standard Normal Distribution

If  $X \sim N(\mu, \delta^2)$ ,  $Z = (X - \mu) / \delta$  has a standard normal distribution. This is established by writing

$$\begin{aligned} P(Z \leq z) &= P\left(\frac{X - \mu}{\delta} \leq z\right) = P(X \leq z\delta + \mu) \\ &= \frac{1}{\sqrt{2\pi}\delta} \int_{-\infty}^{z\delta + \mu} e^{-(x-\mu)^2 / 2\delta^2} dx = \frac{1}{\sqrt{2\pi}} \int_{-\infty}^z e^{-t^2 / 2} dt \end{aligned}$$

where  $t = \frac{x - \mu}{\delta}$

### 1-2 Standard Normal and Chi Squared Distribution

Let X have the standard normal distribution

$$f_X(x) = \frac{1}{\sqrt{2\pi}} e^{-x^2/2}, \quad -\infty < x < \infty \quad (1)$$

We consider the distribution of  $Y = X^2$ . By transformation

$$f_Y(y) = \frac{1}{\sqrt{2\pi}} \frac{1}{\sqrt{y}} e^{-y/2} \quad (2)$$

So, the probability density function (pdf) of Y is a chi squared distribution with 1 degree of freedom. Denote  $\chi_{(p)}^2$  as chi squared distribution with p degrees of freedom.

### 1-3 Summation of Chi Squared Distribution

Let  $X_1, \dots, X_n$  are independent and  $X_i \sim \chi_{p_i}^2$ . We consider the distribution of

$Y' = X_1 + \dots + X_n$ . From the moment generation function of chi squared distribution, we obtain

$$M_{X_i}(t) = \left(\frac{1}{1-2t}\right)^{p_i/2} \quad (3)$$

$$M_{Y'}(t) = \prod_1^n M_{X_i}(t) = \left(\frac{1}{1-2t}\right)^{(P_1+\dots+P_n)/2} \quad (4)$$

It is obvious that  $Y'$  has a chi squared distribution with  $(P_1 + \dots + P_n)$  degrees of freedom ( $\chi_{(P_1+\dots+P_n)}^2$ ).

### 1-4 Standard Normal, Chi Squared and Student's t Distribution

We can get Student's  $t_v$  distribution from the ratio of a standard normal variable to an independent variable distributed as  $\sqrt{\chi_v^2 / v}$ .

Let  $X_1, X_2, \dots, X_{v+1} \stackrel{idd}{\sim} Normal(0,1)$ ,  $\frac{X_{v+1}}{\sqrt{\sum_{i=1}^v X_i^2 / v}}$  is a  $t_v$  distribution.

Proof: It is obvious that random variable  $W = \sum_{i=1}^v X_i^2$  has a Chi square( $v$ ) distribution,

while  $U = X_{v+1}$  is a  $N(0,1)$  and independent of  $W$ . The joint pdf of  $U$  and  $W$  is

$$f_{U,W}(u, w) = \frac{1}{\sqrt{2\pi}} e^{-u^2/2} \frac{1}{\Gamma(v/2)2^{v/2}} w^{(v/2)-1} e^{-w/2}, \quad -\infty < u < \infty, 0 < w < \infty$$

Now make the transformation

$$t_1 = \frac{u}{\sqrt{w/v}}, \quad t_2 = w \quad \Rightarrow \quad u = t_1 \sqrt{t_2/v}, \quad w = t_2$$

The Jacobian of the transformation is  $\sqrt{t_2/v}$ , and the marginal pdf of  $t_1$  is given by

$$\begin{aligned} f_{T_1}(t_1) &= \int_0^\infty (f_{U,W}(t_1 \sqrt{t_2/v}, t_2) \sqrt{t_2/v}) dt_2 \\ &= \frac{1}{\sqrt{2\pi}} \frac{1}{\Gamma(v/2) 2^{v/2}} \int_0^\infty (e^{-(1/2)t_1^2 t_2/v} t_2^{(v/2)-1} e^{-t_2/2} \sqrt{t_2/v}) dt_2 \\ &= \frac{1}{\sqrt{2\pi}} \frac{1}{\Gamma(v/2) 2^{v/2} \sqrt{v}} \int_0^\infty (e^{-(1/2)t_2(1+t_1^2/v)} t_2^{((v+1)/2)-1}) dt_2 \end{aligned}$$

Recognize the integrand as the kernel of a gamma  $((v+1)/2, 2/(1+t_1^2/v))$

$$f_{T_1}(t_1) = \frac{1}{\sqrt{2\pi}} \frac{1}{\Gamma(v/2) 2^{v/2} \sqrt{v}} \Gamma\left(\frac{v+1}{2}\right) \left[\frac{2}{1+t_1^2/v}\right]^{(v+1)/2}$$

## 2. W-S FORMULA DERIVATION

Let  $x_1, \dots, x_n$  be a random sample from a normal distribution  $n(\mu, \delta^2)$ , then

$$s^2 = \left[\frac{1}{n-1}\right] \sum_{i=1}^n (x_i - \bar{x})^2 = \frac{\delta^2}{n-1} \sum_{i=1}^n \left(\frac{x_i - \bar{x}}{\delta}\right)^2 \quad (5)$$

Since  $u_i = \frac{x_i - \bar{x}}{\delta} \sim N(0,1)$ , i.e., standard normal distribution, we obtain  $u_i^2 \sim \chi_{(1)}^2$  and

$$s^2 \sim \frac{\delta^2}{n-1} \chi_{(n-1)}^2.$$

$$E(s^2) = \frac{\delta^2}{n-1} (n-1) = \delta^2 \quad (6)$$

$$\text{Var}(s^2) = \text{Var}\left(\frac{\delta^2}{n-1} \chi_{(n-1)}^2\right) = \left(\frac{\delta^2}{n-1}\right)^2 2(n-1) = \frac{2\delta^4}{n-1} \quad (7)$$

Define

$$S^2 = a_1 s_1^2 + \dots + a_k s_k^2 = \sum_1^k a_i s_i^2 \quad (8)$$

where the  $a_i$  are known constants (e.g.  $a_i = \left(\frac{\partial f}{\partial x_i}\right)^2$ );

$s_i$  are the variances of normal distributions  $n(\mu_i, \delta_i^2)$ , has the degrees of

freedom of  $\nu = n-1$ , and  $E(s_i^2) = \delta_i^2$

$$\text{Var}(S^2) = \text{Var}\left(\sum_1^k a_i s_i^2\right) = \sum_1^k a_i^2 \text{Var}(s_i^2) = \sum_1^k a_i^2 \frac{2\delta_i^4}{n-1} \quad (9)$$

We propose to approximate the distribution of  $S^2$  by  $R^2$ , which has a chi squared

distribution with degrees of freedom of  $f'$ ,  $\chi_{(f')}^2$ , so that they have the same expected value

and variance.

$$E(R^2) = E(S^2) = E\left(\sum_1^k a_i s_i^2\right) = \sum_1^k a_i E(s_i^2) = \sum_1^k a_i \delta_i^2 \quad (10)$$

Generally, for chi squared distribution,  $V(X) = \frac{2E(X)^2}{\text{DegreesOfFreedom}}$

$$V(R^2) = \frac{2(E(R^2))^2}{f'} = \frac{2\left(\sum_1^k a_i \delta_i^2\right)^2}{f'} \quad (11)$$

Equating (9) and (11)

$$f' = \frac{\left(\sum_1^k a_i \delta_i^2\right)^2}{\sum_1^k a_i^2 \frac{\delta_i^4}{n-1}}$$

## REFERENCES

1. Casella, George and Berger, Roger L., "Statistical Inference", 2<sup>nd</sup> Edition, ISBN 0-534-24312-6, 2001.
2. Brownlee, A. K., "Statistical Theory and Methodology in Science and Engineering", 2<sup>nd</sup> Edition, 1967.

## APPENDIX D C-FACTOR DETERMINATION<sup>1</sup>

C factor, i.e., the flow coefficient, is the relative measure of the fluid flow ability of the orifice in the exhaust duct. The flow coefficient is determined by the volume flow rate through the orifice and the pressure difference across the orifice. When holding the inlet and outlet pressures constant, the flow coefficient of a given orifice should be a constant. Figure D-1 shows the vertical part of the exhaust duct of cone calorimeter with orifice plate and the pressure ports.

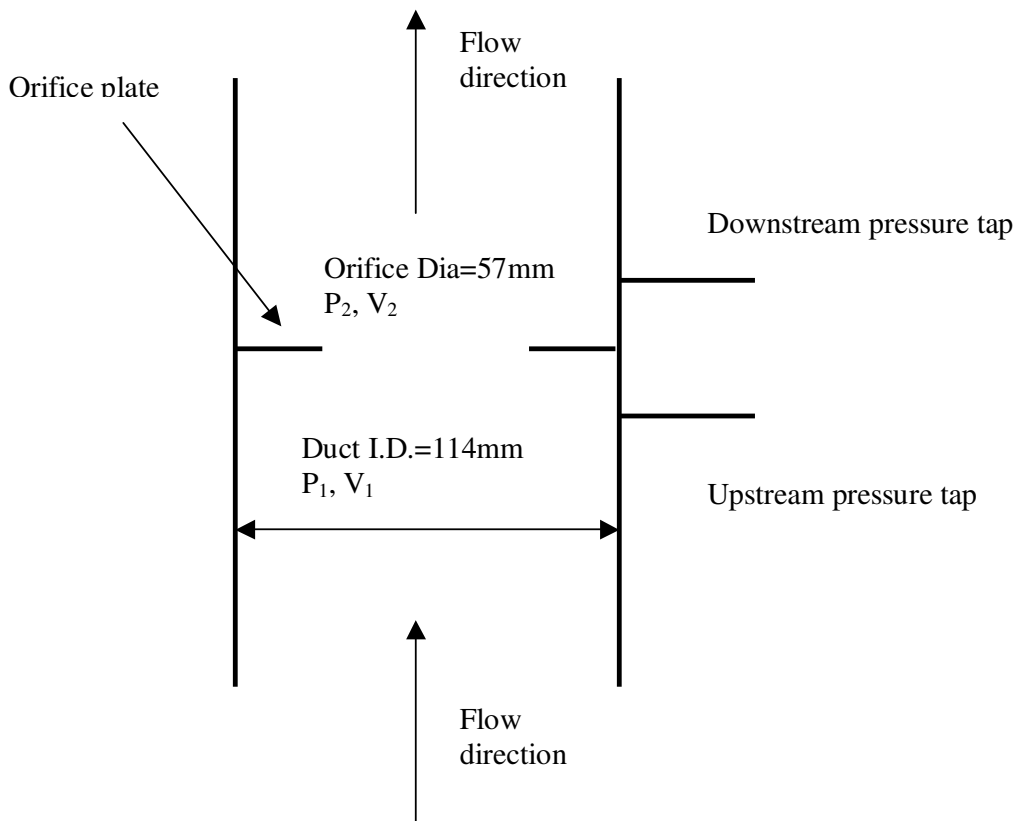


**Figure D-1 Illustration of the Vertical Part of the Exhaust Duct of Cone Calorimeter with Orifice Plate and Pressure Ports**

Since the fluid speed in the duct is sufficiently subsonic ( $<0.3\text{mach}$ ), the incompressible Bernoulli's equation describes the flow reasonably well. Applying this equation to the fluid in duct (ignore gravitational force):

$$\Delta P = P_1 - P_2 = 0.5\rho V_1^2 - 0.5\rho V_2^2$$

Along with the continuity equation

$$A_1 V_1 = A_2 V_2$$

The volumetric flow rate can be calculated as:

$$Q = A_2 \sqrt{\frac{2\Delta P}{\rho_e \left(1 - \left(\frac{A_2}{A_1}\right)^2\right)}}$$

Where:  $A_1$  is the inside diameter of duct ( $\text{m}^2$ );

$A_2$  is the diameter of the orifice ( $\text{m}^2$ );

$P_1$  is the pressure of upstream fluid (Pa);

$P_2$  is the pressure of downstream fluid (Pa);

$Q$  is the volumetric flow rate in the duct ( $\text{m}^3/\text{s}$ );

$V_1$  is the velocity of upstream fluid (m/s);

$V_2$  is the velocity of downstream fluid (m/s);

$\rho_e$  is the density of the fluid in the duct ( $\text{kg}/\text{m}^3$ );

The above equation applies only to perfectly laminar, inviscid flows. For the fluid in the duct of cone calorimeter, viscosity and turbulent are present and act to convert kinetic energy into heat. To account for this effect, a discharge coefficient  $C_d$  is introduced in to the above equation to marginally reduce the flow rate  $Q$ . Also, since the value of  $(\frac{A_2}{A_1})^2$  is very small, we ignore that in the equation:

$$Q = C_d A_2 \sqrt{\frac{2\Delta P}{\rho_e}} \quad (1)$$

It is assumed that the exhausted fluid in the duct of cone calorimeter has the same properties as air and behaves as ideal gas. The density of the fluid can be calculated as:

$$\rho_e = \rho_0 T_0 / T_e \quad (2)$$

Where:

$$\rho_0 = 1.29 \text{ kg/m}^3$$

$$T_0 = 273 \text{ K}$$

The mass flow rate can be calculated as:

$$m = C_d A_2 \rho_e \sqrt{\frac{2\Delta P}{\rho_e}} = C \sqrt{\frac{\Delta \rho}{T_e}} \quad (3)$$

The constant  $C$  value in equation (3) is the  $C$  Factor of the cone calorimeter.

## **REFERENCE**

1. Emmons, Howard W., "Vent Flows", Fire Protection Engineering Handbook, 2<sup>nd</sup> Edition, ISBN 0-87765-354-2, 1995.

## **APPENDIX E LASER PHOTODIODES POWER CYCLE INVESTIGATION**

There is a power variation in the laser photodiodes. The variation will definitely affect the uncertainty of the laser measurements. To investigate the nature of the power variation, three groups of test were conducted at different obscuration levels, i.e., 0%, 16%, 48%, and 100%. These obscuration levels are routinely checked in our day-to-day calibration activities. In all the tests, output voltage was collected once per second.

In the first group of test, the voltages were collected for 1800s for each reference obscuration level. Four files were created. In the second group test, start a data file and check various obscuration levels for 0%, 16%, 48%, and 100% for back to back 300 seconds periods. "Randomly" vary which obscuration is used for each 300-second period. After about 6000 seconds stop and close the data file. The third group data was randomly selected from the day-to-day calibration files. In the day-to-day calibration, voltage output of the reference obscuration was recorded for 60s. The power cycle phenomenon of the laser can be illustrated by Figure E-1 through Figure E-4. The four Figures were drawn by using the data from the first group.

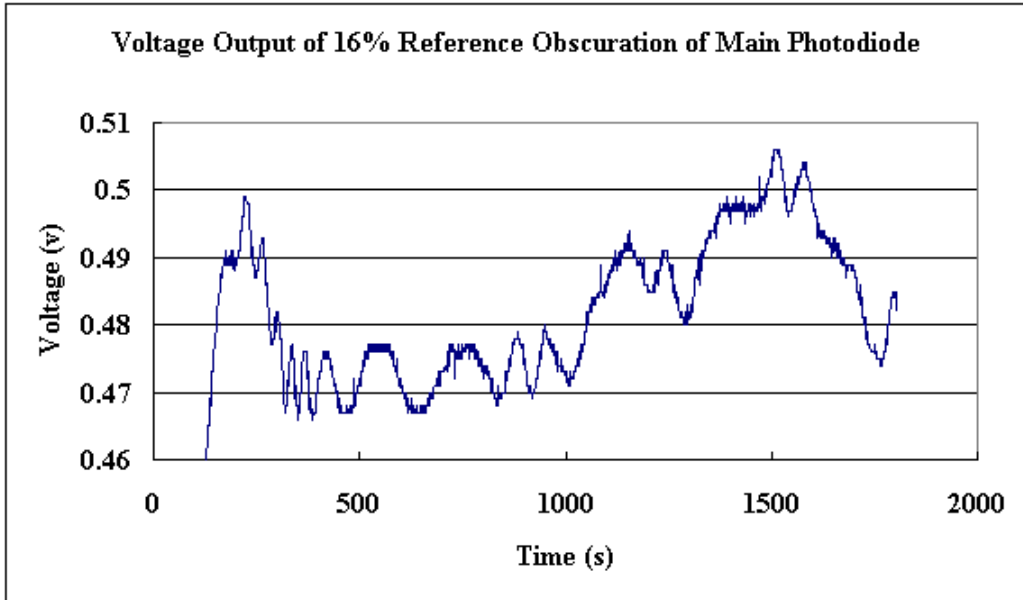


**Figure E-1 Power Cycle Illustration of Main Photodiode at 16% Reference Obscuration**

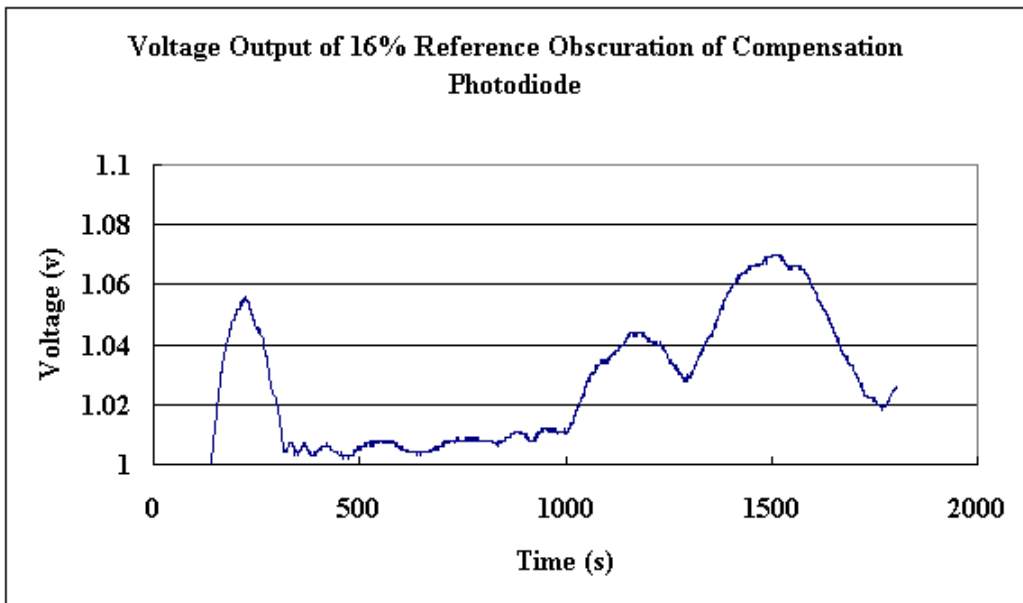


**Figure E-2 Power Cycle Illustration of Compensation Photodiode at 16% Reference Obscuration**

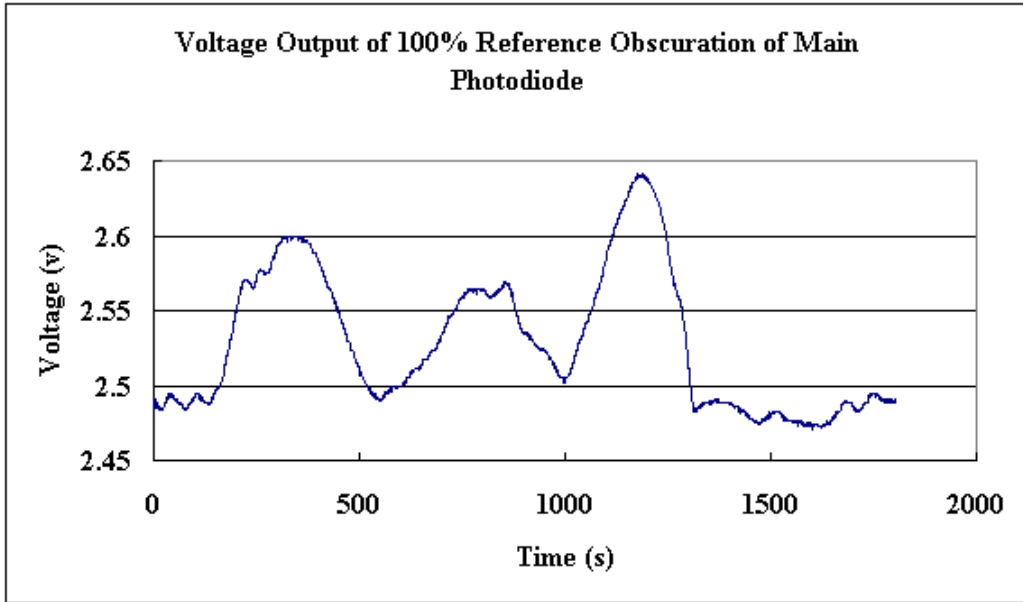


**Figure E-3 Power Cycle Illustration of Main Photodiode at 100% Reference Obscuration**

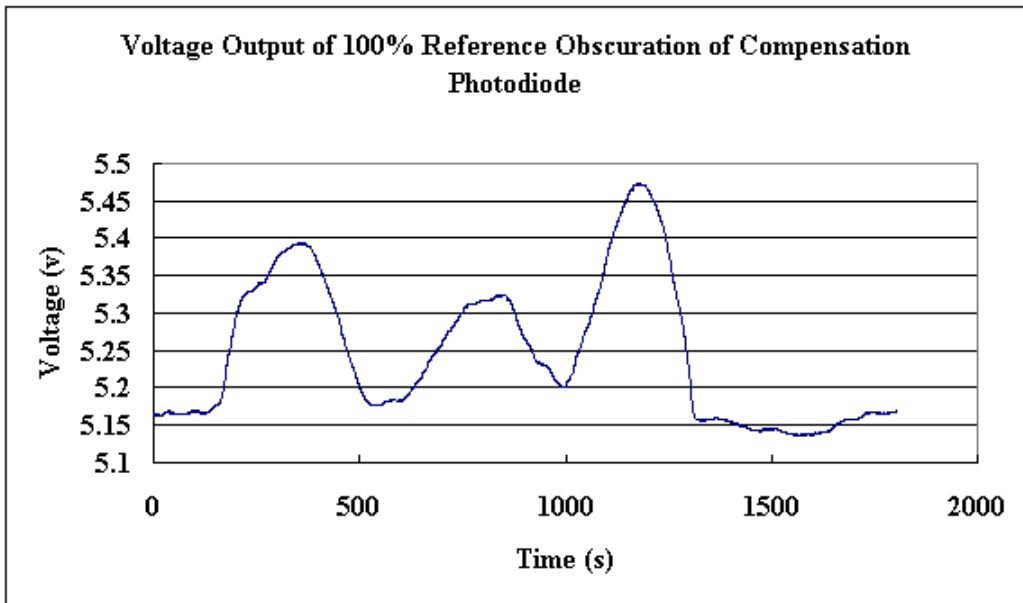


**Figure E-4 Power Cycle Illustration of Compensation Photodiode at 100% Reference Obscuration**

The average and standard deviation of the output voltage are shown in Table E-1 and Table E-2. The standard deviation is illustrated in Figure E-5 and Figure E-6.

**Table E-1 Average and Standard Deviation of Output Voltage of Main Photodiode**

Test Period	Reference Obscuration	Average (v)	Standard Deviation (v)
1800s	0%	-0.0041	0.0031
	16%	0.4780	0.0199
	48%	1.1979	0.0231
	100%	2.5289	0.0461
300s	0%	-0.0044	0.0029
	16%	0.4660	0.0124
	48%	1.2260	0.0262
	100%	2.5460	0.0324
60s	0%	-0.0034	0.0026
	16%	0.5155	0.0031
	48%	1.5732	0.0047
	100%	3.424	0.0155

**Table E-2 Average and Standard Deviation of Output Voltage of Compensation Photodiode**

Test Period	Reference Obscuration	Average (v)	Standard Deviation (v)
1800s	0%	-0.0019	0.0011
	16%	1.0181	0.0412
	48%	2.5185	0.0473
	100%	5.2474	0.0954
300s	0%	-0.0020	0.0010
	16%	0.9862	0.0248
	48%	2.5741	0.0540
	100%	5.2957	0.0665
60s	0%	-0.0002	0.0008
	16%	1.0416	0.0016
	48%	3.1979	0.0092
	100%	6.6893	0.0332

As seen in Figure E-5 and Figure E-6, the standard deviation of 60s has the smallest values at each reference obscuration. The reason for this is that 60s collected data is only a part of a period. The uncertainty analysis based on 60s data collection should be an underestimate. However, the uncertainty of laser (based on 60s data collection) propagates to related quantities, such as extinction coefficient, specific extinction area, and results in too big uncertainties for these quantities (These can be found in the corresponding Sections in the paper). The laser used in the cone calorimeter in the Fire Lab at WPI doesn't have the ability to differentiate obscuration related quantities. Therefore, a stabilized laser is needed.

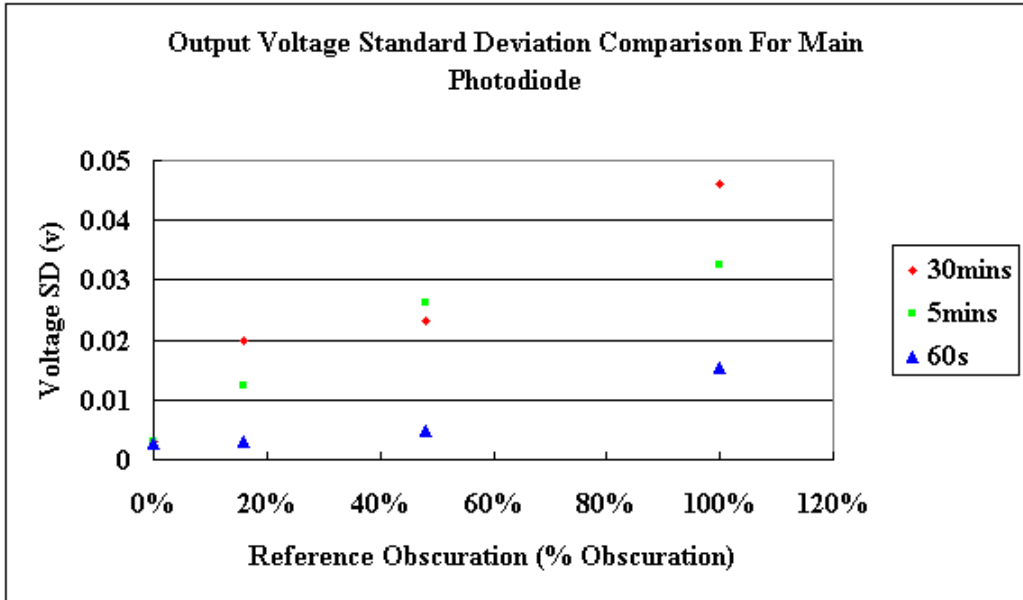


Figure E-5 Output Voltage Standard Deviation of Main Photodiode at Different Reference Obscuration Level

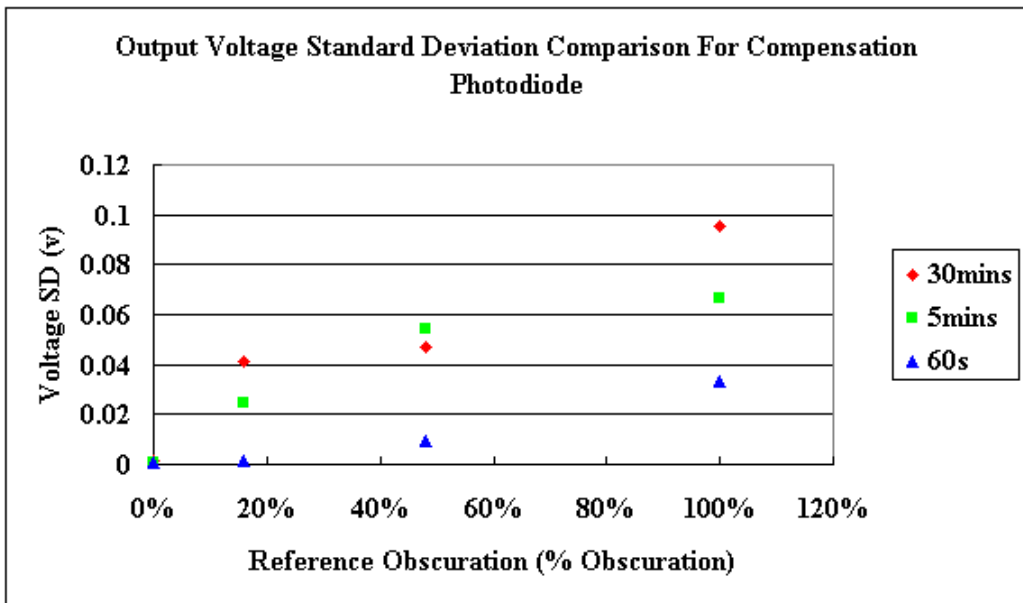


Figure E-6 Output Voltage Standard Deviation of Compensation Photodiode at Different Reference Obscuration Level

## APPENDIX F A HYPOTHETICAL CALIBRATION FOR OXYGEN ANALYZER

The oxygen analyzer is calibrated hypothetically at two points 15% and 25% oxygen.

Suppose we have two gas bottles with the oxygen concentration of 15% and 25% respectively.

The oxygen concentration uncertainty specified by the manufacturer is  $\pm 0.05\%$  oxygen. The uncertainty of the voltage output for 15% and 25% oxygen concentration is assumed to be the same as we measured from 20.9% oxygen concentration.

Since the paramagnetic oxygen analyzer was inherently linear by design based on its transducer and the function was represented by

$$O_2 \% = mV + b$$

where  $m$  is slope determined by

$$m = \frac{O_{2span} \% - O_{2zero} \%}{V_{span} - V_{zero}}$$

$b$  is intercept determined by

$$b = \frac{O_{2zero} \% V_{span} - O_{2span} \% V_{zero}}{V_{span} - V_{zero}}$$

$O_{2zero} \%$  and  $O_{2span} \%$  are defined as accepted value of the reference materials at 15% and 25% oxygen,  $V_{zero}$  and  $V_{span}$  are corresponding oxygen analyzer voltage output at 15% and 25% of oxygen concentration. The standard uncertainty of  $m$  and  $b$  is estimated according to the Law of Propagation of Uncertainty in ISO Guide<sup>1</sup> and NIST Guidelines<sup>2</sup>.

$$u_c^2(y) = \sum \left( \frac{\partial f}{\partial x_i} \right)^2 u^2(x_i)$$

The covariance terms were eliminated since the error sources were uncorrelated, i.e., the measurements didn't share errors from identical sources. Each  $u(x_i)$  was a standard uncertainty of above four direct measured quantities. Standard uncertainty is the uncertainty of the result of a measurement expressed as a standard deviation. The standard uncertainty of voltage output was estimated as

$$u(V) = \sqrt{\frac{1}{n-1} \sum_1^n (V_i - \bar{V})^2}$$

Where: N was times the voltage output recorded (60 for our case)

$$\bar{V} = \frac{V_1 + \dots + V_n}{n}$$

Since the uncertainty of each variable is known, i.e.,  $u(V_{zero}) = u(V_{span}) = 4.9 \times 10^{-5}$  are oxygen analyzer voltage output standard uncertainty at 15% and 25% oxygen respectively;  $u(O_{2zero} \%) = 0.03\%$  and  $u(O_{2span} \%) = 0.03\%$  are oxygen concentration standard uncertainty at 15% and 25% oxygen concentration respectively. The data are from a typical day-to-day calibration case. The standard uncertainty of m and b was estimated as

$$\delta m = \sqrt{\left( \frac{(O_{2zero} \% - O_{2span} \%)}{(V_{span} - V_{zero})^2} u(V_{zero}) \right)^2 + \left( \frac{(O_{2span} \% - O_{2zero} \%)}{(V_{span} - V_{zero})^2} u(V_{span}) \right)^2 + \left( \frac{-1}{V_{span} - V_{zero}} u(O_{2zero} \%) \right)^2 + \left( \frac{1}{V_{span} - V_{zero}} u(O_{2span} \%) \right)^2}$$

$$\delta b = \sqrt{\left(\frac{V_{span}(O_{2zero} \% - O_{2span} \%)}{(V_{span} - V_{zero})^2} u(V_{zero})\right)^2 + \left(\frac{V_{zero}(O_{2span} \% - O_{2zero} \%)}{(V_{span} - V_{zero})^2} u(V_{span})\right)^2 + \left(\frac{V_{span}}{V_{span} - V_{zero}} u(O_{2zero} \%)\right)^2 + \left(\frac{-V_{zero}}{V_{span} - V_{zero}} u(O_{2span} \%)\right)^2}$$

The standard uncertainty of oxygen measurement result can be represented as

$$u(O_2 \%) = k_p (\delta m V + \delta b)$$

A typical calculation showed that  $\delta m$  was approximated as 0.000106 volume fraction of oxygen per volt, and  $\delta b$  as 0.000875 volume fraction of oxygen for standard uncertainty. In our day-to-day calibration, the sampling size is 60 at both of zero and span point.

If a physics quantity  $y$  (for now,  $y$  is  $m$  or  $b$ ) is not measured directly, but is determined from  $n$  other statistically independent quantities  $x_1, \dots, x_n$  through a functional relationship  $f$  :  
 $y = f(x_1, \dots, x_n)$ ,

based on ISO<sup>1</sup> and NIST<sup>2</sup>, the coverage factor  $k_p$  of the expanded uncertainty ( $U = k_p u_c(y)$ ), which defines an interval having  $p$  level of confidence ( $p$  is usually selected to be 95%).  $k_p$  was defined by Student's  $t$  distribution based on  $\nu_{eff}$  number of effective degrees of freedom. The effective degrees of freedom was estimated by Welch-Satterthwaite formula

$$\nu_{eff} = \frac{u_c^4(y)}{\sum_{i=1}^n \frac{(\partial f / \partial x_i)^4 u^4(x_i)}{\nu_i}}$$

Where  $\nu_i$  is the degrees of freedom of  $u(x_i)$  and usually  $\nu_i = n - 1$ ,  $n$  is the sampling size.

The effective degrees of freedom calculated by using Welch-Satterthwaite formula was about 60 for both of m and b. Then, 2 was taken as the coverage factor for interval of 95% confidence, the uncertainty was expressed as

$$u(O_2 \%) = 2 \times (0.000106V + 0.000875)$$

The uncertainty is bigger than that based on 0% and 20.9% calibration.

## **REFERENCES**

1. International Organization for Standardization, "Guide to the Expression of Uncertainty in Measurement", ISBN 92-67-10188-9, 1995.
2. Taylor, B. N., and Kuyatt, C. E., Guidelines for Evaluating and Expressing the Uncertainty of NIST Measurement Results, NIST Technical Note 1297, NIST, Gaithersburg, MD, 1994.

## APPENDIX G STANDARD DEVIATION OF UNIFORM DISTRIBUTION<sup>1</sup>

The continuous uniform distribution is defined by spreading mass uniformly over an interval [a, b]. Its probability density function (pdf) is given by

$$f(x|a,b) = \frac{1}{b-a} \quad \text{if } x \in [a,b], \text{ otherwise the pdf is 0.}$$

The expected value or mean of random variable X is

$$EX = \int_{-\infty}^{\infty} xf(x)dx = \int_a^b xf(x)dx$$

For each integer n, the n<sup>th</sup> moment of X,  $\mu_n'$ , is

$$\mu_n' = EX^n$$

The n<sup>th</sup> central moment of X,  $\mu_n$  is

$$\mu_n = E(X - \mu)^n,$$

where  $\mu = \mu_1' = EX$

The variance of a random variable X is the second central moment,

$VarX = E(X - EX)^2$ . The positive square root of VarX is the standard deviation of X.

For the uniform case,

$$EX = \int_a^b \frac{x}{b-a} = \frac{a+b}{2}$$

$$\text{Var}X = E(X - EX)^2 = E[X^2 - 2XEX + (EX)^2]$$

$$= EX^2 - 2(EX)^2 + (EX)^2$$

$$= EX^2 - (EX)^2$$

$$= \int_a^b \frac{x^2}{b-a} - \left(\frac{a+b}{2}\right)^2 = \frac{(b-a)^2}{12}$$

So,

$$\text{std}(X) = +\sqrt{\text{Var}X} = \frac{b-a}{2\sqrt{3}}$$

## REFERENCE

1. Casella, George and Berger, Roger L., "Statistical Inference", 2<sup>nd</sup> Edition, ISBN 0-534-24312-6, 2001

## **APPENDIX H CONE VIs INTRODUCTION**

The cone calorimeter is a fire instrument based on the principle of oxygen consumption calorimetry. All data is acquired via the NI data acquisition system. This data is gathered using Virtual Instruments or VIs. A set of VIs for measurement uncertainty analysis is developed to allow a user to operate the cone calorimeter from start-up to shutdown. Overall uncertainty analysis methods described in Appendix A are implemented in the VIs. At the end of each test, VIs reports all the engineering units with their 95% confidence interval of component instruments and indirect measured quantities.

The process of calibration and testing is incorporated into one main VI, ConeDAQ\_uncer2.vi.

This overall VI is broken down into the following for ease of understanding and operation:

- Calibration (Calibration Procedure 1)
- C Factor (Calibration Procedure 2)
- Test
- Post-test/Shutdown

The details of each subVI are described as following:

- Calibration (Calibration Procedure 1)

1. Pre-Test/Warm Up

Complete the checklist and tick at the end of each item. Make note(s) of any maintenance in the left bottom box. Press Shift+Enter to continue.

2. Change Parameter?

Input a new value for any listed parameters that user wants to change. Press Save button to continue.

3. Smoke Calibration

Four levels of reference obscuration, 0%, 16%, 48%, and 100%, are included in the procedure. After the beginning of each obscuration check, press the red Record button, which stops the data collection after 60s. At the end of the calibration, the calibration factors and the uncertainty of laser show up. If you accept the value, press Done, otherwise, press repeat to redo the procedure.

#### Algorithm

The algorithm of this procedure is based on the “Laser” in “Uncertainty Analysis of Component Instrument” Section in Appendix A.

#### 4. Load Cell

Six levels of reference weight, 0g, 50g, 100g, 150g, 200g, and 230g, are included in the procedure. After the beginning of each check, press the red Record button, which stops the data collection after 60s. At the end of the calibration, the current calibration factors and their uncertainty, manufacturer calibration factors, and the uncertainty of load cell show up. If you accept the value, press Done, otherwise, press Repeat to redo the procedure.

#### Algorithm

The uncertainty of load cell is based on the “Load Cell” in “Uncertainty Analysis of Component Instrument” Section in Appendix A.

#### 5. Specimen Height

Complete the checklist and tick at the end of each item. Press Complete button to continue.

- C Factor (Calibration Procedure 2)

##### 1. Duct Flow and Temperature

Zero and span conditions are checked for pressure transducer. Compare the output voltage with the given range. Compare the reported temperature with the ambient temperature. At the end of the calibration, if you accept the value, press Done, otherwise, press Repeat to redo the procedure.

## 2. Oxygen Analyzer

Zero and span conditions are included in the procedure. After the beginning of each check, press the red Record button, which stops the data collection after 60s. At the end of the calibration, the current calibration factors and their uncertainty, and manufacturer calibration factors of oxygen analyzer show up. If you accept the value, press Done, otherwise, press Repeat to redo the procedure.

### Algorithm

The uncertainty of load cell is based on the “Oxygen Analyzer” in “Uncertainty Analysis of Component Instrument” Section in Appendix A.

## 3. CO/CO<sub>2</sub> Analyzer

Zero and span conditions are checked for CO/CO<sub>2</sub> analyzer. Compare the output voltage with the given range. At the end of the calibration, if you accept the value, press Done, otherwise, press Repeat to redo the procedure.

## 4. Methane Calibration

Complete each item and then make a tick at the end of the item. In this procedure, three levels of heat release rate, i.e., 1 kW, 3 kW, and 5 kW, are obtained as standards by burning methane. The heat release rates along with their uncertainties are also calculated based on the C factor value of 0.043 by oxygen consumption theory. At the end of the procedure, the calculated heat release rate and their uncertainties show up. Compare the calculated results with the standards. If you accept the value, press Done, otherwise, press Repeat to redo the procedure.

### Algorithm

The uncertainty of heat release rate calculation is based on the “Heat Release Rate” in “Uncertainty Analysis of Indirect Measurement” Section in Appendix A.

- Cone Calorimeter (Test Procedure)

Press the circle button of “Time of Shutter Open”, “Time of Ignition”, “Time of Flame Out”, and “Time of Clean Air” accordingly to conduct the test procedure. To finish test, press the red STOP button.

### Algorithm

The algorithm in the test procedure is based on Appendix A.

- Post-Test

Complete the checklist and tick at the end of each item. Press Complete button to end the overall test.

# APPENDIX I LOAD CELL SYSTEM AND LASER SYSTEM RESPONSE TIME

Load cell system refers to the devices from load cell all the way to the computer. Laser system refers to the devices from laser all the way to the computer.

## 1. Laser System Response Time

Tests were conducted by using the reference obscurations of 0% and 100%. The obscurations were tested one and the other at the scan rate of 0.2s per scan. Zero seconds response time was found for the laser system, see Figure I-1 and Figure I-2.

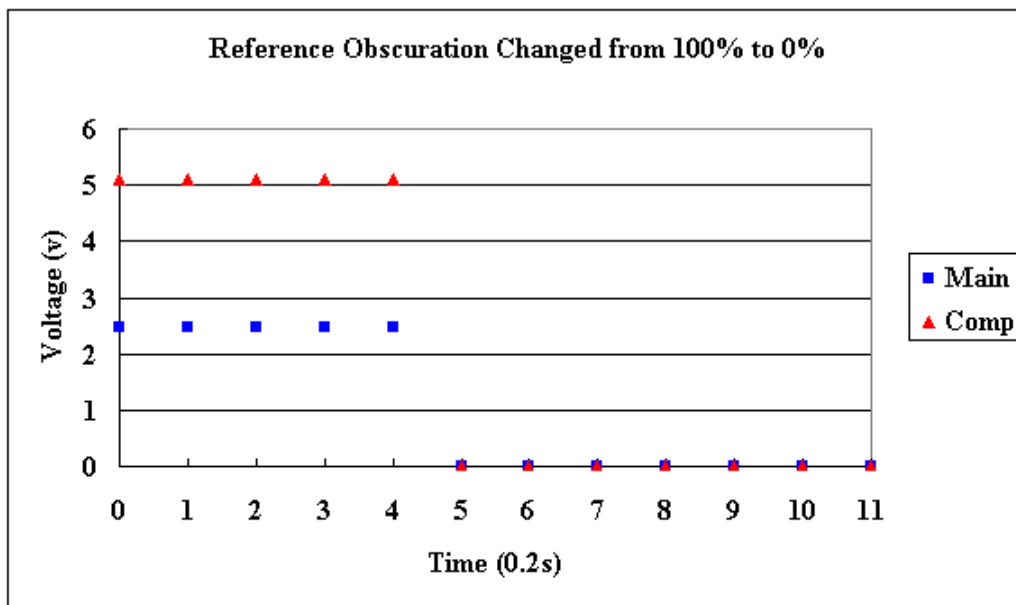


**Figure I-1 Main and Compensation Photodiodes Response Time shown by Changing from 100% Obscuration to 0% Obscuration**

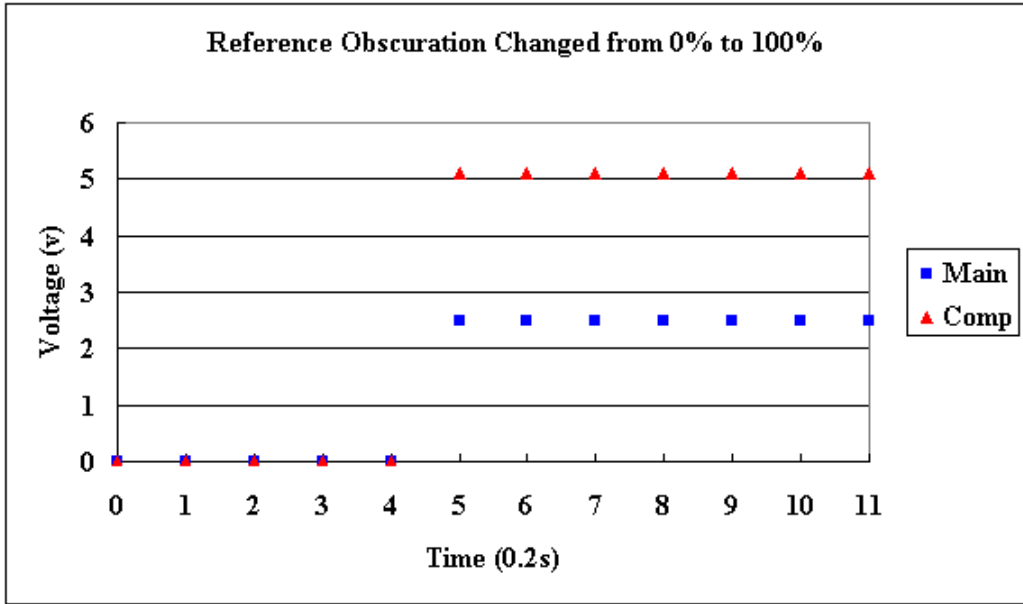


**Figure I-2 Main and Compensation Photodiodes Response Time shown by Changing from 0% Obscuration to 100% Obscuration**

## 2. Load Cell System

Tests were conducted by using two 50g reference weights. One of the weights stayed on load cell during the test. The other weight was gently dropped and taken away. The test was repeated for several times. The scanning rate is 0.2s per scan. It was found that the response time of load cell system was 0.4s to 0.6s, see the Figure I-3 and Figure I-4.

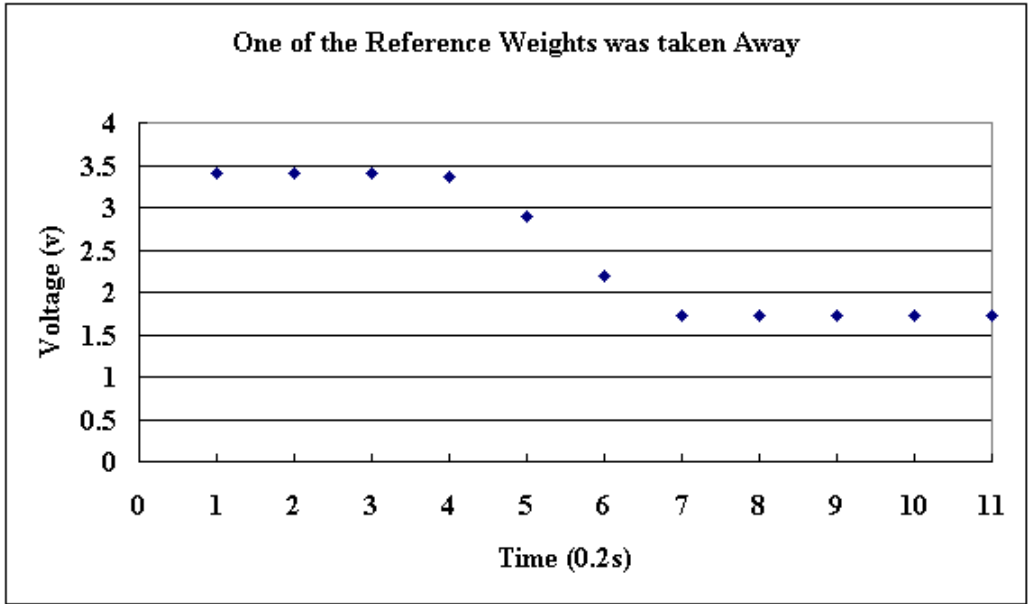


Figure I-3 Load Cell System Response Time by Weight dropped on the Load Cell

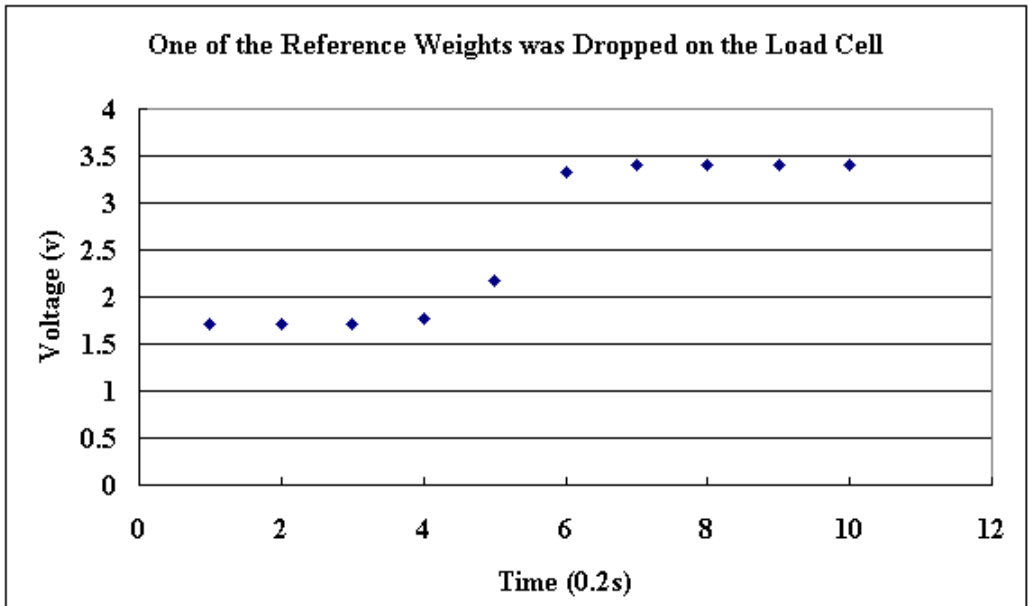


Figure I-4 Load Cell System Response Time by Weight Taken Away from the Load Cell

## APPENDIX J JUSTIFICATION OF UNCERTAINTY PROPAGATION EQUATION<sup>1</sup>

Suppose that, in order to find a value for the function  $q(x, y, \dots)$ , we measure the quantities  $x, y, \dots$ , several times, obtaining  $n$  pairs of data,  $(x_1, y_1, \dots), \dots, (x_n, y_n, \dots)$ . From the data, we can compute the mean  $[x], [y], \dots$ , standard deviation of  $x, y, \dots$  values  $\delta x, \delta y, \dots$ . Also, using the data, we can compute  $n$  values of the quantity of interest

$$q_i = q(x_i, y_i, \dots)$$

Given  $q_i$ , we can now calculate their mean  $[q]$ , and the standard deviation  $\delta q$ .

We consider that all the uncertainties are small so that it may be represented by the first few terms in a Taylor series expansion of  $q$  about points  $x, y, \dots$

$$q_i \approx q(x_i, y_i, \dots) = q([x], [y], \dots) + \frac{\partial q}{\partial x}(x_i - [x]) + \frac{\partial q}{\partial y}(y_i - [y]) + \dots \quad (1)$$

In this expression the partial derivatives are taken at the point  $[x], [y], \dots$

The best estimation of  $q$  can be taken as the average of  $q_i$

$$[q] = \frac{1}{n} \sum q_i = \frac{1}{n} \sum \{q([x], [y], \dots) + \frac{\partial q}{\partial x}(x_i - [x]) + \frac{\partial q}{\partial y}(y_i - [y]) + \dots\}$$

By definition

$$[x] = \frac{x_1 + \dots + x_n}{n}$$

So,

$$\sum (x_i - [x]) = 0$$

Thus we have the simple result

$$[q]=q([x], [y], \dots) \quad (2)$$

The standard deviation of q is calculated as

$$\begin{aligned} \delta_q^2 &= \frac{1}{n} \sum (q_i - [q])^2 \\ &= \frac{1}{n} \sum \left\{ \frac{\partial q}{\partial x} (x_i - [x]) + \frac{\partial q}{\partial y} (y_i - [y]) + \dots \right\}^2 \\ &= \left( \frac{\partial q}{\partial x} \right)^2 \frac{1}{n} \sum (x_i - [x])^2 + \left( \frac{\partial q}{\partial y} \right)^2 \frac{1}{n} \sum (y_i - [y])^2 + \dots + 2 \frac{\partial q}{\partial x} \frac{\partial q}{\partial y} \frac{1}{n} \sum (x_i - [x])(y_i - [y]) + \dots \\ &= \left( \frac{\partial q}{\partial x} \right)^2 \delta_x^2 + \left( \frac{\partial q}{\partial y} \right)^2 \delta_y^2 + \dots + 2 \frac{\partial q}{\partial x} \frac{\partial q}{\partial y} \delta_{xy} + \dots \end{aligned} \quad (3)$$

where:  $\delta_x$  is the standard deviation of x

$\delta_y$  is the standard deviation of y

$\delta_{xy} = \frac{1}{n} \sum (x_i - [x])(y_i - [y])$  is called covariance of x and y.

#### Discussion 1

If the uncertainties of x, y, ... are independent and random, on the average, we should expect to find equal distributions of positive and negative values for each the covariance term in

equation (3). Therefore, we should expect the term to vanish in finite number of observations.

This is often a reasonable approximation and equation then reduces to

$$\delta_q = \sqrt{\left(\frac{\partial q}{\partial x} \delta_x\right)^2 + \left(\frac{\partial q}{\partial y} \delta_y\right)^2 + \dots} \quad (4)$$

## Discussion 2

If the measurements of  $x$ ,  $y$ , ... are not independent, then covariance need not to be zero. For instance, it is easy to imagine a situation where an overestimate of  $x$  will always be accompanied by an overestimate of  $y$ , ..., and vice versa. The value of covariance will always be positive. When the covariance is not zero, we say that the errors in  $x$  and  $y$  are correlated.

Suppose an arbitrary number  $t$  and consider the function

$$A(t) = \frac{1}{n} \sum \{(x_i - [x]) + t(y_i - [y])\}^2 \geq 0$$

Since  $A(t)$  is positive whatever the value of  $t$ , the minimum value  $A_{\min}$  can be found by setting its derivative  $dA/dt$  equal to zero, and this  $A_{\min}$  is still greater than or equal to zero.

$$A(t) = \delta_x^2 + 2t\delta_{xy} + t^2\delta_y^2$$

$$\frac{dA}{dt} = 2\delta_{xy} + 2t\delta_y^2$$

$A_{\min}$  will be obtained when  $dA/dt$  equal to zero, i.e.,  $t = -\frac{\delta_{xy}}{\delta_y^2}$ .

So,

$$A_{\min} = \delta_x^2 - \left(\frac{\delta_{xy}^2}{\delta_y^2}\right) \geq 0, \text{ hence, } |\delta_{xy}| \leq \delta_x \delta_y$$

Equation (3) then can be rewritten as

$$\delta_q^2 \leq \left(\frac{\partial q}{\partial x}\right)^2 \delta_x^2 + \left(\frac{\partial q}{\partial y}\right)^2 \delta_y^2 + \dots + 2 \left|\frac{\partial q}{\partial x} \frac{\partial q}{\partial y}\right| \delta_x \delta_y + \dots = \left(\left|\frac{\partial q}{\partial x}\right| \delta_x + \left|\frac{\partial q}{\partial y}\right| \delta_y + \dots\right)^2$$

$$\delta_q \leq \left|\frac{\partial q}{\partial x}\right| \delta_x + \left|\frac{\partial q}{\partial y}\right| \delta_y + \dots \quad (5)$$

Whether or not the errors in  $x, y, \dots$  are independent, and whether or not they are normally distributed, the uncertainty in  $q$  will never exceed the RHS of equation (5).

## REFERENCE

1. Taylor, John R., "An Introduction to Error Analysis", 2<sup>nd</sup> Edition, 1997.

## APPENDIX K HRR UNCERTAINTY BASED ON METHANE

The methane mass flow meter was manufactured by Teledyne Hastings-Raydist. The accuracy is 1% of full scale (0-25 SLPM). The manufacturer's calibration factor is  $y = 0.0833x$ .  $y$  is the flow rate in l/s,  $x$  is the voltage output in volt. We assume the voltage output is normally distributed and manufacturer specified uncertainty has 95% confidence. The standard uncertainty is estimated as 0.00208 l/s ( $25 \times 1\% / 60 / 2$ ). Gas phase methane density at 1.013 bar and 25C is 0.657 g/l. Therefore, the standard mass flow rate uncertainty is 0.00137 g/s ( $0.00208 \times 0.657$ ).

The purity of the methane in bottle is at least 99.5% based on ASTM E 1354<sup>1</sup>. We assume methane concentration has uniform distribution with 99.75% average concentration in the range of 99.5% to 100%. The heat of combustion of methane is 50 kJ/g. The standard uncertainty is 0.072 kJ/g ( $50 \times 0.5\% / 2 / 50 \times 0.5\% / 2 \sqrt{3}^{2,3}$ ).

HRR based on methane flow rate is determined as

$$HRR(CH_4) = MassFlowRate \times HoC$$

With the standard uncertainty of mass flow rate and heat of combustion estimated above, the HRR uncertainty can be estimated by using the following equation of Law of Propagation of Uncertainty recommended by ISO and NIST Guide<sup>2,3</sup>

$$u(HRR) = \sqrt{(\delta(MassFlowRate) * HoC)^2 + (\delta(HoC) * MassFlowRate)^2}$$

where  $\delta(MassFlowRate)$  and  $\delta(HoC)$  are the standard uncertainty of mass flow rate and heat of combustion respectively.

Then, the HRR uncertainty with 95% confidence is pressed as  $2u(HRR)$ , where 2 is the coverage factor of 95% confidence with large degrees of freedom.

Based on above information the HRR uncertainty with 95% confidence from methane is calculated as a constant 0.14 kW for 1, 3, and 5 kW of HRR.

## **REFERENCES**

1. ASTM E 1354, “Standard Test Method for Heat and Visible Smoke Release Rates for Materials and Products Using an Oxygen Consumption Calorimeter”, Annual Book of ASTM Standards, American Society for Testing Materials, Philadelphia, PA. 2002.
2. International Organization for Standardization, “Guide to the Expression of Uncertainty in Measurement”, ISBN 92-67-10188-9, 1995.
3. Taylor, B. N., and Kuyatt, C. E., Guidelines for Evaluating and Expressing the Uncertainty of NIST Measurement Results, NIST Technical Note 1297, NIST, Gaithersburg, MD, 1994.

## **APPENDIX L BACKGROUND OF UNCERTAINTY ANALYSIS RELATED TO RECOMMENDED METHODOLOGIES**

In the field of measurement uncertainty analysis, National Bureau of Standards (now NIST) has provided leadership dating all the way back to Mayo Hershey in 1911<sup>1</sup>. Then, scientists from NIST and other organizations have provided a wealth of noteworthy papers and reports on this topic. However, they encountered a big challenge when trying to reach a consensus on the expression of uncertainty. The vast majority of NIST measurement results are accompanied by quantitative statements of uncertainty, but there has never been a uniform approach at NIST to the expression of uncertainty<sup>2</sup>. Similarly, the world's highest authority in metrology CIPM (International Committee for Weights and Measures) also recognized the lack of international consensus on the expression of uncertainty in measurement. Both organizations decided to make their contributions to resolve this problem. In 1977, CIPM requested BIPM (International Bureau of Weights and Measures) to address the problem in conjunction with the national standards laboratories and to make a recommendation. A working group on the Statement of Uncertainties, which was attended by experts from 11 national standards laboratories, developed Recommendation INC-1 (1980), Expression of Experimental Uncertainties. The CIPM approved the Recommendation in 1981 and reaffirmed it in 1986. The latest ISO Guide<sup>3</sup> establishes general rules for evaluating and expressing uncertainty in measurement that are intended to be applicable to a broad spectrum of measurements. The basis of the Guide is Recommendation 1 (CI-1981) of CIPM and Recommendation INC-1 (1980) of the working group on the Statement of Uncertainties. The Guide was prepared by a joint working group consisting of experts nominated by the BIPM, IEC (International Electrotechnical Committee), ISO and OIML (International Organization of Legal Metrology). Instead of categorizing uncertainties as either systematic (bias) or

random (precision), the uncertainty is divided into type A and type B uncertainties in the current Guide. Later, NIST Ad Hoc Committee on Uncertainty Statements was established in 1992 to address this issue. Then, the first edition of NIST Technical Note (TN 1297), i.e., NIST uncertainty standard<sup>4</sup> was initially published in 1993. The latest 1994 edition was published in order to recognize the official publication of the ISO Guide to the Expression of Uncertainty in Measurement on which TN 1297 is based<sup>2</sup>. The 1994 edition is in full harmony with the ISO standard. The guide uses expanded uncertainty  $U$  to report the results of all NIST measurements other than those for which standard deviation ( $U_c(y)$ ) has traditionally been employed. To be consistent with current international practice, the coverage factor value  $k_p$  ( $U = k_p U_c(y)$ ) is, by convention,  $k_p = 2$  for large sampling size ( $N \geq 10$ )<sup>5</sup>. Values of  $k_p$  other than 2 are determined by using Student's t distribution with  $p$  level of confidence and  $\nu_{eff}$  degrees of freedom.  $\nu_{eff}$  was estimated by using Welch-Satterthwaite formula<sup>2,6</sup>.

ISO 11095<sup>7</sup> introduces a methodology of calibrating an instrument by using reference materials. Four assumptions were made: 1) there is no error in the accepted values of the reference materials (RMs); 2) calibration function is linear; 3) repeated measurements of a given reference material are independent and normally distributed; and 4) the residual is either constant or proportional to the accepted value of the reference material. Then, the interval with 95% confidence can be estimated. The details of the method will be introduced in next section.

Above methodologies recommended by ISO<sup>6</sup> and NIST<sup>2</sup> Guides were based on a marvelous theorem—Central Limit Theorem. The theorem may be expressed as: Given a population of values with a finite variance, if we take independent samples from this population, all of size  $n$ , then the population formed by the average of these samples will tend to have a normal

distribution, regardless of what the distribution is of the original population. Mathematically, CLT is an asymptotic law, i.e., the complete identity with the normal distribution actually never takes place (unless the original population is itself normal), but it approached more and more as N increases. The restriction that the population from which the samples are taken must have a finite variance is of no practical importance, since all but a few very special populations possess finite variances. The Guides tell us that if  $y = f(x_1, \dots, x_n)$  can be expressed by the first order of Taylor series expansion, according to CLT, y is approximated to be normally distributed.

The Monte Carlo Simulation technique is any method which solves a problem by generating suitable random numbers and observing that fraction of the numbers obeying some property or properties. The method is useful for obtaining numerical solutions to problems which are too complicated to solve analytically<sup>8</sup>.

Another useful theory was shown by Steele et al<sup>9</sup>. They demonstrated that the determination of precision uncertainty is described for experiments where the test measurements are obtained from single or from a limited number of independent readings. For these cases, the limits of precision uncertainty are best determined from previous experience.

## **REFERENCES**

1. Abernethy, Robert B., The History and Statistical Development of the New ASME-SAE-AIAA-ISO Measurement Uncertainty Methodology, AIAA/SAE/ASME/ASEE Propulsion Conference, 1985.
2. Taylor, B. N., and Kuyatt, C. E., Guidelines for Evaluating and Expressing the Uncertainty of NIST Measurement Results, NIST Technical Note 1297, NIST, Gaithersburg, MD, 1994.

3. International Organization for Standardization, Guide to the Expression of Uncertainty in Measurement, ISBN 92-67-10188-9, ISO, Geneva, 1993. (Corrected and reprinted, 1995)
4. Taylor, B. N., and Kuyatt, C. E., Guidelines for Evaluating and Expressing the Uncertainty of NIST Measurement Results, NIST Technical Note 1297, NIST, Gaithersburg, MD, 1993.
5. Coleman, H. W. and Steele, W. G., “Experimentation and Uncertainty Analysis for Engineers” 2<sup>nd</sup> Edition, 1998.
6. International Organization for Standardization, “Guide to the Expression of Uncertainty in Measurement”, ISBN 92-67-10188-9, 1995.
7. International Organization for Standardization, “Linear Calibration Using Reference Materials”.
8. Eric W. Weisstein, “Monte Carlo Method”, From Mathworld—A Wolfram Web Resource, <http://mathworld.wolfram.com/MonteCarloMethod.html>
9. Steele, W. G., Taylor, R. P., Burrell R. E. and Coleman H. W., “Use of Previous Experience to Estimate Precision Uncertainty of Small Sample Experiments”, AIAA Journal, Vol 31, 10, October 1993.

## APPENDIX M MEASUREMENT ERROR AND UNCERTAINTY

Measurement Uncertainty is a parameter, associated with the result of a measurement, that characterizes the dispersion of the values that could reasonably be attributed to the measurand<sup>1</sup>. The parameter may be a standard deviation or the half-width of an interval having a stated level of confidence. Measurement error is the result of a measurement minus a true value of the measurand<sup>1</sup>. The total measurement error consists of two components: systematic and random error, see Figure M-1.

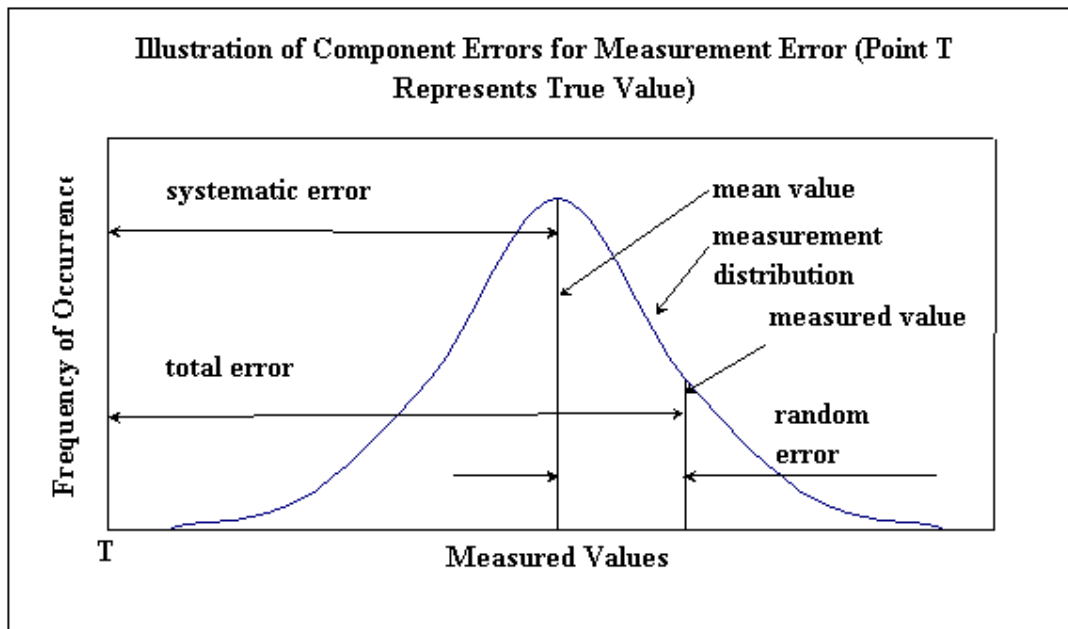


**Figure M-1 Illustration of Systematic Error, Random Error and Total Measurement Error (The Figure is Modified from Figure 4.1 of Test Uncertainty<sup>2</sup>)**

Since the true value cannot be known and therefore only its limits, i.e., its uncertainty can be estimated. ISO Guide<sup>1</sup> groups uncertainty components into two categories based on their method of evaluation, “Type A” and “Type B”. Type A uncertainty is obtained by the statistical analysis of series of observations. Type B uncertainty is obtained by means other

than the statistical analysis of series of observations<sup>1</sup>. These categories apply to uncertainty and are not substitutes for the words “random” and “systematic”. The uncertainty for a known effect may in some cases be obtained by a Type A evaluation while in other cases by a Type B evaluation, as may the uncertainty characterizing a random effect<sup>1</sup>. The purpose of the Type A and Type B classification is to indicate the two different ways of evaluating uncertainty components and is for convenience of discussion only. The classification is not meant to indicate that there is any difference in the nature of the components resulting from the two types of evaluation<sup>1</sup>.

## **REFERENCES**

1. International Organization for Standardization, “Guide to the Expression of Uncertainty in Measurement”, ISBN 92-67-10188-9, 1995.
2. ASME, “Test Uncertainty”, PTC 19.1-1998.

## APPENDIX N MASS LOSS RATE UNCERTAINTY

MLR is calculated using 5-point numerical differentiation method recommended by ASTM E-1354<sup>1</sup>:

$$MLR = \frac{-m_{i-2} + 8m_{i-1} - 8m_{i+1} + m_{i+2}}{12\Delta t}$$

where:  $\Delta t$  is 1 second.

In the burning test, the mass decreases as the time increases, i.e., it should be identified as a time series measurement. Time series is defined as an ordered sequence of values of a variable at equally spaced time intervals<sup>2</sup>. For now, MLR uncertainty was determined experimentally (statistically). Five similar PMMA burning tests were replicated. The mass loss rates were averaged out for the steady state burning duration. Then, the standard uncertainty of MLR was calculated based on the standard deviation of the means. The value turned out to be 0.58 g/sm<sup>2</sup>. The uncertainty was approximated at PMMA steady state burning rate duration about 23 g/sm<sup>2</sup>. Was the uncertainty able to represent the uncertainty at different burning rate level? It is not fully understood and will be put in the future work (see Appendix K). Based on the standard uncertainty, MLR of 2mm red oak at 40 kW/m<sup>2</sup> external heat flux with its 95% confidence interval was shown in Figure N-1. According to the t distribution, the uncertainty of 95% confidence of 5 degrees of freedom is 0.58\*2.57=1.5 g/sm<sup>2</sup>.

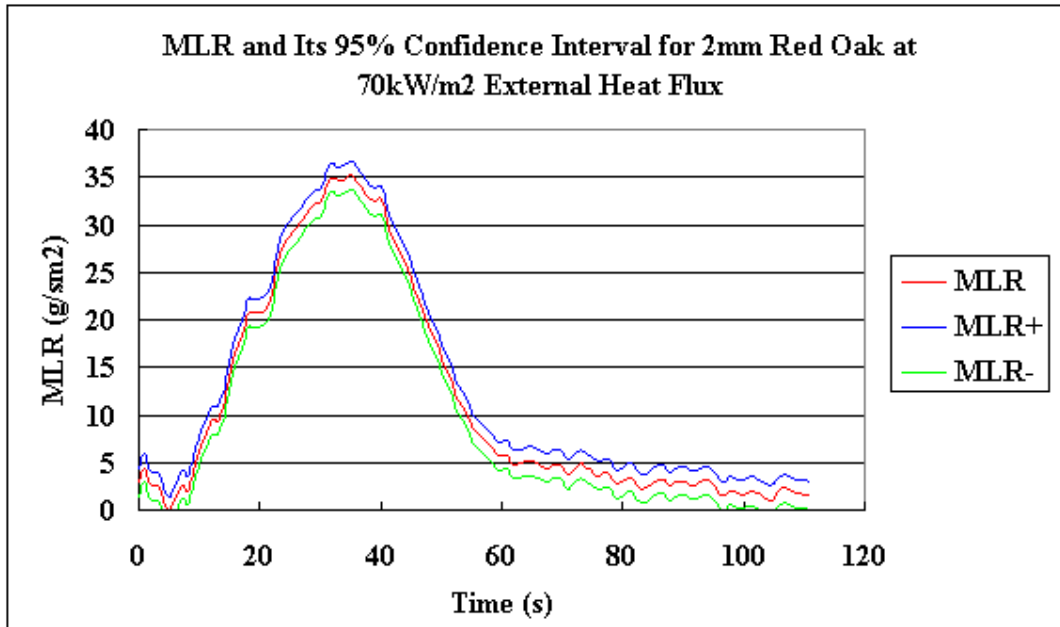


**Figure N-1 MLR and Its 95% Confidence Interval of 2mm Red Oak at 70 kW/m<sup>2</sup> External Heat Flux in Cone Test**

## REFERENCES

1. ASTM E 1354, "Standard Test Method for Heat and Visible Smoke Release Rates for Materials and Products Using an Oxygen Consumption Calorimeter", Annual Book of ASTM Standards, American Society for Testing Materials, Philadelphia, PA. 2002.
2. NIST/SEMATECH e-Handbook of Statistical Methods, <http://www.itl.nist.gov/div898/handbook/>, Nov.1<sup>st</sup>, 2004.

## APPENDIX O SENSITIVITY ANALYSIS FOR HRR

The SC value of each parameter is calculated by using the Equation recommended by NIST

$$SC_i = \left| \frac{\partial y}{\partial x_i} \frac{x_i}{y} \right|_1$$

and the calculation details are shown in the following equations

$$SC_{\Delta h_c / r_0} = \left| \frac{\partial(HRR)}{\partial(\Delta h_c / r_0)} \frac{(\Delta h_c / r_0)}{HRR} \right|$$

$$= 1.10C \sqrt{\frac{\Delta P(t)}{T(t)} \frac{X_{O_2}^0 - X_{O_2}(t)}{1.105 - 1.5X_{O_2}(t)}} \left[ \left( \frac{\Delta h_c}{r_0} \right) 1.10C \sqrt{\frac{\Delta P}{T} \frac{X_{O_2}^0 - X_{O_2}(t)}{1.105 - 1.5X_{O_2}(t)}} \right]^{-1} (\Delta h_c / r_0) = 1$$

$$SC_c = \left| \frac{\partial(HRR)}{\partial C} \frac{C}{HRR} \right|$$

$$= \left( \frac{\Delta h_c}{r_0} \right) 1.10 \sqrt{\frac{\Delta P(t)}{T(t)} \frac{X_{O_2}^0 - X_{O_2}(t)}{1.105 - 1.5X_{O_2}(t)}} \left[ \left( \frac{\Delta h_c}{r_0} \right) 1.10C \sqrt{\frac{\Delta P}{T} \frac{X_{O_2}^0 - X_{O_2}(t)}{1.105 - 1.5X_{O_2}(t)}} \right]^{-1} C = 1$$

$$SC_p = \left| \frac{\partial(HRR)}{\partial P} \frac{P}{HRR} \right|$$

$$= 0.5 \left( \frac{\Delta h_c}{r_0} \right) 1.10C \sqrt{\frac{1}{\Delta P(t)T(t)} \frac{X_{O_2}^0 - X_{O_2}(t)}{1.105 - 1.5X_{O_2}(t)}}$$

$$\left[ \left( \frac{\Delta h_c}{r_0} \right) 1.10C \sqrt{\frac{\Delta P}{T} \frac{X_{O_2}^0 - X_{O_2}(t)}{1.105 - 1.5X_{O_2}(t)}} \right]^{-1} P = 0.5$$

$$SC_T = \left| \frac{\partial(HRR)}{\partial T} \frac{T}{HRR} \right|$$

$$= 0.5 \left( \frac{\Delta h_c}{r_0} \right) 1.10C \sqrt{\frac{\Delta P(t)}{T(t)^3} \frac{X_{O_2}^0 - X_{O_2}(t)}{1.105 - 1.5X_{O_2}(t)}} \left[ \left( \frac{\Delta h_c}{r_0} \right) 1.10C \sqrt{\frac{\Delta P}{T} \frac{X_{O_2}^0 - X_{O_2}(t)}{1.105 - 1.5X_{O_2}(t)}} \right]^{-1} T = 0.5$$

$$SC_{X_{O_2}(t)} = \left| \frac{\partial(HRR)}{\partial X_{O_2}(t)} \frac{X_{O_2}(t)}{HRR} \right|$$

$$= \left( \frac{\Delta h_c}{r_0} \right) 1.10C \sqrt{\frac{\Delta P(t)}{T(t)} \frac{1.5X_{O_2}^0 - 1.105}{[1.105 - 1.5X_{O_2}(t)]^2}} \left[ \left( \frac{\Delta h_c}{r_0} \right) 1.10C \sqrt{\frac{\Delta P}{T} \frac{X_{O_2}^0 - X_{O_2}(t)}{1.105 - 1.5X_{O_2}(t)}} \right]^{-1} O_2(t)$$

$$= \frac{O_2(t)(1.5X_{O_2}^0 - 1.105)}{(1.105 - 1.5X_{O_2}(t))(X_{O_2}^0 - X_{O_2}(t))}$$

The values are shown in Table O-1. In principle, SC was indicating how many percent change for HRR if there is 1% change for a component variable  $x_i$ . As seen in Table O-1, HRR was most sensitive to oxygen volume fraction, i.e., HRR would change 10% to 420% if there was 1% change of oxygen volume fraction. 10% HRR change corresponded to higher level of HRR, while 420% corresponded to lower level of HRR. The higher level of HRR corresponds to 19% of oxygen concentration and the 1% of variation is 0.19% oxygen. The lower level of HRR corresponds to 20.9% of oxygen concentration and the 1% of variation is 0.209% oxygen. The SC was calculated by assuming the oxygen concentration in the incoming air was 20.95% oxygen. It showed that the sensitivity of oxygen volume fraction to HRR increased when HRR decreased.

**Table O-1 SC of Each variable Being Used to Calculate HRR**

	$\frac{\Delta h_c}{r_0}$	C	P	T	$X_{O_2}(t)$ (19%-20.9%)
SC	1	1	0.5	0.5	10 to 420

## **REFERENCE**

1. Bryant, Rodney A., Ohlemiller, Thomas J., Johnsson, Erik L., Hammins, Anthony, Grove, Brian S., Guthrie, William F., Maranghides, Alexander, and Mulholland George W., “The NIST 3 Megawatt Quantitative Heat Release Rate Facility”, NIST Special Publication 1007, December 2003.

## APPENDIX P VOLUME FLOW RATE

Assuming gas in the duct is ideal, volume flow rate can be represented

$$\dot{V} = \frac{C}{353} \sqrt{\Delta P T}$$

Then the uncertainty of volume flow rate can be calculated as following

$$\frac{\partial \dot{V}}{\partial C} = \frac{\sqrt{\Delta P T}}{353} \quad (1)$$

$$\frac{\partial \dot{V}}{\partial (\Delta P)} = \frac{C}{706} \sqrt{\frac{T}{\Delta P}} \quad (2)$$

$$\frac{\partial \dot{V}}{\partial T} = \frac{C}{706} \sqrt{\frac{\Delta P}{T}} \quad (3)$$

The dynamic VFR can be estimated by substituting equations (1)-(3) into the Law of Propagation of Uncertainty recommended by ISO<sup>1</sup> and NIST Guide<sup>2</sup>, i.e.,

$$u_c^2(y) = \sum \left( \frac{\partial f}{\partial x_i} \right)^2 u^2(x_i)$$

then, the uncertainty with 95% confidence is expressed as

$$VFR \pm 2u_c(VFR)$$

A typical VFR calculation for 38mm red oak at 40 kW/m<sup>2</sup> external heat flux is shown in Figure P-1. We have 95% confidence of the uncertainty. The 95% confidence interval was 0.022 to 0.026 m<sup>3</sup>/s, which was the range specified in the ASTM E 1354<sup>3</sup>.

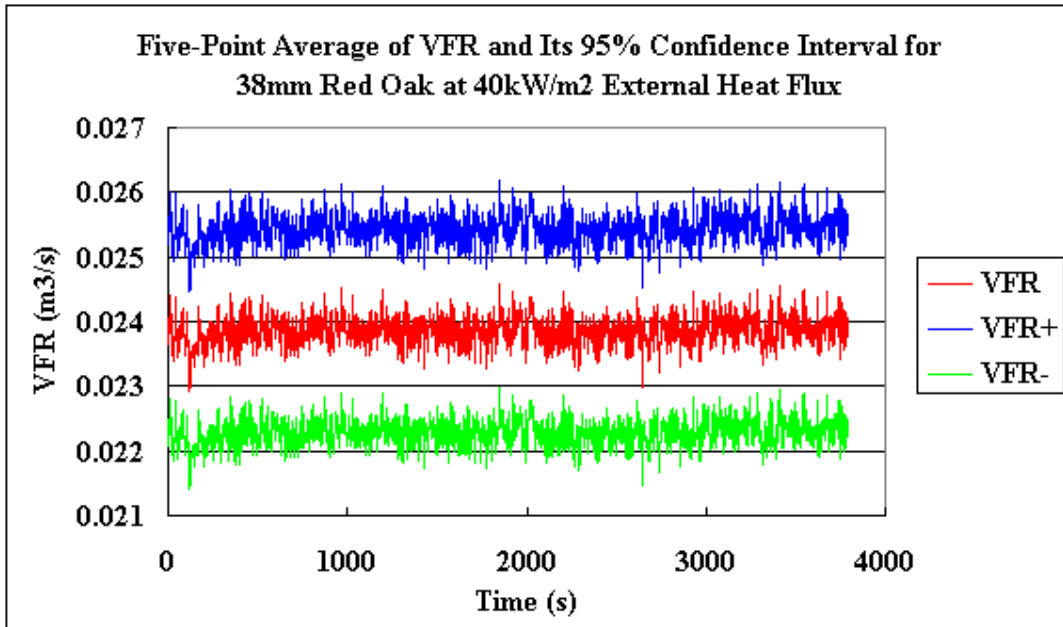


**Figure P-1 Five-point Average of Volume Flow Rate and Its 95% Confidence of Interval for 38mm Red Oak at 40 kW/m<sup>2</sup> External Heat Flux in Cone Test**

The SC value of each parameter is calculated by using the Equation recommended by NIST

$$SC_i = \left| \frac{\partial y}{\partial x_i} \frac{x_i}{y} \right|_4$$

and the calculation details are shown in the following equations

$$SC_c = \left| \frac{\partial(VFR)}{\partial C} \frac{C}{VFR} \right| = \frac{\sqrt{\Delta PT}}{353} \left[ \frac{C}{353} \sqrt{\Delta PT} \right]^{-1} C = 1$$

$$SC_{\Delta P} = \left| \frac{\partial(VFR)}{\partial(\Delta P)} \frac{\Delta P}{VFR} \right| = \frac{C}{706} \sqrt{\frac{T}{\Delta P}} \left[ \frac{C}{353} \sqrt{\Delta P T} \right]^{-1} (\Delta P) = 0.5$$

$$SC_T = \left| \frac{\partial(VFR)}{\partial T} \frac{T}{VFR} \right| = \frac{C}{706} \sqrt{\frac{\Delta P}{T}} \left[ \frac{C}{353} \sqrt{\Delta P T} \right]^{-1} (T) = 0.5$$

The SC is shown in Table P-1. As seen in Table P-1, volume flow rate is most sensitive to C factor.

**Table P-1 SC of Each Variable Being Used to Calculate VFR**

	C Factor	P	T
SC	1	0.5	0.5

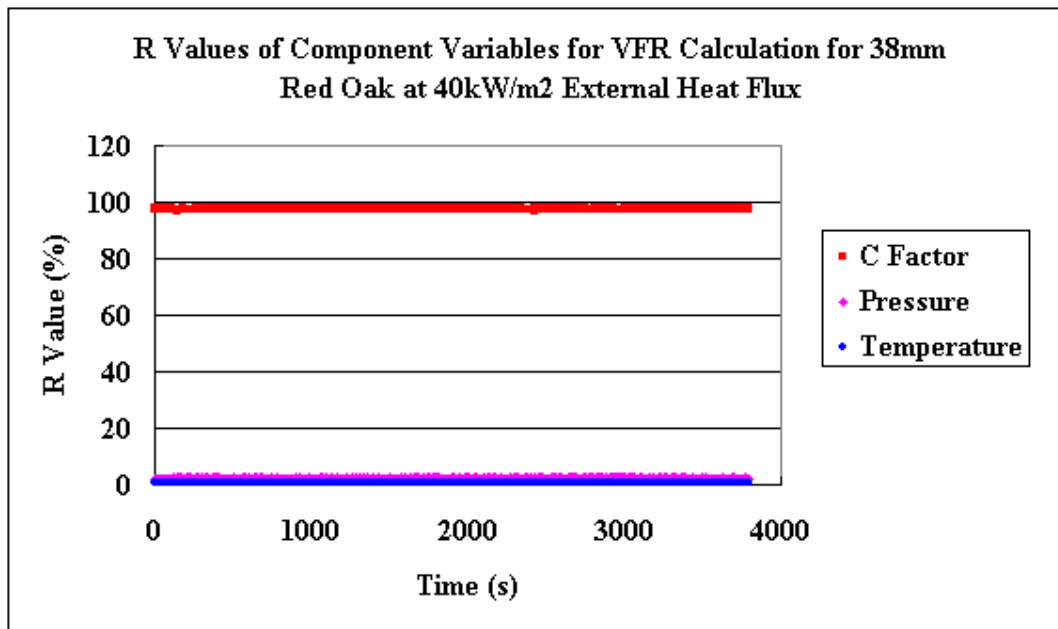


**Figure P-2 R Values of the Component Variables of Volume Flow Rate Calculation for 38mm Red Oak at 40 kW/m<sup>2</sup> External Heat Flux in Cone Test**

As seen in Figure P-2, the R value of C- Factor is almost 100% while the R values of pressure and temperature are almost 0%. From SC and R value analysis, VFR was most sensitive to C-Factor.

## **REFERENCES**

1. International Organization for Standardization, "Guide to the Expression of Uncertainty in Measurement", ISBN 92-67-10188-9, 1995.
2. Taylor, B. N., and Kuyatt, C. E., Guidelines for Evaluating and Expressing the Uncertainty of NIST Measurement Results, NIST Technical Note 1297, NIST, Gaithersburg, MD, 1994.
3. ASTM E 1354, "Standard Test Method for Heat and Visible Smoke Release Rates for Materials and Products Using an Oxygen Consumption Calorimeter", Annual Book of ASTM Standards, American Society for Testing Materials, Philadelphia, PA. 2002.
4. Bryant, Rodney A., Ohlemiller, Thomas J., Johnsson, Erik L., Hammins, Anthony, Grove, Brian S., Guthrie, William F., Maranghides, Alexander, and Mulholland George W., "The NIST 3 Megawatt Quantitative Heat Release Rate Facility", NIST Special Publication 1007, December 2003.

## APPENDIX Q SENSITIVITY ANALYSIS FOR EXTINCTION COEFFICIENT

The SC value of each parameter is calculated by using the Equation recommended by NIST

$$SC_i = \left| \frac{\partial y}{\partial x_i} \frac{x_i}{y} \right|$$

and the calculation details are shown in the following equations

$$SC_{I_0} = \left| \frac{\partial k}{\partial I_0} \frac{I_0}{k} \right| = \frac{1}{LI_0} \left[ \left( \frac{1}{L} \right) \ln \left( \frac{I_0}{I} \right) \right]^{-1} I_0 = 1 / \ln(I_0 / I)$$

$$SC_I = \left| \frac{\partial k}{\partial I} \frac{I}{k} \right| = \frac{1}{LI} \left[ \left( \frac{1}{L} \right) \ln \left( \frac{I_0}{I} \right) \right]^{-1} I = 1 / \ln(I_0 / I)$$

The SC is shown in Table Q-1.

**Table Q-1 SC of Each variable Being Used to Calculate Extinction Coefficient**

	I	I <sub>0</sub>
SC	1/ln(I <sub>0</sub> / I)	1/ln(I <sub>0</sub> / I)

As seen in Table Q-1, k was equally sensitive to I<sub>0</sub> and I. The SC value is in the range of 33 to 3.1×10<sup>6</sup>. Since the uncertainty of main photodiodes is larger than that of compensation photodiode (from the typical calculation), extinction coefficient is more sensitive to main photodiode. Apparent difference in photodiodes and / or circuits used to produce voltage

response. Each photodiode has different amplification in its circuits to make the voltages similar. This effectively indicates that compensation photodiode is not working.

## **REFERENCE**

1. Bryant, Rodney A., Ohlemiller, Thomas J., Johnsson, Erik L., Hammins, Anthony, Grove, Brian S., Guthrie, William F., Maranghides, Alexander, and Mulholland George W., "The NIST 3 Megawatt Quantitative Heat Release Rate Facility", NIST Special Publication 1007, December 2003.

## APPENDIX R SMOKE PRODUCTION RATE

Smoke production rate is calculated by

$$SPR = k * VFR = \frac{C}{353L} \ln\left(\frac{I_0}{I}\right) \sqrt{PT}$$

Then the uncertainty of smoke production rate can be calculated as following

$$\frac{\partial(SPR)}{\partial(C)} = \frac{1}{353L} \ln\left(\frac{I_0}{I}\right) \sqrt{PT} \quad (1)$$

$$\frac{\partial(SPR)}{\partial(P)} = \frac{C}{706L} \sqrt{\frac{T}{P}} \ln\left(\frac{I_0}{I}\right) \quad (2)$$

$$\frac{\partial(SPR)}{\partial(T)} = \frac{C}{706L} \sqrt{\frac{P}{T}} \ln\left(\frac{I_0}{I}\right) \quad (3)$$

$$\frac{\partial(SPR)}{\partial(I_0)} = \frac{C}{353LI_0} \sqrt{PT} \quad (4)$$

$$\frac{\partial(SPR)}{\partial(I)} = -\frac{C}{353LI} \sqrt{PT} \quad (5)$$

The dynamic SPR can be estimated by substituting equations (1)-(5) into the Law of Propagation of Uncertainty recommended by ISO<sup>1</sup> and NIST Guide<sup>2</sup>, i.e.,

$$u_c^2(y) = \sum \left(\frac{\partial f}{\partial x_i}\right)^2 u^2(x_i)$$

then, the uncertainty with 95% confidence is expressed as

$$SPR \pm 2u_c(SPR)$$

A typical SPR calculation for 38mm red oak at 40 kW/m<sup>2</sup> external heat flux is shown in Figure R-1. We have 95% confidence of the uncertainty.

The uncertainty analysis of SPR showed that the uncertainty was about 0.006 m<sup>2</sup>/s. As seen in Figure R-1, during 500s to 3800s, the smoke production rate is around zero, which is much less than the estimated uncertainty. Around the peak value of the smoke production rate, the normalized uncertainty (SPR uncertainty/SPR value) is about 100%. Therefore, the uncertainty is too big relative to the measured smoke production rate due to extinction coefficient.

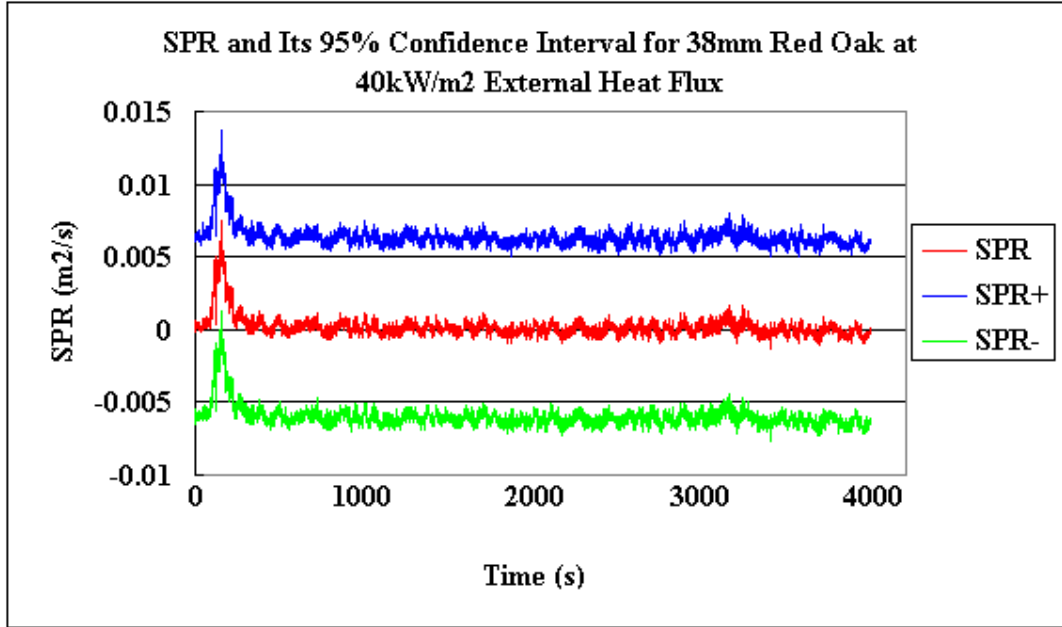


**Figure R-1 Smoke Production Rate and Its 95% Confidence Interval for 38mm Red Oak at 40 kW/m<sup>2</sup> External Heat Flux in Cone Test**

The SC value of each parameter is calculated by using the Equation recommended by NIST

$$SC_i = \left| \frac{\partial y}{\partial x_i} \frac{x_i}{y} \right|_3$$

and the calculation details are shown in the following equations

$$SC_C = \left| \frac{\partial(SPR)}{\partial C} \frac{C}{SPR} \right| = \frac{1}{353L} \ln\left(\frac{I_0}{I}\right) \sqrt{PT} \left[ \frac{C}{353L} \ln\left(\frac{I_0}{I}\right) \sqrt{PT} \right]^{-1} C = 1$$

$$SC_P = \left| \frac{\partial(SPR)}{\partial P} \frac{P}{SPR} \right| = \frac{C}{706L} \sqrt{\frac{T}{P}} \ln\left(\frac{I_0}{I}\right) \left[ \frac{C}{353L} \ln\left(\frac{I_0}{I}\right) \sqrt{PT} \right]^{-1} P = 0.5$$

$$SC_T = \left| \frac{\partial(SPR)}{\partial T} \frac{T}{SPR} \right| = \frac{C}{706L} \sqrt{\frac{P}{T}} \ln\left(\frac{I_0}{I}\right) \left[ \frac{C}{353L} \ln\left(\frac{I_0}{I}\right) \sqrt{PT} \right]^{-1} T = 0.5$$

$$SC_I = \left| \frac{\partial(SPR)}{\partial I} \frac{I}{SPR} \right| = \frac{C}{353LI} \sqrt{PT} \left[ \frac{C}{353L} \ln\left(\frac{I_0}{I}\right) \sqrt{PT} \right]^{-1} I = 1/\ln(I_0/I)$$

$$SC_{I_0} = \left| \frac{\partial(SPR)}{\partial I_0} \frac{I_0}{SPR} \right| = \frac{C}{353LI_0} \sqrt{PT} \left[ \frac{C}{353L} \ln\left(\frac{I_0}{I}\right) \sqrt{PT} \right]^{-1} I_0 = 1/\ln(I_0/I)$$

The SC is calculated and shown in Table R-1.

**Table R-1 SC of Each variable Being Used to Calculate SPR**

	C Factor	P	T	I	I <sub>0</sub>
SC	1	0.5	0.5	1/ln(I <sub>0</sub> /I)	1/ln(I <sub>0</sub> /I)

Since the absolute value of 1/ln(I<sub>0</sub>/I) is always greater than 1, SPR was equally sensitive to I<sub>0</sub> and I. The SC value of I<sub>0</sub> and I is in the range of 33 to 3.1×10<sup>6</sup>. However, the uncertainty of main photodiodes was larger from the typical calculation, therefore, the R value of main photodiode was also larger, see Figure R-2. Apparent difference in photodiodes and / or circuits used to produce voltage response. Each photodiode has different amplification in its circuits to make the voltages similar. This effectively indicates that compensation photodiode is not working. From the SC and R value analysis, SPR is most sensitive to main photodiode.

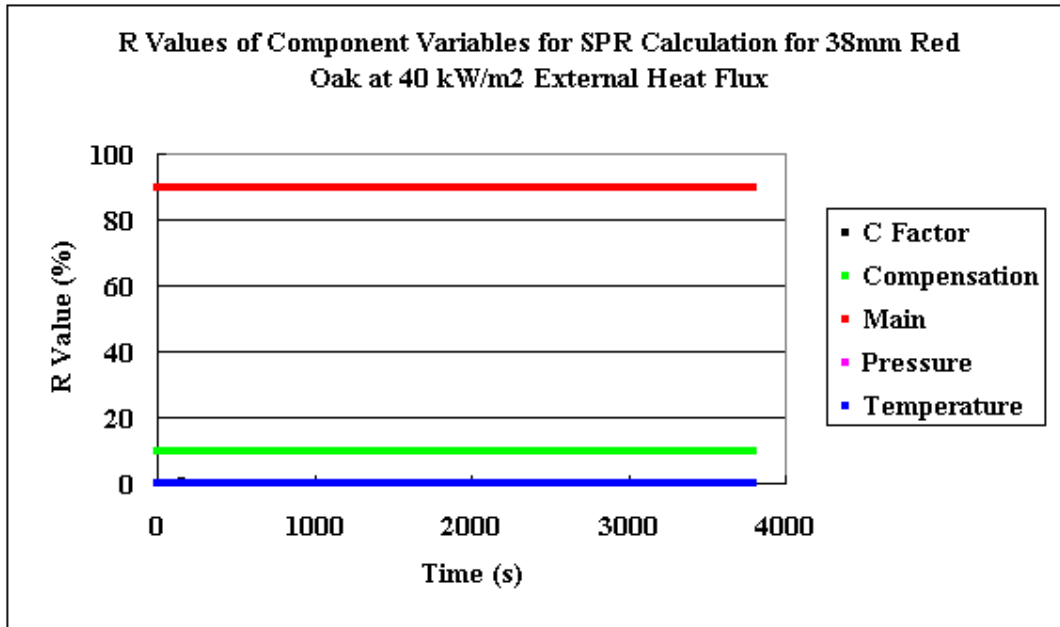


**Figure R-2 R Values of the Component Variables of Smoke Production Rate Calculation for 38mm Red Oak at 40 kW/m<sup>2</sup> External Heat Flux in Cone Test**

## REFERENCES

1. International Organization for Standardization, "Guide to the Expression of Uncertainty in Measurement", ISBN 92-67-10188-9, 1995.
2. Taylor, B. N., and Kuyatt, C. E., Guidelines for Evaluating and Expressing the Uncertainty of NIST Measurement Results, NIST Technical Note 1297, NIST, Gaithersburg, MD, 1994.
3. Bryant, Rodney A., Ohlemiller, Thomas J., Johnsson, Erik L., Hammins, Anthony, Grove, Brian S., Guthrie, William F., Maranghides, Alexander, and Mulholland George W., "The NIST 3 Megawatt Quantitative Heat Release Rate Facility", NIST Special Publication 1007, December 2003.

## APPENDIX S DYNAMIC SPECIFIC EXTINCTION AREA

The dynamic SEA can be estimated by substituting equations (1)-(6) into the Law of Propagation of Uncertainty recommended by ISO<sup>1</sup> and NIST Guide<sup>2</sup>, i.e.,

$$u_c^2(y) = \sum \left( \frac{\partial f}{\partial x_i} \right)^2 u^2(x_i)$$

$$\frac{\partial(SEA_i)}{\partial(C)} = \frac{\sqrt{P_i T_i} \frac{1}{L} \ln\left(\frac{I_{0i}}{I}\right)}{MLR_i} \quad (1)$$

$$\frac{\partial(SEA_i)}{\partial(I_{0i})} = \frac{C \sqrt{P_i T_i}}{353 L I_{0i} MLR_i} \quad (2)$$

$$\frac{\partial(SEA_i)}{\partial(I_i)} = \frac{C \sqrt{P_i T_i}}{353 L I_i MLR_i} \quad (3)$$

$$\frac{\partial(SEA_i)}{\partial(P_i)} = \frac{C \ln\left(\frac{I_{0i}}{I_i}\right) \sqrt{\frac{T_i}{P_i}}}{706 L MLR_i} \quad (4)$$

$$\frac{\partial(SEA_i)}{\partial(T_i)} = \frac{C \ln\left(\frac{I_{0i}}{I_i}\right) \sqrt{\frac{P_i}{T_i}}}{706 L MLR_i} \quad (5)$$

$$\frac{\partial(SEA_i)}{\partial(MLR_i)} = \frac{-\frac{C\sqrt{P_i T_i}}{353} \frac{1}{L} \ln\left(\frac{I_{0i}}{I_i}\right)}{MLR_i^2} \quad (6)$$

A typical dynamic SEA calculation for 38mm red oak at 40 kW/m<sup>2</sup> external heat flux is shown in Figure S-1. We have 95% confidence of the uncertainty. As seen in Figure S-1, the uncertainty is at least one magnitude larger than that of SEA.

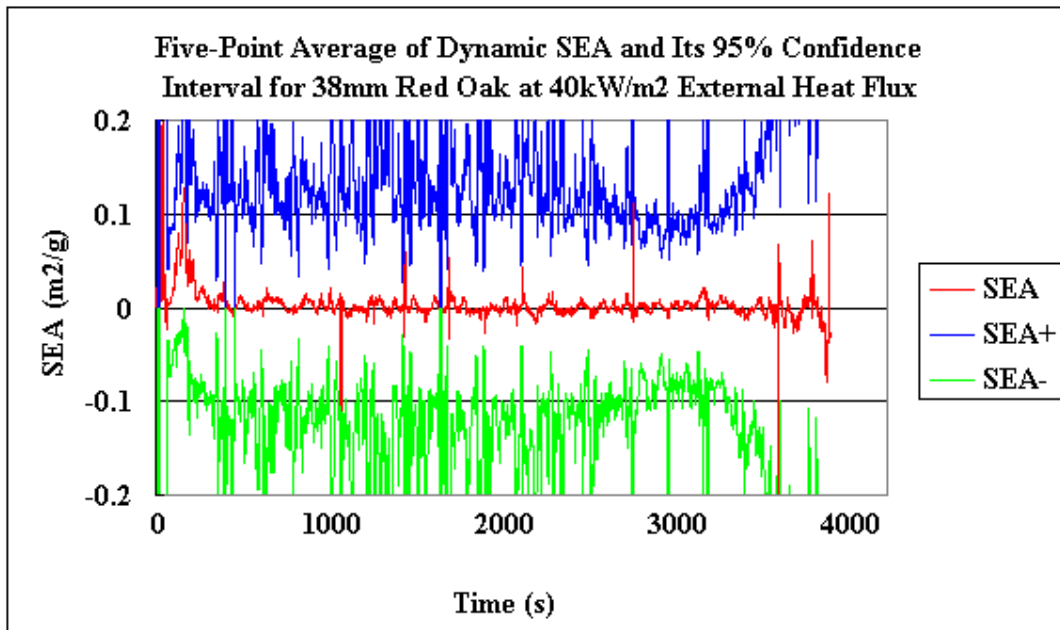


**Figure S-1 Five-Point Average of Dynamic Specific Extinction Area and Its 95% Confidence Interval of 38mm Red Oak at 40 kW/m<sup>2</sup> External Heat Flux in Cone Test**

The SC value of each parameter is calculated by using the Equation recommended by NIST

$$SC_i = \left| \frac{\partial y}{\partial x_i} \frac{x_i}{y} \right|_3$$

and the calculation details are shown in the following equations

$$SC_C = \left| \frac{\partial(SEA)}{\partial C} \frac{C}{SEA} \right| = \frac{\frac{\sqrt{P_i T_i}}{353} \frac{1}{L} \ln\left(\frac{I_{0i}}{I_i}\right)}{MLR_i} \left[ \frac{\frac{C \sqrt{P_i T_i}}{353} \frac{1}{L} \ln\left(\frac{I_{0i}}{I_i}\right)}{MLR_i} \right]^{-1} C = 1$$

$$SC_{I_{0i}} = \left| \frac{\partial(SEA)}{\partial I_{0i}} \frac{I_{0i}}{SEA} \right| = \frac{\frac{C \sqrt{P_i T_i}}{353 L I_{0i}} \frac{1}{L} \ln\left(\frac{I_{0i}}{I_i}\right)}{MLR_i} \left[ \frac{\frac{C \sqrt{P_i T_i}}{353} \frac{1}{L} \ln\left(\frac{I_{0i}}{I_i}\right)}{MLR_i} \right]^{-1} I_{0i} = 1 / \ln(I_{0i} / I_i)$$

$$SC_{I_i} = \left| \frac{\partial(SEA)}{\partial I_i} \frac{I_i}{SEA} \right| = \frac{\frac{C \sqrt{P_i T_i}}{353 L I_i} \frac{1}{L} \ln\left(\frac{I_{0i}}{I_i}\right)}{MLR_i} \left[ \frac{\frac{C \sqrt{P_i T_i}}{353} \frac{1}{L} \ln\left(\frac{I_{0i}}{I_i}\right)}{MLR_i} \right]^{-1} I_i = 1 / \ln(I_{0i} / I_i)$$

$$SC_{P_i} = \left| \frac{\partial(SEA)}{\partial P_i} \frac{P_i}{SEA} \right| = \frac{\frac{C}{706 L} \ln\left(\frac{I_{0i}}{I_i}\right) \sqrt{\frac{T_i}{P_i}}}{MLR_i} \left[ \frac{\frac{C \sqrt{P_i T_i}}{353} \frac{1}{L} \ln\left(\frac{I_{0i}}{I_i}\right)}{MLR_i} \right]^{-1} P_i = 0.5$$

$$SC_{T_i} = \left| \frac{\partial(SEA)}{\partial T_i} \frac{T_i}{SEA} \right| = \frac{\frac{C}{706 L} \ln\left(\frac{I_{0i}}{I_i}\right) \sqrt{\frac{P_i}{T_i}}}{MLR_i} \left[ \frac{\frac{C \sqrt{P_i T_i}}{353} \frac{1}{L} \ln\left(\frac{I_{0i}}{I_i}\right)}{MLR_i} \right]^{-1} T_i = 0.5$$

$$SC_{MLR_i} = \left| \frac{\partial(SEA)}{\partial (MLR_i)} \frac{MLR_i}{SEA} \right| = \frac{\frac{C \sqrt{P_i T_i}}{353} \frac{1}{L} \ln\left(\frac{I_{0i}}{I_i}\right)}{MLR_i^2} \left[ \frac{\frac{C \sqrt{P_i T_i}}{353} \frac{1}{L} \ln\left(\frac{I_{0i}}{I_i}\right)}{MLR_i} \right]^{-1} MLR_i = 1$$

The SC values are shown in Table S-1

**Table S-1 SC of Each variable Being Used to Calculate Dynamic SEA**

	C Factor	Main	Compensation	Pressure	Temperature	MLR
SC	1	1/ln(I <sub>0</sub> /I)	1/ln(I <sub>0</sub> /I)	0.5	0.5	1

Since the absolute value of  $1/\ln(I_0/I)$  is always greater than 1, theoretically, dynamic SEA is equally sensitive to  $I_0$  and  $I$ . The SC value of  $I_0$  and  $I$  is in the range of 33 to  $3.1 \times 10^6$ .

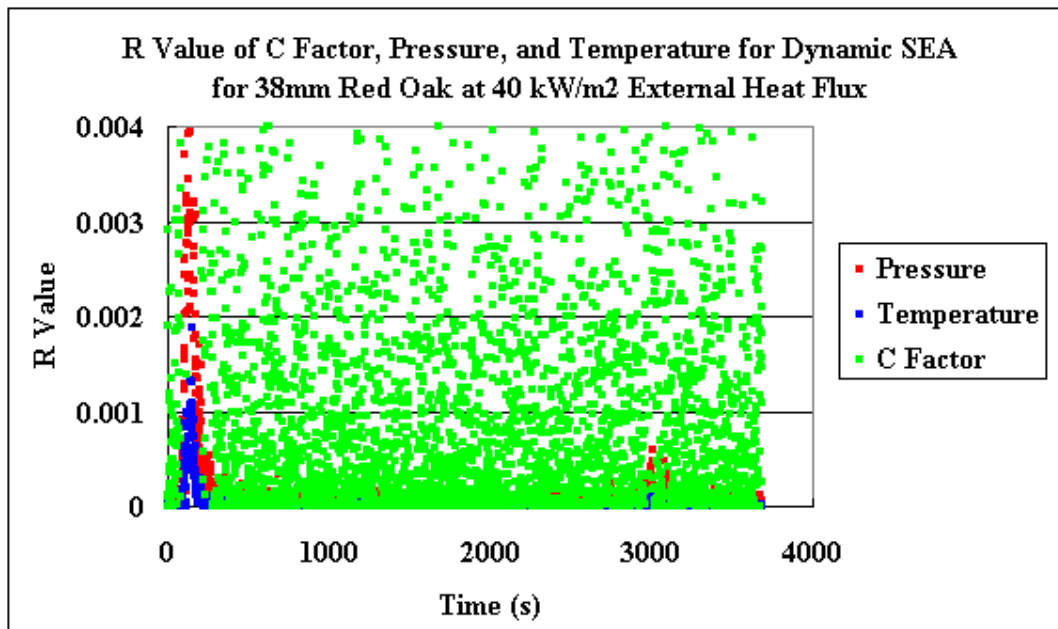


Figure S-2 R Values of C Factor, Pressure, and Temperature for Dynamic Specific Extinction Area Calculation for 38mm Red Oak at 40 kW/m<sup>2</sup> External Heat Flux in Cone Test

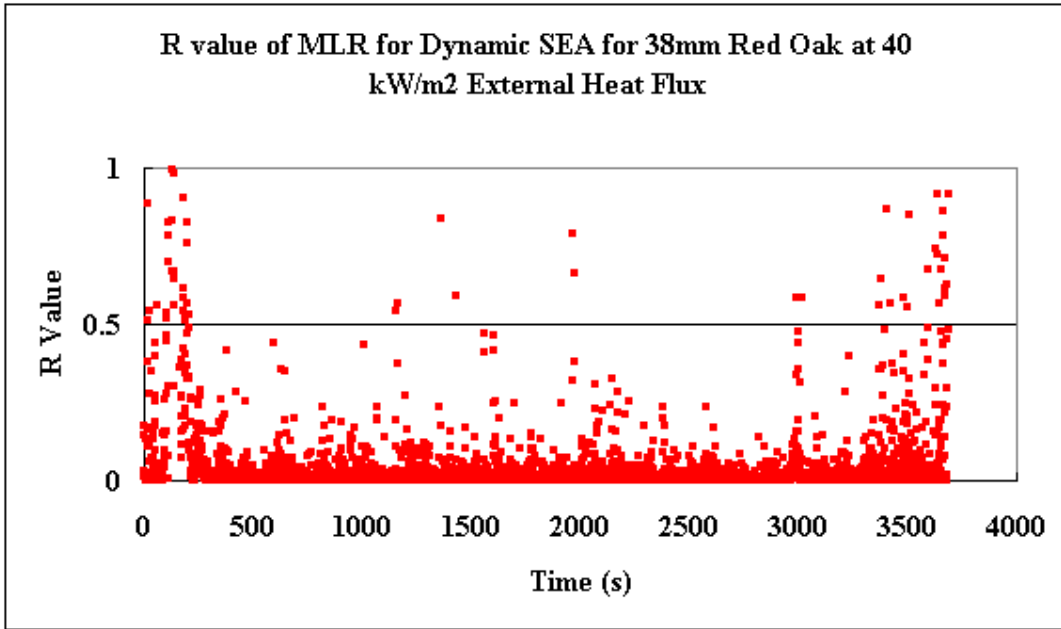


Figure S-3 R Value of Mass Loss Rate for Dynamic Specific Extinction Area Calculation of 38mm Red Oak at 40 kW/m<sup>2</sup> External Heat Flux in Cone Test

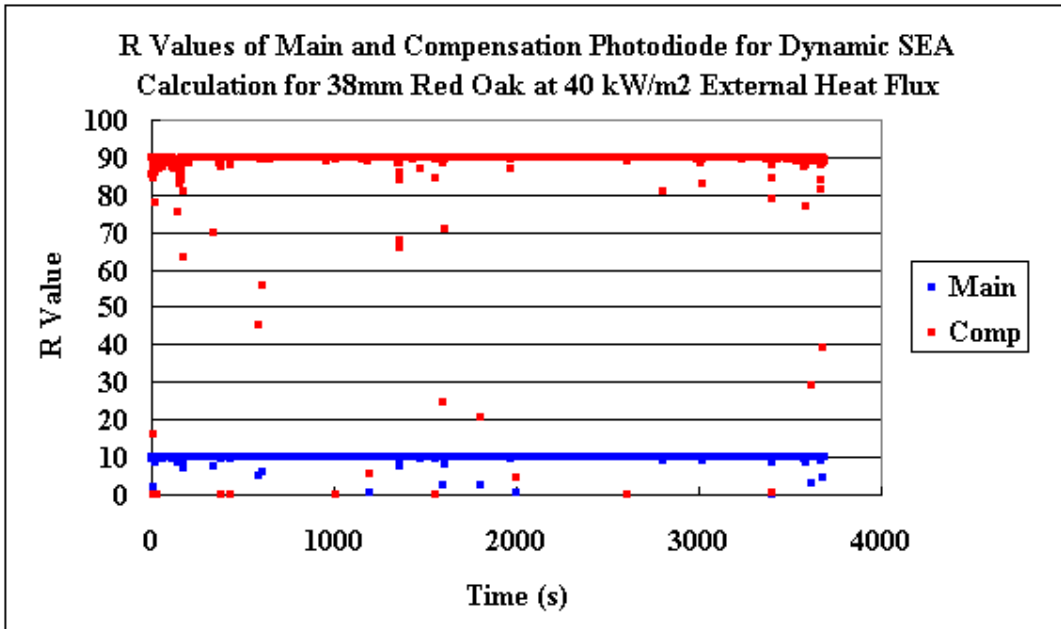


Figure S-4 R Values of Main and Compensation Photodiodes for Dynamic Specific Extinction Area Calculation of 38mm Red Oak at 40 kW/m<sup>2</sup> External Heat Flux in Cone Test

Similar to the analysis of average SEA, R values for dynamic SEA were shown in Figure S-2, Figure S-3, and Figure S-4. Figure S-2 showed the “first group” R values of C factor,

pressure and temperature, Figure S-3 showed the “second group” R value of mass loss rate, and Figure S-4 showed the “third group” R values of main and compensation photodiodes. The R values of the “first group” were found very small compared to the other two groups. Most of the R values of the second group is less than 1%. In the “third group”, it was obvious that the uncertainty of main photodiode dominated the uncertainty of dynamic SEA. Theoretically, the dynamic SEA should be equally sensitive to main and compensation photodiode, which can be found from equation (2) and (3). Apparent difference in photodiodes and / or circuits used to produce voltage response. Each photodiode has different amplification in its circuits to make the voltages similar. This effectively indicates that compensation photodiode is not working. Since the uncertainty of main photodiodes is larger than that of compensation (from the typical calculation), the R value is also larger.

## **REFERENCES**

1. International Organization for Standardization, “Guide to the Expression of Uncertainty in Measurement”, ISBN 92-67-10188-9, 1995.
2. Taylor, B. N., and Kuyatt, C. E., Guidelines for Evaluating and Expressing the Uncertainty of NIST Measurement Results, NIST Technical Note 1297, NIST, Gaithersburg, MD, 1994.
3. Bryant, Rodney A., Ohlemiller, Thomas J., Johnsson, Erik L., Hammins, Anthony, Grove, Brian S., Guthrie, William F., Maranghides, Alexander, and Mulholland George W., “The NIST 3 Megawatt Quantitative Heat Release Rate Facility”, NIST Special Publication 1007, December 2003.

## APPENDIX T DYNAMIC HEAT OF COMBUSTION

The dynamic HOC can be estimated by substituting equations (1)-(2) into the Law of Propagation of Uncertainty recommended by ISO<sup>1</sup> and NIST Guide<sup>2</sup>, i.e.,

$$u_c^2(y) = \sum \left( \frac{\partial f}{\partial x_i} \right)^2 u^2(x_i)$$

$$\frac{\partial(HOC_i)}{\partial(\dot{q}_i(t))} = \frac{1}{MLR_i} \quad (1)$$

$$\frac{\partial(HOC_i)}{\partial(m_i)} = \frac{-\dot{q}_i(t)}{MLR_i^2} \quad (2)$$

A typical dynamic HOC calculation for 38mm red oak at 40 kW/m<sup>2</sup> external heat flux is shown in Figure T-1. We have 95% confidence of the uncertainty.

The SC value of each parameter is calculated by using the Equation recommended by NIST

$$SC_i = \left| \frac{\partial y}{\partial x_i} \frac{x_i}{y} \right|_3$$

and the calculation details are shown in the following equations

$$SC_{HRR} = \left| \frac{\partial(HOC)}{\partial HRR} \frac{HRR}{HOC} \right| = \frac{1}{MLR_i} \left[ \frac{HRR_i}{MLR_i} \right]^{-1} (HRR) = 1$$

$$SC_{MLR} = \left| \frac{\partial(HOC)}{\partial(MLR)} \frac{MLR}{HOC} \right| = \frac{HRR}{MLR_i^2} \left[ \frac{HRR_i}{MLR_i} \right]^{-1} (MLR_i) = 1$$

From the SC calculation, we find HRR and MLR have the same SC in terms of dynamic HOC calculation.

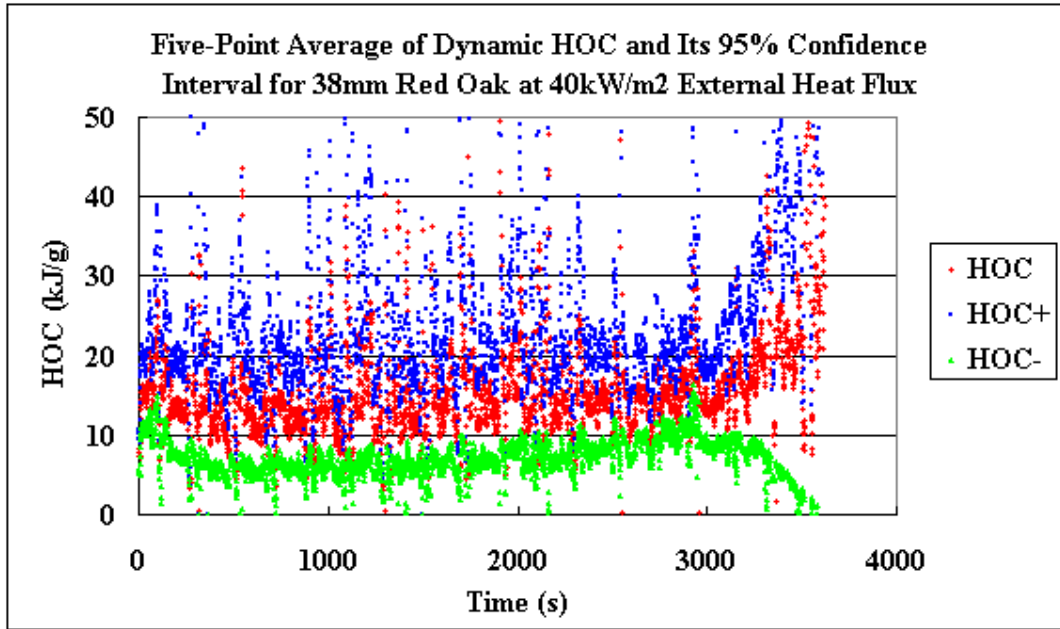


**Figure T-1 Five-Point Average of R Values of Component Variables for Dynamic HOC Calculation for 38mm Red Oak at 40 kW/m<sup>2</sup> External Heat Flux in Cone Test**

R values are shown in Figure T-2. As seen in Figure T-2, for the current case, HRR uncertainty contributes more uncertainty to the dynamic HOC than that of MLR.

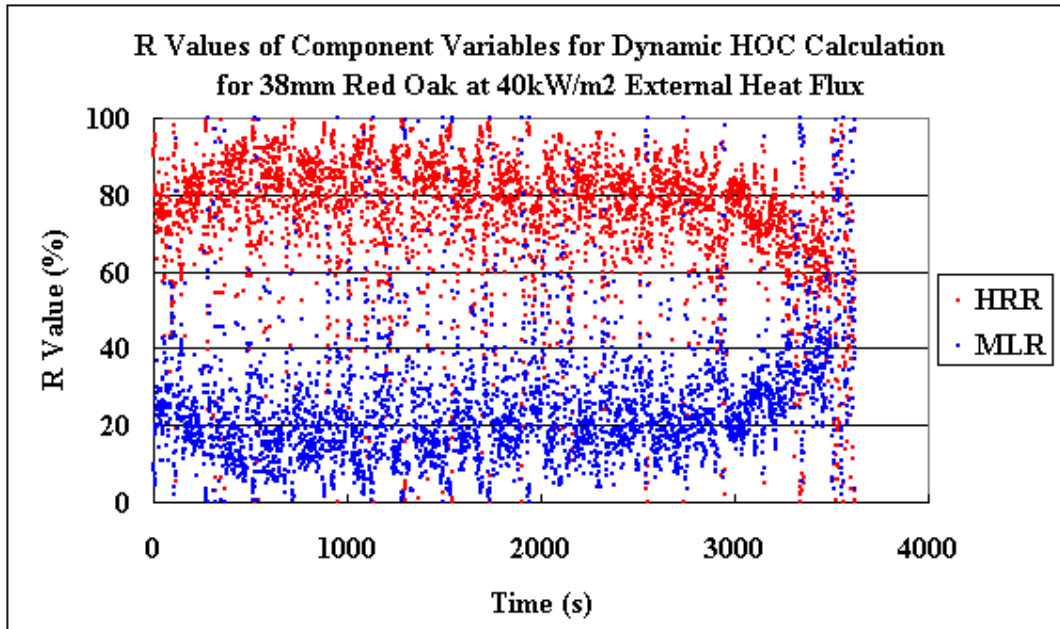


**Figure T-2 R Values of Component Variables for Dynamic HOC Calculation for 38mm Red Oak at 40 kW/m<sup>2</sup> External Heat Flux in Cone Test**

## REFERENCES

1. International Organization for Standardization, "Guide to the Expression of Uncertainty in Measurement", ISBN 92-67-10188-9, 1995.
2. Taylor, B. N., and Kuyatt, C. E., Guidelines for Evaluating and Expressing the Uncertainty of NIST Measurement Results, NIST Technical Note 1297, NIST, Gaithersburg, MD, 1994.
3. Bryant, Rodney A., Ohlemiller, Thomas J., Johnsson, Erik L., Hammins, Anthony, Grove, Brian S., Guthrie, William F., Maranghides, Alexander, and Mulholland George W., "The NIST 3 Megawatt Quantitative Heat Release Rate Facility", NIST Special Publication 1007, December 2003.

## APPENDIX U CONSTANT MLR GENERATOR FOR FUTURE WORK

In order to estimate the MLR uncertainty at different MLR level, a device can be designed and built in the future, see the Figure K-1 below.

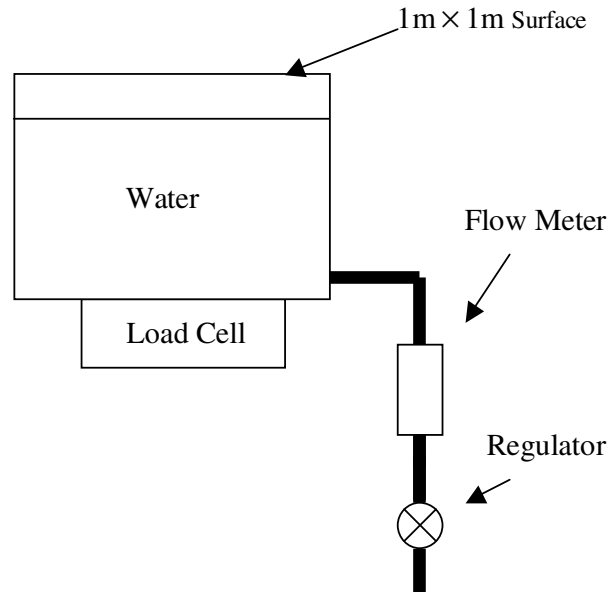


**Figure U-1 Constant Mass Loss Rate Generator for MLR Uncertainty Estimate**

As seen in Figure K-1, a stable MLR at different level can be obtained by adjusting the water flow rate. Mass can be recorded for many times, then the MLR is calculated by using

$$MLR = \frac{-m_{i-2} + 8m_{i-1} - 8m_{i+1} + m_{i+2}}{12\Delta t}$$